Title	Mechanistic and kinetic study on the anomerisation reaction and application in pharmaceutical research
Author(s)	Holland, Trish
Publication Date	2024-01-08
Publisher	NUI Galway
Item record	http://hdl.handle.net/10379/18009

Mechanistic and Kinetic Study on the Anomerisation Reaction and Application in Pharmaceutical Research

By Trish Holland

A Thesis presented to

The University of Galway, Ireland

For the Degree of Master of Science in Chemistry Research

Based on research carried out in the

School of Biological and Chemical Sciences, The University of Galway,

Supervisor: Prof. Paul V. Murphy

Head of School: Prof. Olivier Thomas

August 2023

Table of Contents

Declaration

This thesis has not been submitted before, in whole or in part, to this or any other university for any degree, and is, except where otherwise stated, the original work of the author.

Trish Holland

Abstract

It is becoming increasingly apparent that carbohydrate-based pharmaceutically active compounds (PACs) play a key role in pharmaceutical advancement. Many new carbohydrate-based PACs have recently been developed with a plethora of functions ranging from antiviral and anticancer effects to drug delivery systems.

With this increased interest in carbohydrate-based pharmaceutical research, gaps in the knowledge of carbohydrate chemistry have become apparent, with many challenges still being faced by carbohydrate chemists, including the stereoselective synthesis of anomers. The synthesis of glycosidic links is an essential aspect in the development of carbohydrate-based PACs. A possible route to the selective synthesis of carbohydrate anomers is the anomerisation reaction that is generally preformed using a Lewis acid catalyst. The aim of this thesis was to synthesise the new galacturonic acid derivative 2,3,4-tri-O-acetyl-β-D-galactopyranosiduronic acid, methyl ester using the Koenigs-Knorr glycosylation reaction and investigate the kinetics of the anomerisation of this compound. The rate constant for this compound was calculated to be 5×10^{-5} at RT. This result led to an interest in the varying kinetic rate constants of different uronic acid derivatives. Therefore, further study of the kinetics of the anomerisation reaction of previously synthesised compounds was undertaken, specifically the change in rate constants of the reaction when varying the temperature, uronic acid derivative and catalyst concentration was investigated. The three uronic acid derivatives investigated were 2,3,4-Tri-O-acetyl-β-D-galactopyranosiduronic acid, methyl ester ,Butyl 2-O-(4-phenylbenzoyl)-3,4-di-O-benzoyl-α-D-glucopyranosiduronic acid methyl ester,

Butyl 2-O-(4-bromolbenzoyl)-3,4-di-O-benzoyl-α-D-glucopyranosiduronic acid methyl ester and Butyl 2-O-(4-methylbenzoyl)-3,4-di-O-benzoyl-α-D-glucopyranosiduronic acid, methyl ester

By varying the temperature at which the anomerisation reaction takes place, the activation energy could be calculated from a set of experimentally determined rate constants and were found to be 17.71, 60.43 and 30.94 KJ/Mol respectively.

This showed that EDG groups on the C2 substituent tended to increase the activation energy of the anomerisation reaction for compounds (5) and (6). Compound (7) activation energy was Due to probable experimental error, the rate constant calculated for compound (7) at 45°C was disregarded. Therefore the activation energy calculated may not be as accurate and more investigation is needed to evaluate trends in the effect of EDG and EWG groups on activation energy.

Catalyst concentration studies were carried out and it was found that increasing the concertation above a 1:1 ratio had little to no effect on the reaction rate, indicating that the rate determining step of this reaction only requires one $SnCl_4$ molecule.

Abbreviations and Symbols

α	alpha
β	beta
δ	chemical shift in ppm downfield from TMS
$[\alpha]_D$	specific rotation
°C	degrees Celsius
Å	Angstrom
Ac	acetate
Ac_2O	acetic anhydride
Bu	butyl
Bz	benzoate
$CDCl_3$	deuterated chloroform
COSY	Correlation Spectroscopy
d	doublet
DCM	dichloromethane
dd	doublet of doublets
DMF	Dimethylformamide
DNJ	1-Deoxynojirimycin
dt	double of triplets
E_a	activation energy
ESI-HRMS	High-Resolution Mass Spectrometry

	Electrospray ionisation
EtOAc	ethyl acetate
GPI	glycosyl-phosphatidylinositol
h	hours
HAT	Human American Trypanosomiasis
HSQC	Heteronuclear Single Quantum Correlation
Hz	hertz
J	coupling constant, in Hz
LG	leaving group
M	molar
m	multiplet
Me	methyl
MeOH	methanol
min	minutes
mL	millilitre
mol, mmol	mole, millimole
MUC1	Mucin 1
NMR	nuclear magnetic resonance
PG	protecting group
Ph	Phenyl
ppm	parts per million

q	quartet
RT	room temperature
s	singlet
S_N2	bimolecular nucleophilic substitution
t	triplet
T	temperature
TLC	thin layer chromatography

Acknowledgements

Firstly, I would like to thank my supervisor Professor Paul V. Murphy for the opportunity to pursue a master's degree within his group. You have helped me to learn so many skills and allowed me to grow as a scientist. Thank you so much for your guidance throughout this year.

Next, I want to extend my deepest gratitude to the Murphy group for your constant support. A special mention to Aaron McCormack, thank you for all the time you took to teach me. Your constant patience and guidance are so greatly appreciated. I'd also like to thank Ashis, Kishan, Jack, and Saidulu for all your help throughout the year.

Thank you to the technical staff of the School of Chemistry, in particular, Dr. Roisin Doohan and James Donnellan for their help with my arrays and for their upkeep of the NMR machine.

To the other members of the chemistry department, my lunchtimes this year have been unlike anything I've had before, with the strangest but the most interesting of conversation topics. Thank you all for being so welcoming and making me feel like part of the team. It's because of ye I really do believe "Ireland is still the land of opportunity".

To the members and honorary members of Number 10 past and present, my kayaking stronghold. I could not have done this without ye. In particular, to Maeve for the countless cups of tea, sing along's in the car and never-ending support, Fionn for adding the perfect soundtrack to my year, and Niall for the debates and constant tips on how to keep my plants alive.

To the rest of the kayakers, I arrived in Galway just over a year ago and you made me feel more welcome than I ever have before, ye have become my family and my best friends who have kept me motivated and focused through training, pints, and a good pep talk whenever I needed it, I absolutely couldn't have done it without all of you.

To my grandparents who ensured I was afforded every opportunity in life and who, no matter what have been so proud.

To my mom. You have been my inspiration since day one. Your strength, independence, and resilience are awe-inspiring. You have been at the end of the phone with words of wisdom and constant support every day and I can never thank you enough. While I have been working toward my master's you have been doing exactly the same, and it will be an honour to stand next to you in your cap and gown.

1. Introduction

1.1 Introduction to Carbohydrates

Carbohydrates are the most abundant biomolecules. They vary widely in their structure and functions in biochemistry and pharmaceuticals. They have been extensively studied as an essential food group and are now also being investigated as pharmaceutically active agents.

Carbohydrates are organic molecules that have a clearly defined chemical structure composed of carbon, oxygen, and hydrogen with the general formula $C_n(H_2O)_n$.[1] These substances were once known as hydrates of carbon and were hence referred to as carbohydrates.[2] The term "carbohydrate" now refers to polyhydroxylated aldehydes or ketones, or compounds that form these compounds when hydrolysed.[3]

Carbohydrates are sub-categorised as monosaccharides, disaccharides, oligosaccharides, or polysaccharides. Monosaccharides are known as the building blocks of more complex sugars. They are comprised of one sugar unit that combines to form larger structures. Disaccharides have two sugar units; oligosaccharides contain three to ten sugar units and polysaccharides contain more than ten and can be thought of as polymers made of carbohydrate units (Figure 1).[3]
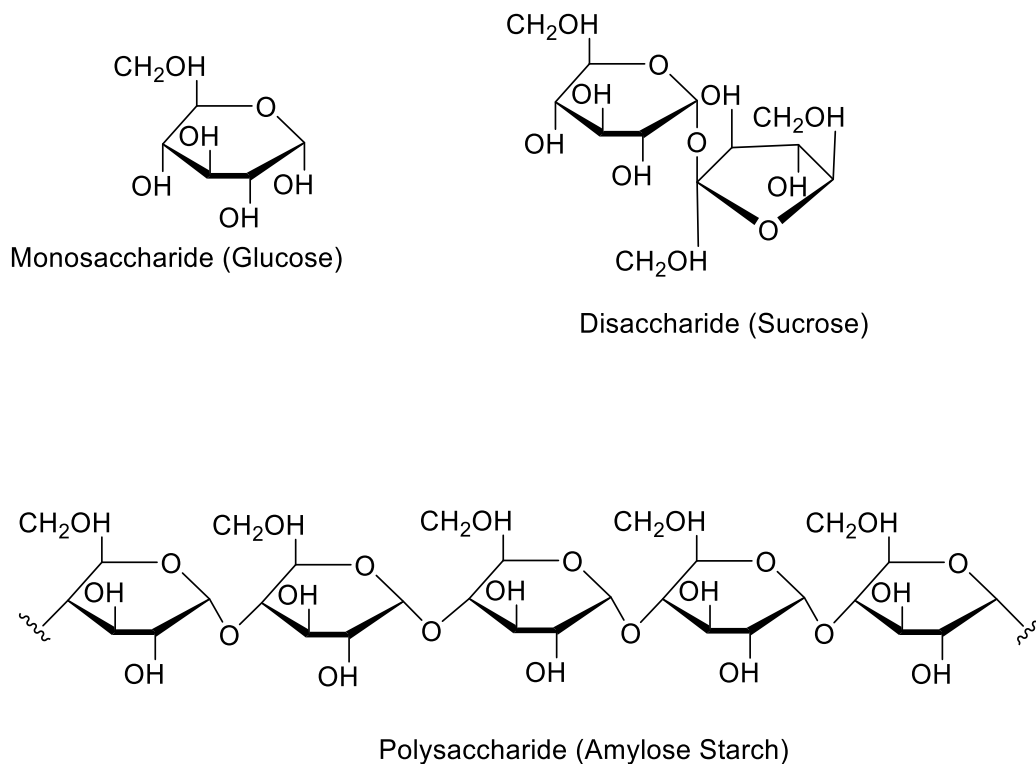
Figure 1. *Depiction of a monosaccharide, disaccharide and polysaccharide carbohydrate compound.*

Carbohydrates play a crucial role in many biological processes in both plants and animals. Carbohydrates are commonly known as essential macronutrients and are found in many varieties of food and drinks in simple and complex forms.[4] These compounds break down into simple sugars (glucose) in the human body and are used for energy.[4]

Carbohydrates are also essential compounds in chemistry and biochemistry, they are the most abundant complex biomolecules and are involved in a myriad of biological and pharmaceutical processes such as molecular recognition, components of glycoproteins and glycolipids and are used in some antiviral and antiseptic treatments. [5]

1.2 Carbohydrates in the Pharmaceutical Industry

Carbohydrates play a critical role in the pharmaceutical industry, as they can be pharmaceutically active (PACs) or bioactive compounds. Carbohydrate compounds are now being used as therapeutic agents for many diseases, with 54 new carbohydrate-based drugs being FDA-approved between 2000 and 2021.[6]

Until recently the study of carbohydrate chemistry and biochemistry focused on their role in energy storage and supply, with very little thought given to their possible role in drug discovery. [7]

The study of carbohydrates is now very important in the pharmaceutical industry with their role in biological processes such as molecular signalling, and their presence in cells in the form of glycoproteins and glycolipids making them impossible to ignore.

1.2.1 Molecular Recognition

Molecular Recognition In both intracellular and intercellular molecular recognition, carbohydrates are essential, as they can coat the outside of cells which carry information essential for cell-cell signalling.[8] Numerous physiological and pathological processes including glycoprotein fate and stability, fertilization, immune reactions, inflammation, cell defence, infection, and cancer are triggered by these recognition events.[9] Sugar-specific receptors (lectins) can be present on the surface of cells which leads to interaction and adhesion of apposing cells via specific carbohydrate recognition domains (CRD) and carbohydrates.[8] These CRDs have structural diversity that influences the binding of sugar moieties (Figure 2).[10]
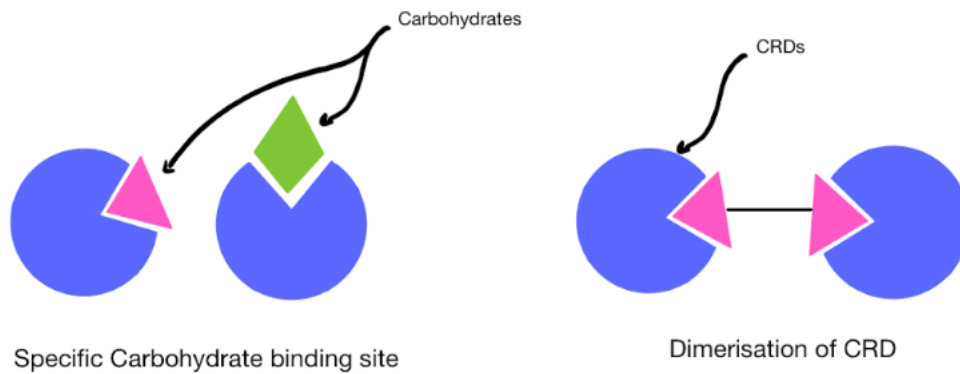
Figure 2. lectin proteins influence the binding of sugar moieties to CRDs. Image adapted from ref [10] [10]

1.2.2 Glycoproteins and Glycolipids

Combining carbohydrates with non-carbohydrate entities vastly increases carbohydrate compounds' diversity, complexity, and functions. The combination of carbohydrates with non-carbohydrate entities such as proteins and lipids are known as glycoconjugates and are formed through an enzymatic reaction known as glycosylation.[11]

Glycoproteins are proteins that have undergone this glycosylation reaction with one or more carbohydrate compounds.

Glycoproteins are formed when oligosaccharides form covalent bonds with proteins through two kinds of linkages: N-linkages or O-linkages (Figure 3).[12]
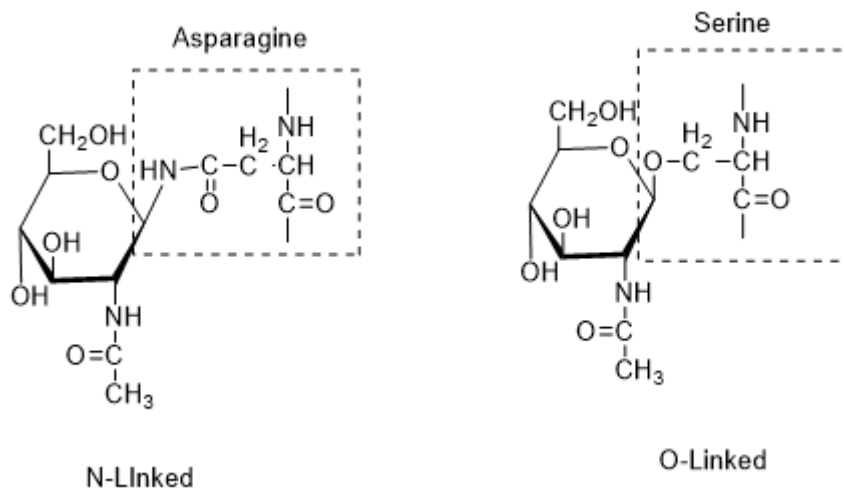
Figure 3. N-linked and O-Linked Glycoproteins

N-linked glycosylation occurs in the endoplasmic reticulum (ER) and usually occurs co-translationally, while O-linkages occur in the Golgi apparatus and occur post-translationally. O-linked glycosylation covalently attaches oligosaccharides to proteins in particular serine on threonine residues.[13] N-linked glycosylation attaches the oligosaccharides to the side chain of the amide group on the asparagine residues in some Asn-X-Ser/Thr sequence.[14] The biosynthesis of these N and O-linked glycoproteins depends on the level of gene expression, mRNA, enzyme protein activity, and substrate and cofactor concentrations.[14] These variables lead to a huge range of structures that differ with cell and tissue type as well as differing among different species.

Glycans play a key role in protein folding and having the correct moiety is essential for correct protein folding. The presence of glycans on proteins may also affect the protein's solubility and stability.[14]

Glycolipids are a class of molecules that contain carbohydrates covalently attached to a lipid. These molecules have a wide range of structures and functions as is the case for glycoproteins.[15] Glycolipids can often be found in eukaryotic cell membranes where they provide stability and have a role in cell-cell signalling.[16]

Many cells contain a layer known as the glycocalyx, a grass-like meshwork covering the cell membrane. This layer is comprised of branched and linear oligosaccharides and transmembrane-associated glycolipids and glycoproteins.[17] The glycocalyx has many important functions, for instance in bacterial cells the glycocalyx mediates cell attachment, protects the cell against molecular and cellular bacterial agents (e.g., antibiotics) and retains humidity when the cell is exposed to dry environments.[17]

In diseases such as cancer, metastasis, and a variety of other diseases, diverse alterations of these glycoproteins occur.[18] This is due to alterations in the oligosaccharide assembly in the Golgi apparatus which influences glycoprotein processing steps. Understanding these steps is vital in the understanding and treatment of human disease.[18]

1.2.3 Pharmaceutically Active Compounds

<u>Antibacterial Agents</u>

Carbohydrate-based drugs span a wide range of applications and are used to treat a variety of diseases daily. For example, carbohydrate-based antibiotics play a key role in fighting bacterial infections, such as the antibiotic gentamicin

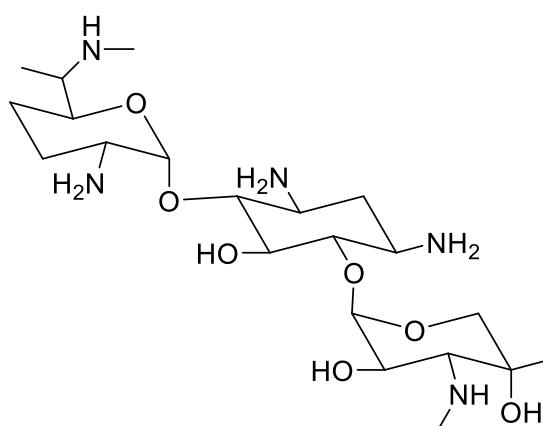which is an aminoglycoside used daily in surgical prophylaxis and for the treatment of bacterial meningitis (Figure 4).[19]

Figure 4. Structure of Gentamicin

Many of these antibiotic drugs target the bacteria's ribosomal function, which prevents protein synthesis.[6] Nine new antibacterial drugs have been developed since 2000.[6] The development of new antibacterial drugs is becoming increasingly important due to ongoing bacterial resistance.

Antiviral Agents

Carbohydrates are used to treat viral pathogens which are one of the biggest threats to human health, responsible for nearly 60% of the past pandemics, including SARS-Cov, MERS-CoV, Ebola and Covid-19.[6] Carbohydrates are quickly showing a particular advantage in the fight against viral diseases with eight new antiviral drugs that target the viral DNA or RNA replication mechanism being developed since 2000.[6] Notably the development of remdesivir (Figure 5), a saccharide-based drug being used to treat patients who are at high risk of serious illness or death with Covid-19 as it reduces the virus's ability to multiply within the body.[20]
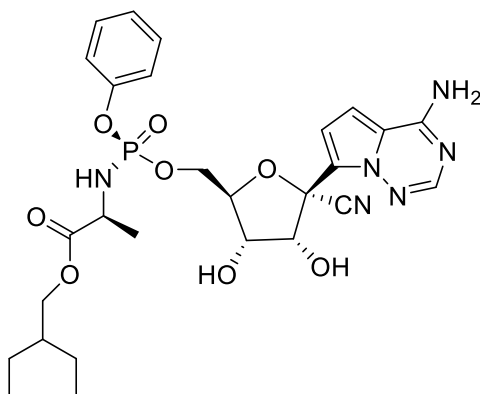
Figure 5. *Structure of Remdesivir*

Anticancer Agents

Cancer cells express extracellular tumour-associated carbohydrate antigens (TACAs) which are biomarkers for cancer detection and prognosis.[5] TACAs antigens alone have a poor ability to induce an immune response thus efforts have been made to create anti-tumour vaccines. Anti-tumour vaccines are currently being designed to aid the killer T-cell-dependent host immune response.[5] The anti-tumour vaccines help the host immune system to recognise and react to the target antigens and destroy the cancer cells by combining TACAs with polysaccharides and other components.[5] Mucin 1 (MUC1) is a glycoprotein that is over-expressed in many solid tumours. MUC1 Glycopeptide vaccines modified with GalNAc Glycoclusters have been studied in the Murphy group by Dr. Adele Gabba. This work looked at how these anti-tumour vaccines, elicited an improved humoral response.[21]

Many chemotherapy drugs are also carbohydrate based such as adriamycin which is used to treat a wide range of cancers such as breast cancer, acute lymphoblastic leukaemia, and thyroid cancer (Figure 6). [22]
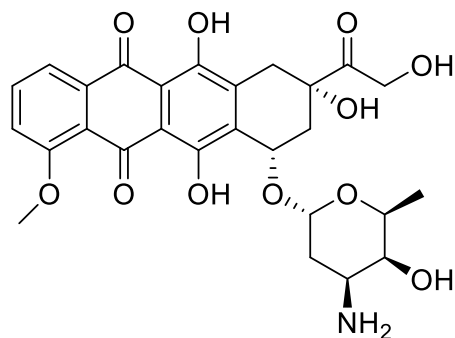
8

Figure 6. Structure of Adriamycin

Drug Delivery Systems

Typically drug delivery systems have been based on lipid and polymer chemistry, however, carbohydrate polymers are showing an increasing versatility and potential in drug delivery systems.[23] Polysaccharides are biocompatible, have low toxicity and are often biodegradable making them great constituents for the development of drug delivery systems.[23]

An example of these such delivery systems is the use of carbohydrate-based amphiphilic nano delivery systems for chemotherapy drugs. "Naked" oligonucleotide-based chemotherapy drugs can show poor therapeutic efficiency as they can be degraded by ribosomes in the bloodstream. Using these drug delivery systems will increase the half-life of the drug, therefore increasing cell uptake and making the drug more potent.[23]

Antiparasitic treatments

Several tropical parasitic diseases are treated and prevented with carbohydrate-based pharmaceutically active agents. A study done on mice shows the potential

for a carbohydrate-based vaccine to treat malaria. The malaria parasite causes cells to express a large amount of glycosyl-Phosphatidylinositol (GPI) on the cell's surface (Figure 7). There is evidence to suggest that the cascade triggered by GPI when the host cell is ruptured is what is responsible for morbidity and mortality caused by malaria.[24] The mice were vaccinated with chemically synthesised GPI and exposed to the malaria toxin. Between 65-70% of treated mice survived while 0-9% of the untreated mice survived. [24]
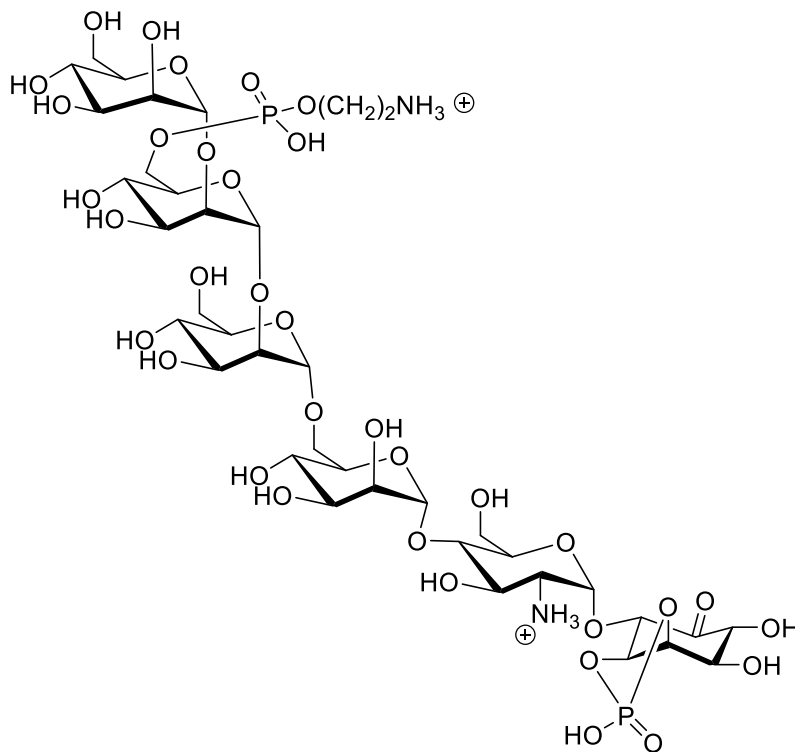

Figure 7. *GPI malarial toxin 1*

Carbohydrate-naphthalene diimide conjugates are now being considered as treatments for trypanosomatid parasites that are the cause of diseases such as African sleeping sickness and Human American Trypanosomiasis (HAT). [25]

Glycoprocessing Inhibitors

Carbohydrates can be used as glycoprocessing inhibitors. Iminopyranose' are monosaccharide sugars where the oxygen in the ring structure has been replaced with an imino group. Due to these sugars similar structure to α-glucosidase (which plays a role in carbohydrate hydrolysis in humans), they can inhibit its activity, possibly leading to anti-diabetic, antiviral, and anticancer effects.[26] 1-Deoxynojirimycin (DNJ) is an iminopyranose found naturally in mulberry tree leaves. DNJ is widely used in anti-diabetic, antioxidant, and anti-inflammatory medications (Figure 8).[26] Work has previously been done in the Murphy group on the use of flow chemistry to improve the synthesis of DNJ.[27]
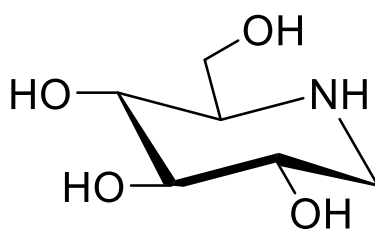

Figure 8. *1-deoxynojirimycin*

1.3 Depictions of Carbohydrates

There are multiple ways to depict carbohydrate structures. Fischer projections is one of the most popular for linear carbohydrates. Fischer projections show the carbohydrate in its open-chain form, from a 2D perspective.[28] These structures are drawn with the aldehyde group orientated to the top. Stereochemical information is easily provided through this illustration.

Vertically pointing groups bend back into the plane of the page, while horizontal groups point forward, away from the plane of the page allowing for one stereoisomer to be distinguished from another, i.e. displaying stereochemical information (Figure 9 and 10).[28]
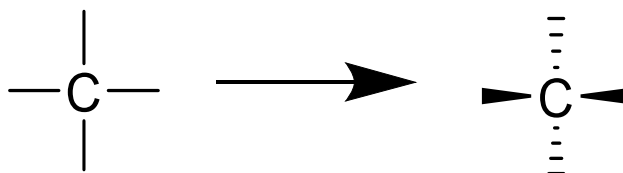

Figure 9. *Simplified Fischer Projection demonstrating how stereochemical information is conveyed.*
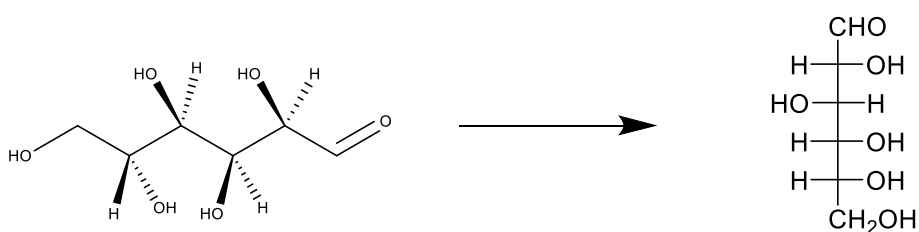

Figure 10. *Structural formula of D- Glucose converted into the Fischer projection.*

Fischer projections are very useful in distinguishing the stereochemical differences between sugar isomers such as L and D sugar forms. The L and D sugars are characterised by the hydroxyl configuration at the highest-numbered stereogenic carbon (Figure 11). If the hydroxyl group is on the right, it is a D sugar and if the hydroxyl group is on the left it is an L-sugar (Figure 11).
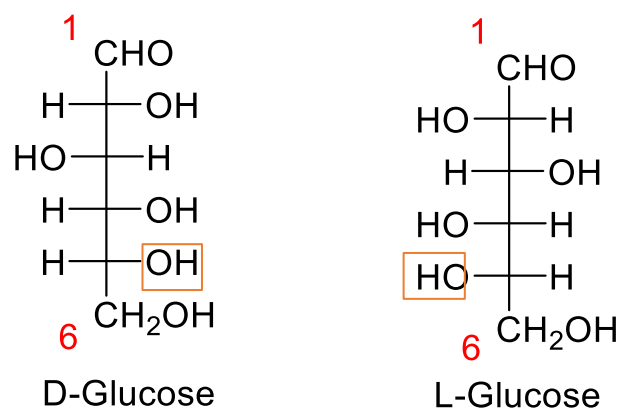
Figure 11. *Fischer Projection of D-Glucose (left) and L-Glucose (right)*

Monosaccharides that contain five or more carbon molecules have both an open chain and a cyclic form. The straight-form carbohydrate converts into the cyclic form in aqueous solutions.[29]

The straight chain carbohydrate form undergoes a cyclisation reaction through the nucleophilic attack on the aldehyde at C-1.[28] This forms a stereo-centre giving two diastereomers known as anomers (an alpha (α) and beta (β) form). Ratios of α to β products can differ depending on many variables including substituents, temperature, pH and type of sugar. (Figure 12).
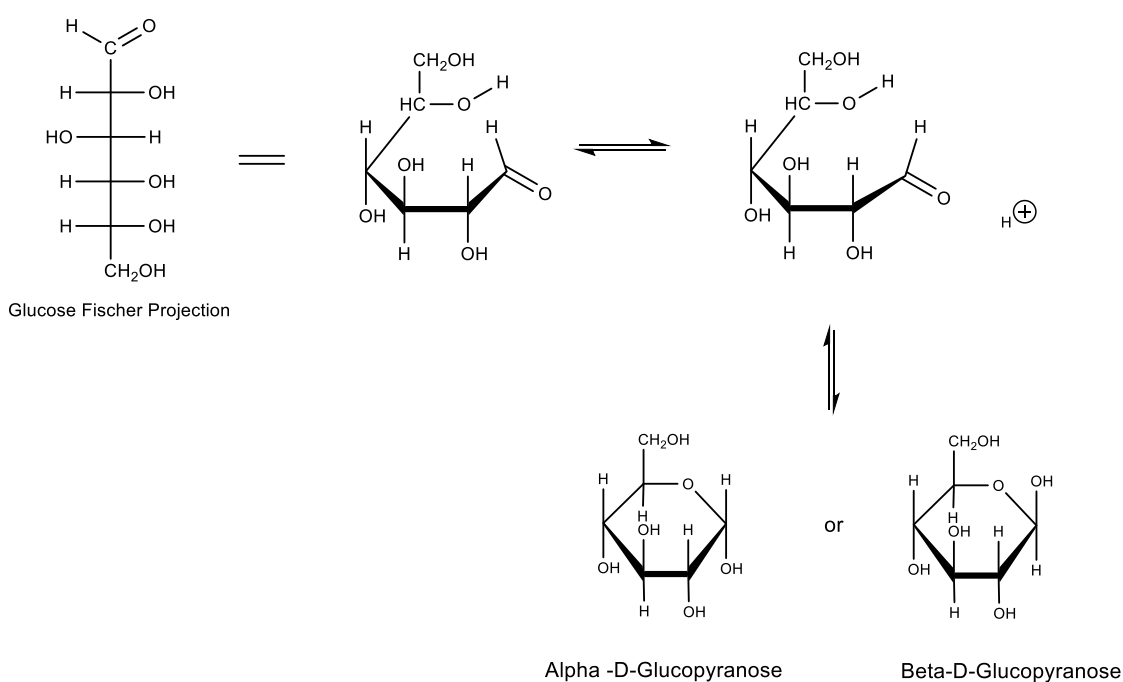
These ratios can be determined by nuclear magnetic resonance (NMR) spectroscopy due to signals appearing at differing chemical shifts of the anomeric proton. The signal for the α anomer will usually have a higher ppm value as it is more de-shielded than the β anomer due to the equatorial orientation of the proton in the α anomer vs the axial orientation in the β anomer. Ratios can also be identified by $[\alpha]_D$ measurements using a polarimeter along with a variety of other methodologies.[30]

The Haworth projection is used to depict sugars that have cyclised. This projection differs from the Fischer projection as it shows the sugar in its closed chain form in a 3D perspective.[31] In this form, the sugar is depicted as a ring and the substituents point either straight up or straight down, making the stereochemical differences between enantiomers identifiable (Figure 13).
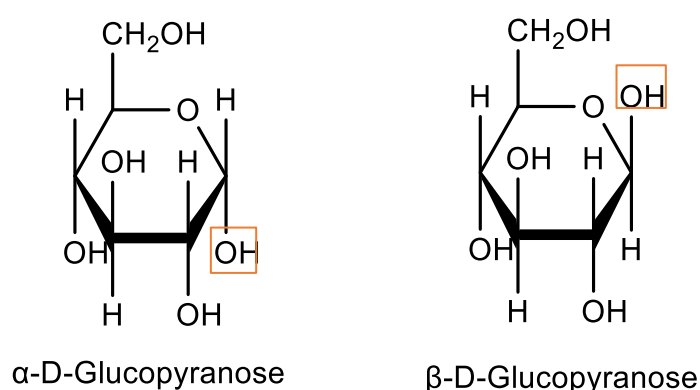

α-D-Glucopyranose   β-D-Glucopyranose

Figure 13. Haworth projections of glucopyranose anomers

1.3.1 Carbohydrate Conformations

Carbohydrates can exist in a variety of conformations, ranging from high energy to low energy. Six-membered rings exist mainly in a chair conformation, which is the lowest energy form of the structure as all substituents are staggered, leading to less steric strain.

Carbohydrate rings may adopt other conformations such as planar, half chair, boat, or twist boat conformation depending on the molecule's environment (for example temperature, pH and solvent type). Within these conformations, substituents may be partially eclipsed or eclipsed leading to higher energy conformations (Figure 14).

| Planar | Half-Chair | Boat | Twist Boat | Chair |
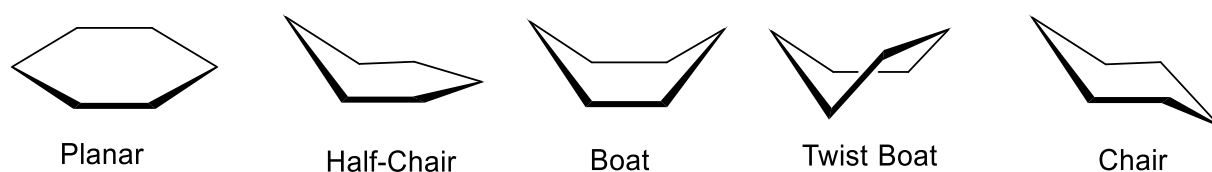
Figure 14. Depiction of different carbohydrate conformations

1.4 Uronic Acids

Uronic Acids are derived from monosaccharides where the hydroxyl group on the C-6 of the sugar unit has been oxidised to form the carboxylate (Figure 15). [32] Uronic acids play a significant role in many biological processes, including metabolism and the excretion of drugs.[32] Uronic acids are of interest to organic chemists as they are difficult to find in nature in the required volumes and purity, therefore if required they must be synthesised.[33]

Some uronic acids are used in the pharmaceutical industry. For example, Heparin is a uronic acid that is used for medicinal purposes. Heparin is an anti-

coagulant used to decrease blood clotting, preventing clot formation, and hindering clots that have already formed from increasing in size.[34]
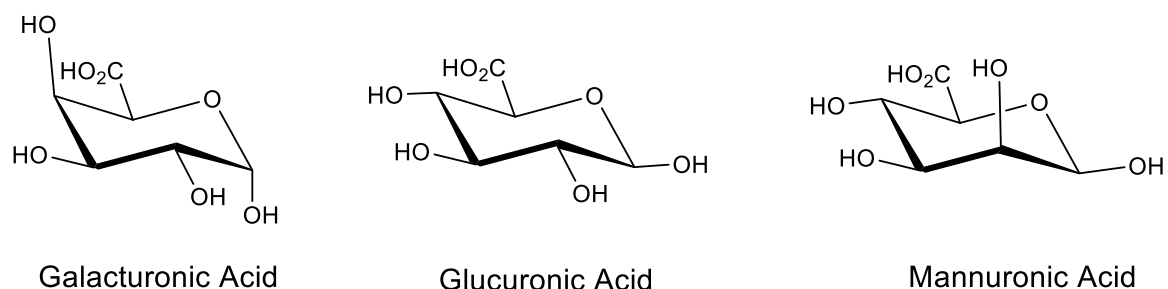

Figure 15. *Examples of Uronic Acid Sugars*

Previous studies within the Murphy group have proven that uronic acids anomerise faster than the corresponding glucopyranosides.[35] This is due to the formation of a five-membered chelate between the carbonyl oxygen and the pyranose oxygen brought together by a TiCl4 or SnCl$_4$ catalyst. [36] The faster the reaction the more feasible it is to use as an effective synthetic route to a target compound. This speed also makes the study of the anomerisation reaction easier as the reaction will reach equilibrium faster. Therefore, requiring lower NMR usage, making it cheaper and more convenient to run. In some cases cases the reaction may be too fast to study accurately.

Galacturonic acid is a commercially available uronic acid that is widely used within the food industry.[37] This makes galacturonic acid a good starting point for the study of glycosidic linkages, and anomerisation reactions and is used widely throughout this research.

1.5 Glycosidic links (synthesis and mechanism)

Glycosidic links are the bonds that hold sugar units together to create carbohydrate chains. A major aspect of carbohydrate synthesis is the formation of these bonds with the first glycosylation reaction occurring in the 1800s. [38]

A glycosyl donor containing a leaving group (LG) reacts with an alcohol group (the acceptor molecule), which can either be an aliphatic alcohol or a free hydroxyl group on another single sugar unit to form an acetal bond through a condensation reaction (Figure 16).
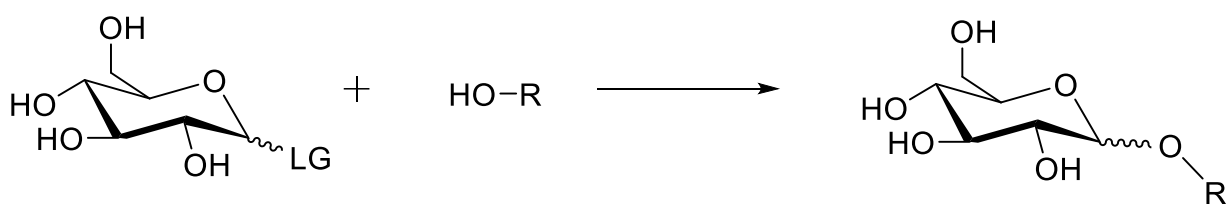

Figure 16. Glycosylation Reaction

Monosaccharide sugar units react to form glycosidic links from the hemiacetal C of one sugar unit to the hydroxyl functional group of another unit to give a disaccharide and subsequently oligo and polysaccharides as these units polymerise.

This reaction can be complicated and non-specific as there is the possibility of the formation of two anomers from this reaction (α and β).[38] The hydroxyl groups on the glycosyl donor are reactive, therefore protecting groups on these sites are required to prevent unwanted reactions and side products.

The synthesis of glycosidic bonds is affected by many variables, including leaving groups, solvents, additives and protecting groups but all follow the same general process: activation of the anomeric LG, dissociation, nucleophilic attack, and proton transfer (Figure 17). [38]
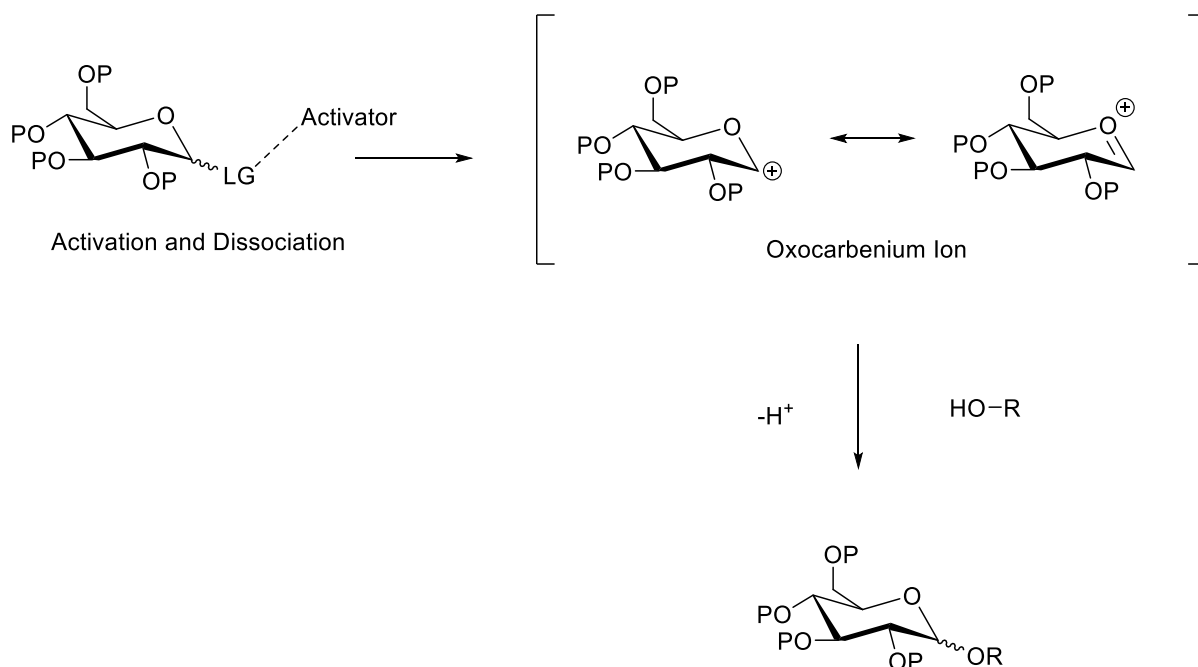
Figure 17. *Mechanism of glycosylation*

1.5.1 Koenigs–Knorr glycosylation reactions.

There are many methods of synthesising glycosidic links. A common method being the Koenigs-Knorr glycosylation reaction which is the one used throughout this research, the reaction scheme is depicted below (Figure 18). Koenigs-Knorr glycosylation reaction is the synthesis of a glycosidic link between a glycosyl halide and an alcohol. It is a substitution reaction done in the presence of silver carbonate (Ag_2CO_3) with the addition of a catalytic amount of iodine (I_2) to improve the reaction yield.[39] Originally this Ag_2CO_3 compound was used to scavenge the hydrogen halide byproduct of the reactant, but with time it was also shown to assist with leaving group departure. [38] [39] The halide group in the glycosyl will be in an axial orientation due to the anomeric effect, meaning this configuration is more thermodynamically favourable.[39]

Koenigs-Knorr glycosylation method of synthesis was found to be very selective as the mechanism of reaction requires that the nucleophile attacks from the

opposite side to the leaving group creating an inversion at the anomeric centre. [38]
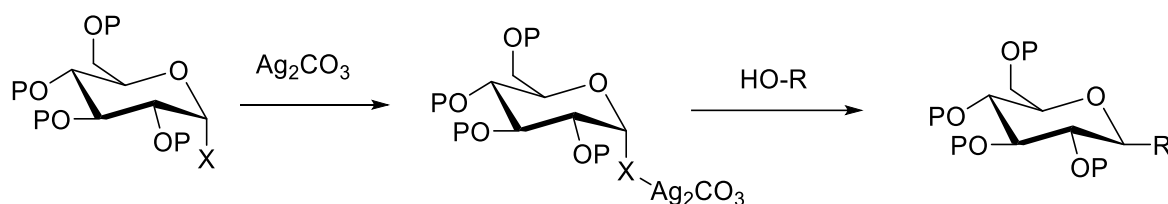

Figure 18. *Koenigs–Knorr glycosylation reaction where HO-R is a hydroxyl group attached to an alkyl group*[38]

1.5.2 Protecting Groups

One of the major challenges in synthetic organic chemistry is selectivity. In a molecule with multiple functional groups, it can be difficult to selectively react at a particular group. Therefore, it may be necessary to use protecting groups (PG). PGs are added to create derivatives of the existing functional groups that render these functional groups unreactive. i.e., blocking reactivity.

In carbohydrates free reactive hydroxyl functional groups are present. During carbohydrate synthesis, it is important to protect these groups so the target molecule can be synthesised. Acetates and benzoate PG are common in carbohydrate chemistry and can be removed commonly with a base.[40] Using PG in organic synthesis adds at least two extra steps to the synthetic route through the addition and removal of these groups (protection and deprotection). This will inevitably reduce the yield and efficiency of the synthesis.[41]

PG can influence glycosylation rates due to the neighbouring group participation i.e., a participating group on the C-2 as shown in the image below (Figure 19). [42]

Previous work by the Murphy group has looked at neighbouring group participation in both the glycosylation and anomerisation rates and how they can influence stereoselectivity. [35]

Acetoxonium ion

1,2 Trans
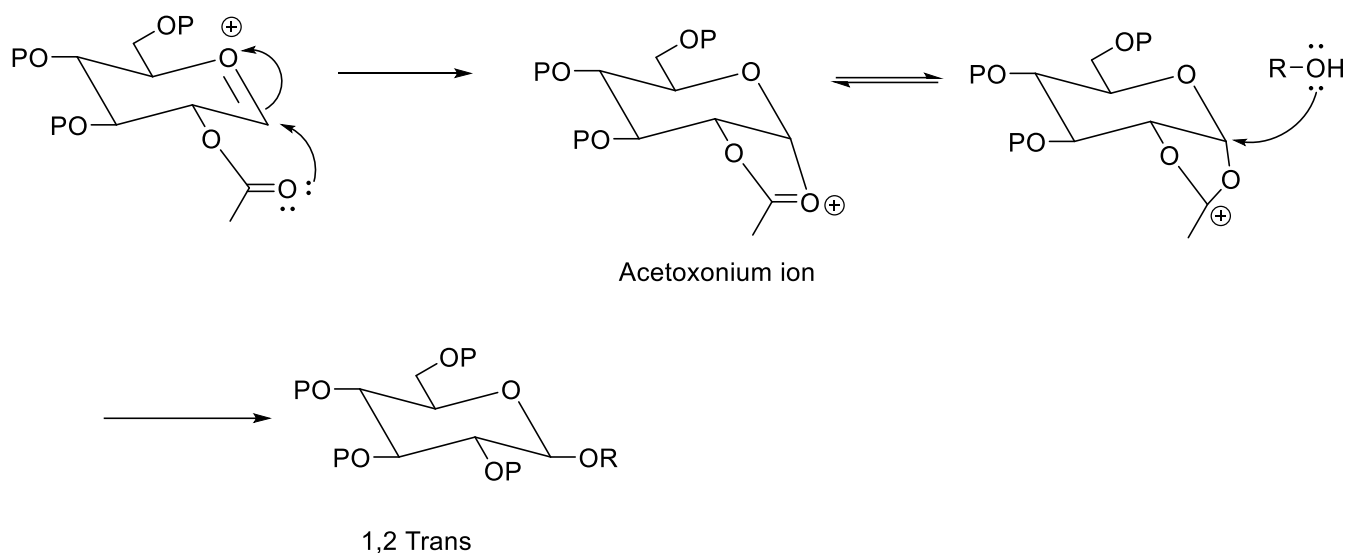
Figure 19. *Neighbouring Group Participation*

1.6 Anomerisation

Anomers are cyclic carbohydrates that differ from one another by the configuration at the hemiacetal carbon also known as the anomeric carbon i.e. they are diastereomers.[43] Anomers are positioned, as α or β compounds, depending on the orientation of the anomeric substituent on the anomeric carbon.[43] If the anomeric substituent is in the axial position then the sugar is known to be in the α configuration, and if the anomeric substituent is equatorial then it is said to be in the β configuration (Figure 20 and 21).[43]

Figure 20. Glucose-α form   *Figure 21. Glucose-β form*

Anomers are important as they differ in their physical and chemical properties such as stability, solubility, and bioavailability. For example, α and β glucose differ in a few w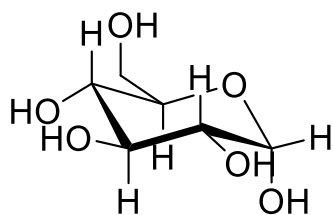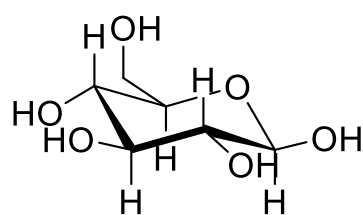ays. The β-glucose anomer is more stable than its alpha counterpart due to reduced steric hindrance, α glucose has a melting point of 146°C while β glucose has a melting point of 150°C, and α glucose has a specific rotation of 112.2° while β glucose has a specific rotation of 18.7° [44] In pharmaceuticals, the difference in anomer properties is vital as different anomers will interact with enzymes and receptors differently which will influence the drug's efficacy and safety. [45]

Anomerisation is the interconversion of one anomer to the other usually to give the more thermodynamically favoured product which in glucose is the α anomer. The anomerisation reaction is extremely important in pharmaceutical chemistry as it allows for the stereoselective synthesis of glycosides which is essential in drug development.[46]

1.6.1 Mechanism

The work outlined in this thesis investigates the movement from the β anomer to the α anomer.[30] The currently proposed and accepted mechanism for anomerisation involves endocyclic cleavage (Figure 22), [30] but it is possible that

anomerisation through exocyclic cleavage could occur in some cases (Figure 23).[30]

X= O, S
M= Sn, Ti
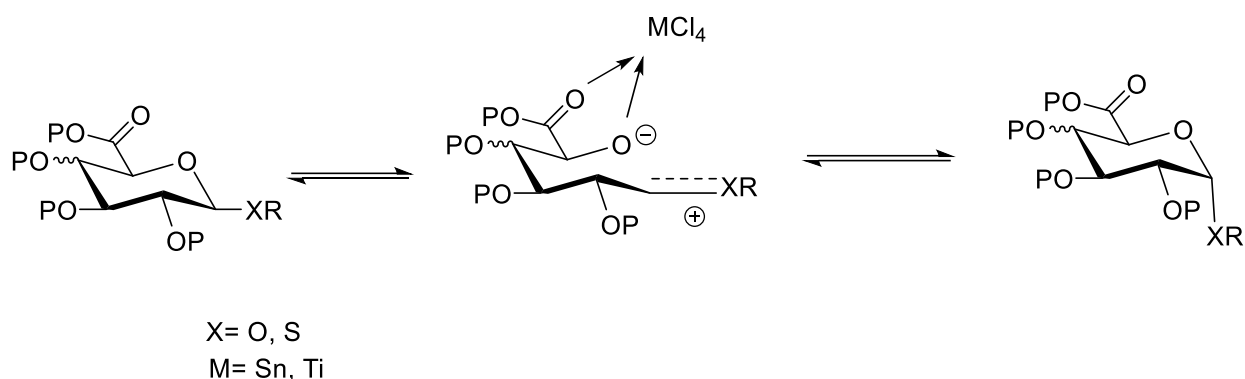
Figure 22. Anomerisation by endocyclic cleavage

X= O, S
M= Sn, Ti
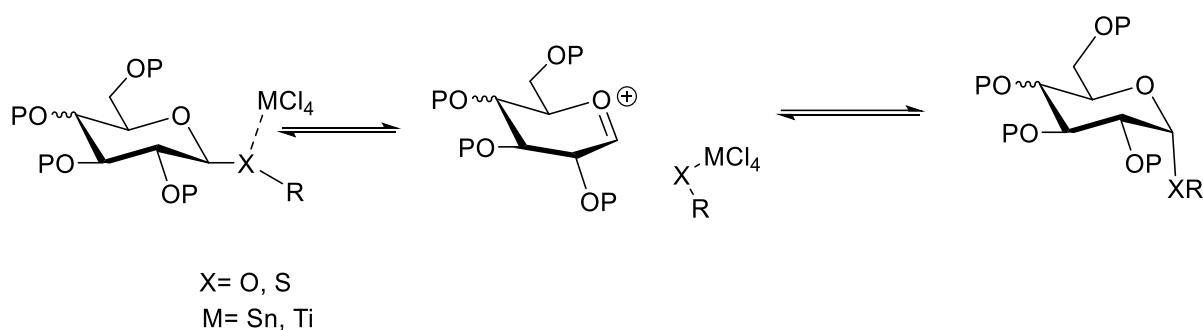
Figure 23. Anomerisation by exocyclic cleavage

1.6.2 Lewis Acid Catalyst

A Lewis acid is a compound that is an electron pair acceptor. Lewis acids accept pairs of non-bonding electrons from an electron donor. By extension, a Lewis acid catalyst is a Lewis acid which acts as an electron pair acceptor that then activates the substrate and increases the reactivity but is not used up within the reaction itself.[47]

This anomerisation reaction is induced by Lewis acids, most commonly tin tetrachloride ($SnCl_4$) and titanium tetrachloride ($TiCl_4$). These compounds catalyse the reaction (endocyclic cleavage mechanism) by coordinating the non-bonding electrons on the O attached to the anomeric carbon. This activates the molecule by withdrawing electron density allowing for the breaking of the C-O bond. A bond rotation then occurs which moves the group of interest from the equatorial to the axial position (I.e., from the α to the β anomer). $SnCl_4$ is the catalyst used throughout this research. $SnCl_4$ reacts quickly with water to create tin oxides which precipitate out of the reaction solution. This precipitate can cloud NMR tubes and reaction vessels making it impossible to take accurate readings. Therefore, it is very important to adequately dry all glassware and reagents to prevent this precipitation.

1.6.3 The Anomeric Effect

The anomeric effect also known as the Edward–Lemieux effect was originally defined as "the thermodynamic preference for polar groups bonded to C-1 to take up an axial position."[48] This is now considered to be a special case of the generalised anomeric effect for gauche conformations along the C-Y bond in a system X-C-Y-C, where X and Y are heteroatoms commonly nitrogen, oxygen, sulphur, or fluorine.[48] Essentially the anomeric effect describes the preference certain anomers have to adopt particular conformations due to electronic and steric effects.

Cyclohexane adopts a chair conformation which prevents torsional strain. When substituents are added to the cyclohexane ring, they have a strong preference for the equatorial position for steric reasons (Figure 24).
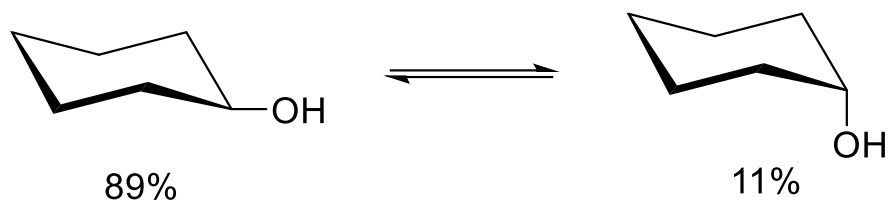
Figure 24. β to α cyclohexanol equilibrium percentages

In carbohydrate compounds, the β anomer is generally more stable than the α due to decreased steric hindrance meaning β forms can often predominate in many carbohydrate interconversions.

Mutarotation is the process of interconversion of α and β cyclic sugars which changes the optical rotation accompanying epimerisation. For example, if a sample of D-glucose is dissolved to form an aqueous solution, both α and β forms of glucose will exist in the solution and equilibrium will form when there is 63% β and 37% α D glucose in the solution (Figure 25). [49] These equilibrium percentages would eventually occur no matter the ratios of α and β initially present in the solution. Trace amounts of the open-chain form would also be present in the solution.

Figure 25. β to α D-glucose equilibrium percentages

This relatively high percentage of α anomer is initially surprising, as assumed steric effects should favour the β conformation more heavily. Many theories

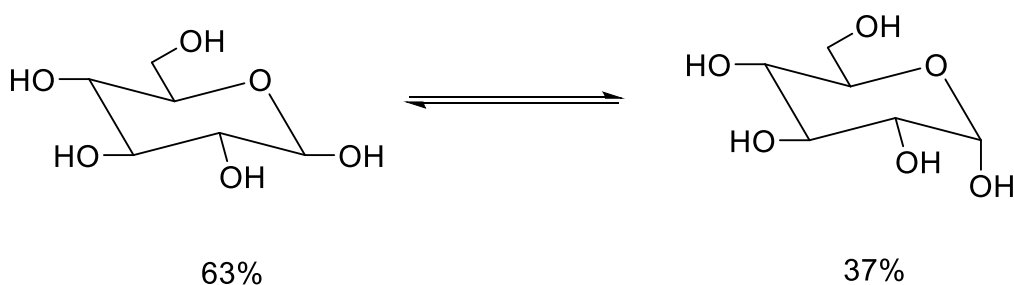were put forward to explain this, with the most likely explanation being interactions between the orbitals on the oxygen in the sugar ring and the substituent on the anomeric carbon (Figure 26). When the substituent is aligned with these dipoles in the equatorial position, it can have a destabilising electrostatic interaction, leading to an increased percentage of molecules in the α form.
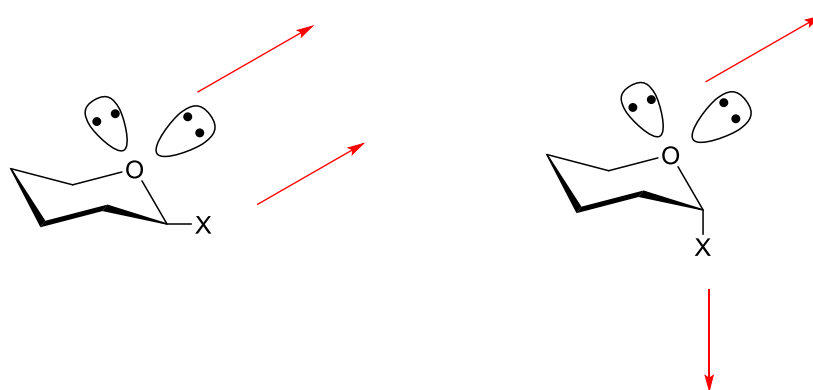
Figure 26. Dipole alignments of equatorial (left) and axial (right) substituents

1.6.4 Optical Rotation

Optical activity is a substance's ability to rotate plane polarised light. This is an intrinsic property of chiral compounds. Optical activity is measured using a polarimeter where plane polarised light is passed through a sample and the degree of rotation is measured (Figure 27). Specific rotation can give insightful information as to the enantiomeric excess of a solution or the enantiomeric purity.

The optical rotation is calculated using the following formula:

$$[\alpha] = \frac{a}{c \cdot l}$$

Equation 1. optical rotation

Where [α] is the specific rotation in degrees, α is the observed rotation in degrees, c is the concentration of the sample on g/ml and l is the path length of the light in dm.
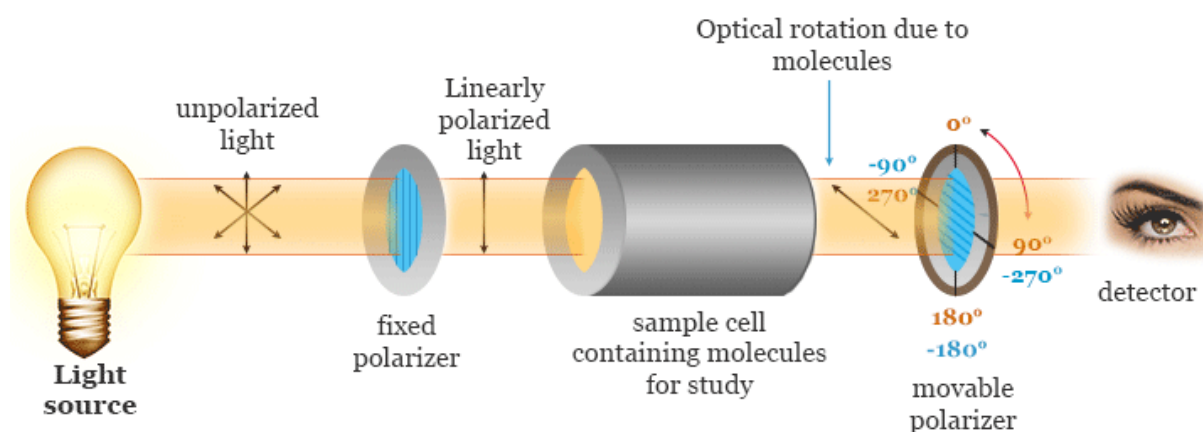
Figure 27. Diagram of a polarimeter [50]

1.7 Kinetics

Rates of the anomerisation reaction have been examined previously and are found to vary depending on the substituents on the sugar ring. Mainly due to the differing effects of electron withdrawing and donating groups, and neighbouring group participation. The anomerisation reaction is reversible and follows first-order equilibrium kinetics ($\alpha \rightleftharpoons \beta$). A first-order reaction is a reaction where the rate of the reaction depends on the concentration of just one reactant to the power of unity.[51][OBJ]

The reaction rate constants can be obtained: (k_r + k_f), where k_r is the rate of the reverse reaction (α-β) and k_f is the rate of the forward reaction (β-α).[30] This can be performed using the following formula for first-order reversible kinetics:

$$\ln\left(\frac{[\beta]_o - [\beta]_e}{[\beta]_t - [\beta]_e}\right) = -(k_f + k_r)$$

Equation 2. First order reversible kinetics

Where $[\beta]_o$ is the initial concentration of the β anomer substrate, $[\beta]_e$ is the concentration of the β anomer when the reaction has reached equilibrium and $[\beta]_t$ is the concentration of the β anomer at time t.

By plotting the minus log of the experimentally observed rate constants (k_f + k_r) vs time (s), a straight-line plot is obtained where the slope of the line is the overall rate constant -k.

The reaction rate constant (k) can be determined by looking at the starting material's disappearance rate or through the product's appearance rate. Rates of formation or rates of loss can be measured by looking at the NMR spectra of the reaction mixture as concentration can be determined by integration of signals corresponding to the anomers present.

This reversible reaction differs from classic first-order kinetics where the reaction is not reversible. First-order reaction kinetics can be examined using the following formula:

$$\ln(\frac{[A]_t}{[A]_o}) = -kt$$

Equation 3. First order reaction kinetics

Where $[A]_t$ is the concentration of the β anomer at time t and $[A]_0$ is the initial concentration of the β anomer.

By plotting ln[β] vs time (s), a straight-line plot with the slope -k is created, determining the overall rate constant.

In many cases, the rate of the reverse anomerisation reaction may be negligible, meaning that the first-order reversible rate equation and the first-order rate equation can give the same or very similar slope, showing the anomerisation reaction to be almost a first-order reaction.

The rate of this reaction can be influenced by many factors including carbohydrate compound type, temperature, and catalyst concentration which are the focus of this research.

1.7.1 Activation energy

The activation energy of a reaction is the amount of energy needed within the system for a reaction to occur. Reactants must overcome an energy barrier to be converted into products. Knowledge of the activation energy of a reaction gives us a deeper understanding of the reaction (Figure 28).

Activation energy will be altered when using a catalyst. As previously stated, to perform an anomerisation reaction, Lewis acid catalysts are used. This lowers the activation energy of the reaction making the reaction possible under mild conditions. Anomerisation is not spontaneous and therefore the use of a catalyst is needed to lower the activation energy/alter the reaction pathway so the reaction can occur.
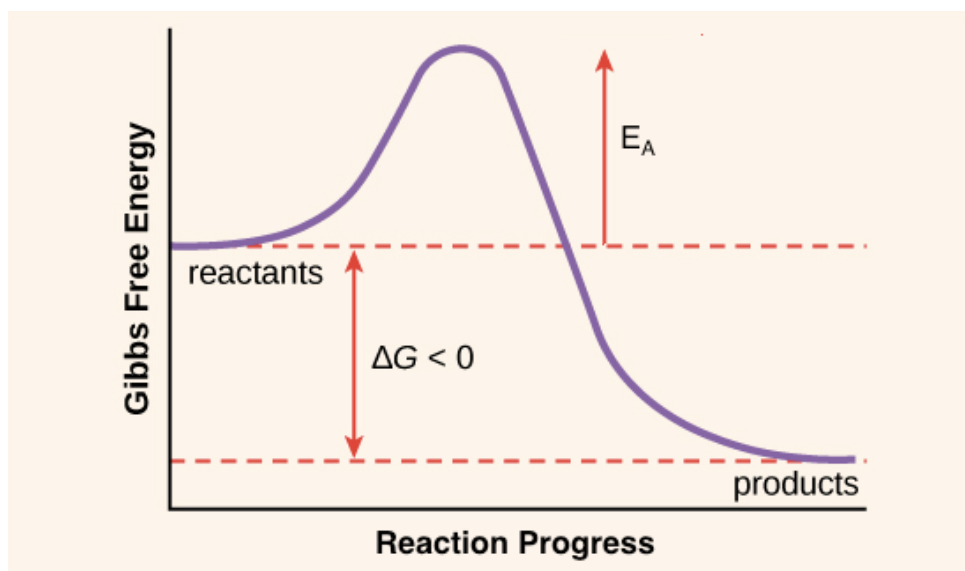
Figure 28. Graphical image of Activation Energy taken from ref [47] [51]

Activation energy can be calculated using the Arrhenius equation.[52]

$$k = Ae^{\frac{-Ea}{RT}}$$

Equation 4. Arrhenius equation

where k = rate constant, A= pre-exponential factor, Ea= Activation energy, R= universal gas constant and T = temperature in Kelvin.

The Arrhenius equation can be rearranged to give the following equation in a linear form:

$$\ln k = \frac{-E_a}{RT} + \frac{1}{T}$$

Equation 5. Arrhenius equation in linear form

Using this equation and experimentally measuring the rate constant at multiple temperatures the activation energy of the reaction can be calculated by graphing the measured rate constants against 1/T.

1.8 Aim of Thesis

The first part of this thesis aimed to synthesise and fully characterise a D-galacturonic acid derivative with a benzoate group on the anomeric carbon using the Koenigs–Knorr glycosylation reaction.

The second part of this thesis investigated the anomerisation reaction. It is already established that carbohydrates play a key role in pharmaceuticals, but there is still a lack of understanding of factors influencing the anomerisation reaction This thesis aims to investigate this Lewis acid catalysed anomerisation reaction mechanism further, taking a deeper look into the kinetics and activation energies.

The objectives of this thesis are as follows:

1. To synthesise and fully characterise the uronic acid derivative 2,3,4-tri-O-acetyl-β-D-galactopyranosiduronic acid, methyl ester using the Koenigs-Korr glycosylation reaction.

2. To further investigate the lewis acid catalysed anomerisation reaction mechanism and determine the kinetics of a variety of anomerisation reactions using different uronic acid derivatives.

3. To determine the activation energies of the anomerisation reaction of three different uronic acid derivatives with differing EWG and EDG groups on the C2 carbon.

2. Results and Discussion

2.1 Synthesis of 2,3,4-tri-O-acetyl-β-D-galactopyranosiduronic acid, methyl ester.

Commercially available galacturonic acid was used to synthesise a new derivative of the compound with a benzoate group on the anomeric carbon, using the addition of protecting groups and the well-established Koenigs-Knorr glycosylation reaction.

The synthesis of the derivative can be broken up into four steps:

1. Protection of the hydroxide functional groups with acetate protecting groups.
2. Protection of the carboxylic acid functional group by conversion to an ester protecting group.
3. Bromination of the anomeric carbon.
4. Koenigs-Knorr glycosylation reaction[39]
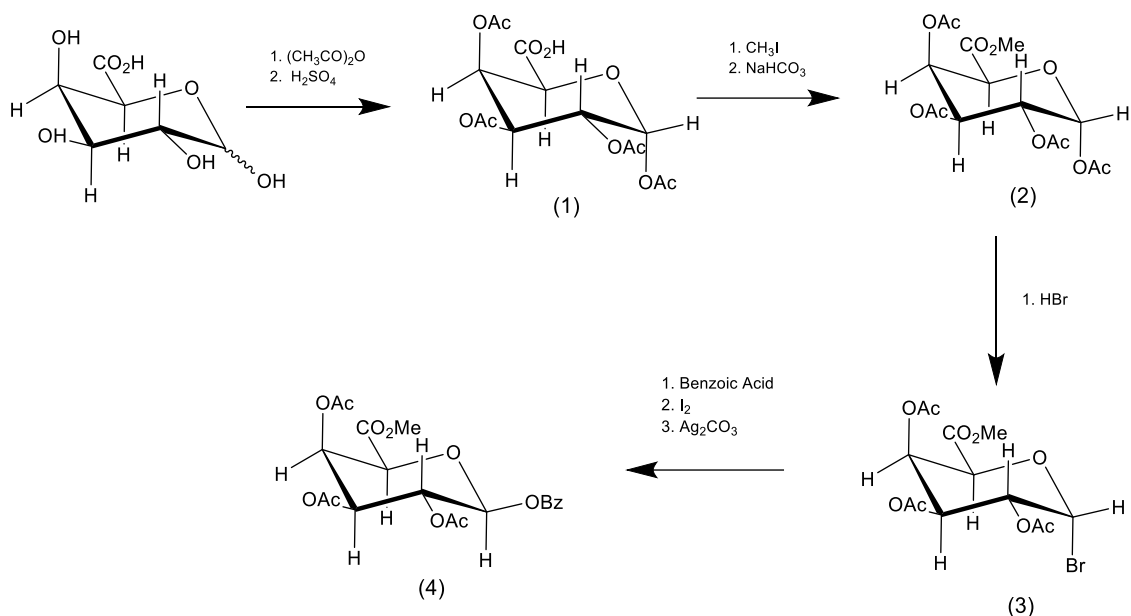
Scheme 1. *Synthetic route to title compound*

Step 1- Addition of Acetate Protection groups
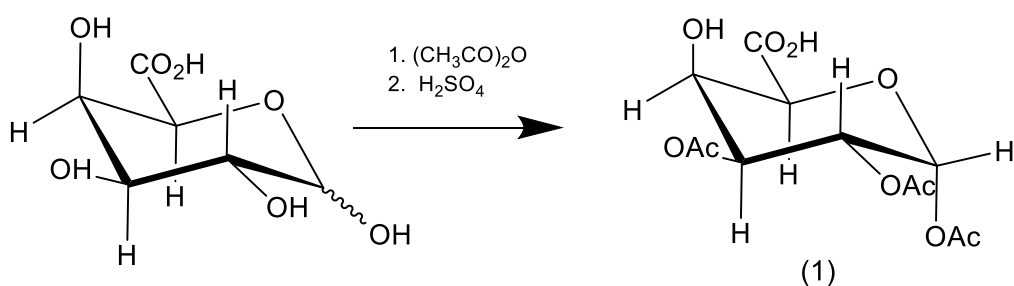
Figure 29. *Synthesis step 1, addition of acetate PG*

The addition of protecting groups is essential in this synthesis to prevent unwanted reactions at the hydroxyl functional groups on C-2, C-3, and C-4. Reactivity of the hydroxyl group at the anomeric carbon differs to the other hydroxyl groups in the compound due to the interactions of the orbitals of the oxygen within the sugar ring.[53] Acetic anhydride (79 equiv.) and sulphuric acid

(1 equiv.) were combined and cooled on ice in a round bottom flask. Acetic anhydride acts as the reaction solvent as well as the source of acetate protecting groups. The sulphuric acid acts as an acid catalyst. This reaction is exothermic and therefore was done on ice to mitigate the risk of overheating involved. This solution was then removed from the ice and left to stir for 20 minutes to allow it to return to room temperature. Galacturonic acid (6 molar equiv) which is commercially available, was added to this solution and stirred for two hours.

The reaction was monitored by thin-layer chromatography (TLC) on a silica gel with 1:1 cyclohexane and ethyl acetate (EtOAc) mixture as eluant. The reaction was left to proceed until no reactant remained and **(1)** was produced. TLCs taken during the reaction showed streaking which was likely due to the polarity of intermediates with unprotected hydroxyl groups. This streaking did not occur when the reaction had gone to completion.

The reaction solution was neutralised with saturated aqueous sodium bicarbonate ($NaHCO_3$) and then partitioned with H_2O and EtOAc. The organic layer was washed with H_2O and brine and then dried with sodium sulfate (Na_2SO_4). The solution was filtered, and the solvent was removed under reduced pressure. The residue was azeotroped twice with toluene to remove the acetic acid byproduct of the reaction and any remaining acetic anhydride. The residue was dried under a high vacuum pump to produce a white solid.

This step gave an average yield of 82% over five attempts using a 1, 2, 4 and 5 g scale.
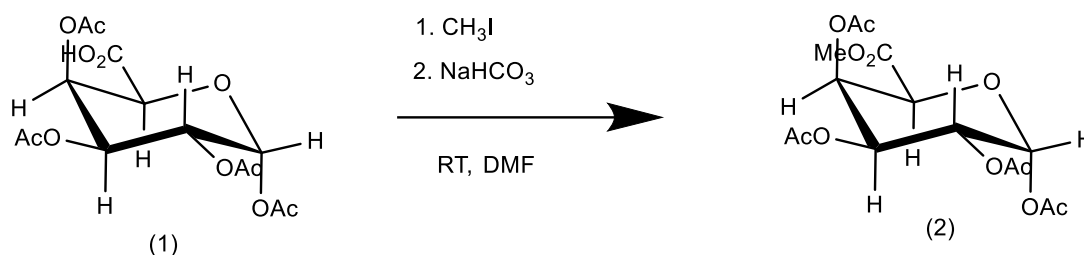
Figure 30. *Synthesis step 2, introduction of ester PG*

The next step of the synthesis was to add an ester protecting group (PG) to the carboxylic acid functional group of the uronic acid. This PG is again used to prevent unwanted reactions at this site in the molecule.

Compound **(1)** was dissolved in DMF. Sodium bicarbonate (NaHCO$_3$, two equiv.) was added to the solution along with iodomethane (CH$_3$I, 2.5 equiv). NaHCO$_3$ acts as a base that activates the carboxylic acid group to nucleophilic attack, with CH$_3$I being the source of CH$_3$ to produce the ester group. The solution was left to stir for 4 hours until there was full consumption of the starting material and compound **(2)** was produced. The reaction was monitored using TLC (silica gel plate, 1:1 cyclohexane-EtOAc).

The reaction solution was then diluted with water and extracted into EtOAc. The organic layer was washed with H$_2$O and Brine and then dried with NaSO$_4$. The solution was filtered, and the solvent was removed under low pressure. The compound was purified by silica gel column chromatography using a gradient elution of 25 % EtOAc in cyclohexane.

This step gave an average yield of 46% over 5 attempts on a 1, 1.5, 2 and 4 g scale
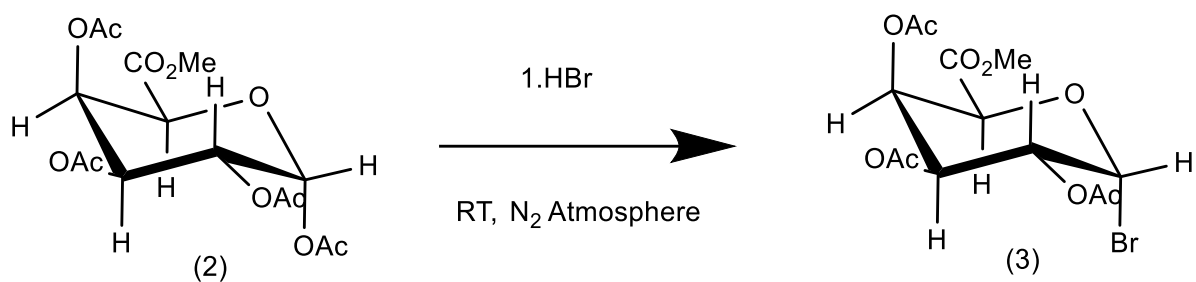
Step 3- Bromination of the Anomeric Carbon

Figure 31. *Synthesis step 3, bromination of anomeric carbon*

The next step of the reaction was the bromination of the anomeric carbon to selectively form the α glycosyl bromide. This is done as Br is a very good halogen leaving group and this reaction gives the required glycosyl donor for the Koenigs-Knorr synthesis. i.e. a glycosyl halide.

Compound **(2)** was dissolved in dry CH_2Cl_2. HBr (nine equivalents) was added (30% in AcOH). The reaction mixture was stirred for two hours until the starting material had been consumed and compound **(3)** a glycosyl bromide compound was produced. The reaction was monitored using TLC (silica gel plate, 1:1 cyclohexane-EtOAc).

The reaction mixture was then poured onto ice-water in a separation funnel and shaken to remove any unreacted HBr. The mixture was separated, and the aqueous layer was washed multiple times with EtOAc. Organic layers were combined and neutralised with saturated sodium bicarbonate. Again, the aqueous and organic layers were separated, and the organic layer was dried with Na_2SO_4. The solution was filtered, and the solvent was removed under high pressure.

This step gave an average yield of 63% over 3 attempts on a 0.5, 1.7, and 2 g scale.
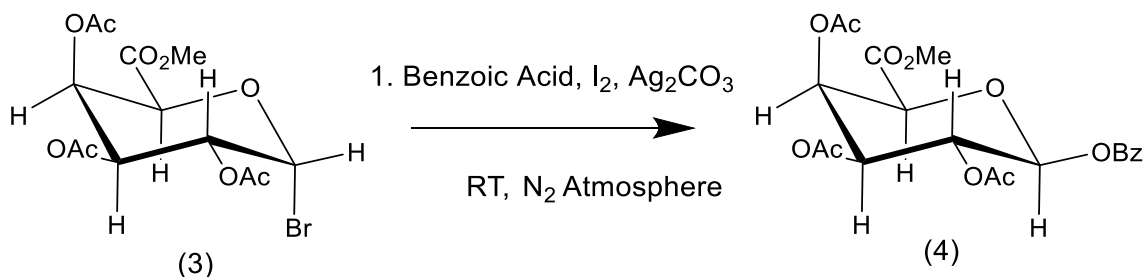
Step 4 – Koenigs-Knorr glycosylation reaction

Figure 32. *Synthesis step 4, Koenigs Knorr glycosylation reaction*

This Koenigs-Knorr reaction gives rise to the formation of a glycosidic link between the glycosyl bromide and benzoic acid acceptor. The attack of the glycosyl bromide by the benzoic acid when neighbouring group participation occurs the reaction seems to undergo a complex form of an S_N2 mechanism, meaning there is an inversion of stereochemistry. While we begin with an α glycosyl bromide, we selectively obtain a β product. Throughout this reaction, all glassware was flame dried and performed under an inert nitrogen atmosphere. **(3)** was dissolved in dry CH_2Cl_2 and left to stir in a round bottom flask with 4 Å molecular sieves to remove all the water.

In another round bottom flask, dry CH_2Cl_2 was added to silver carbonate (Ag_2CO_3, ten equiv.), benzoic acid (5.5 equiv.), and a catalytic amount of I_2. Ag_2CO_3 acts as a scavenger of any halide side product produced and aids in the removal of the leaving group (Br). Benzoic Acid is the Bz source, and I_2 is used to increase the yield of the reaction as it activates the glycosyl bromide.[54] The reaction flask was covered with aluminium foil as the Ag_2CO_3 in the reaction is sensitive to light. This mixture was stirred for 15 minutes. The solution of glycosyl bromide was

36

added dropwise into the second round-bottom flask and the reaction solution was stirred for 16 hours to produce the title compound **(4)**.

The reaction mixture was diluted with EtOAc and filtered through Celite clay to remove the Ag$_2$CO$_3$. The solution was washed with sodium bicarbonate. The filtrate was concentrated and then purified with silica gel column chromatography using a gradient elution from 15 to 22 % EtOAc in cyclohexane.

This step gave an average yield of 48% over two attempts on a a 1.8 and 1.5 g scale.

This overall reaction mechanism gave a yield of 11.4% over four steps from galacturonic acid.

Presence of compound (4) was confirmed using ESI-HRMS (Appendix 1)

2.2 Characterisation

The characterisation of this compound was completed using 1D and 2D NMR spectroscopy techniques including ^{1}H NMR, ^{13}C NMR, COSY, and HSQC along with LC-MS. The following is the characterisation of benzoyl 2,3,4-tri-O-acetyl-β-D-galactopyranosiduronic acid, methyl ester **(4)**.
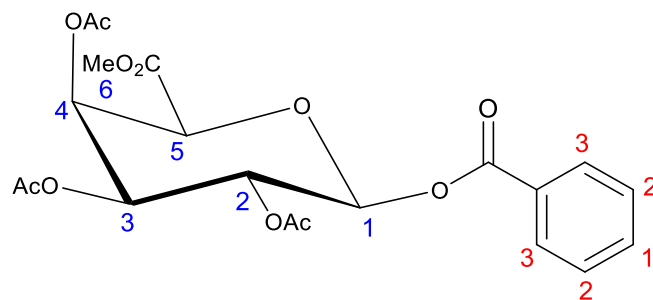
Figure 33. *Molecular structure of title compound* **(4)** *with hydrogen environments labelled for NMR assignments.*

^{1}H-NMR signals were interpreted using 2D-COSY NMR. ^{1}H-NMR and COSY signals are summarised in Table 1.
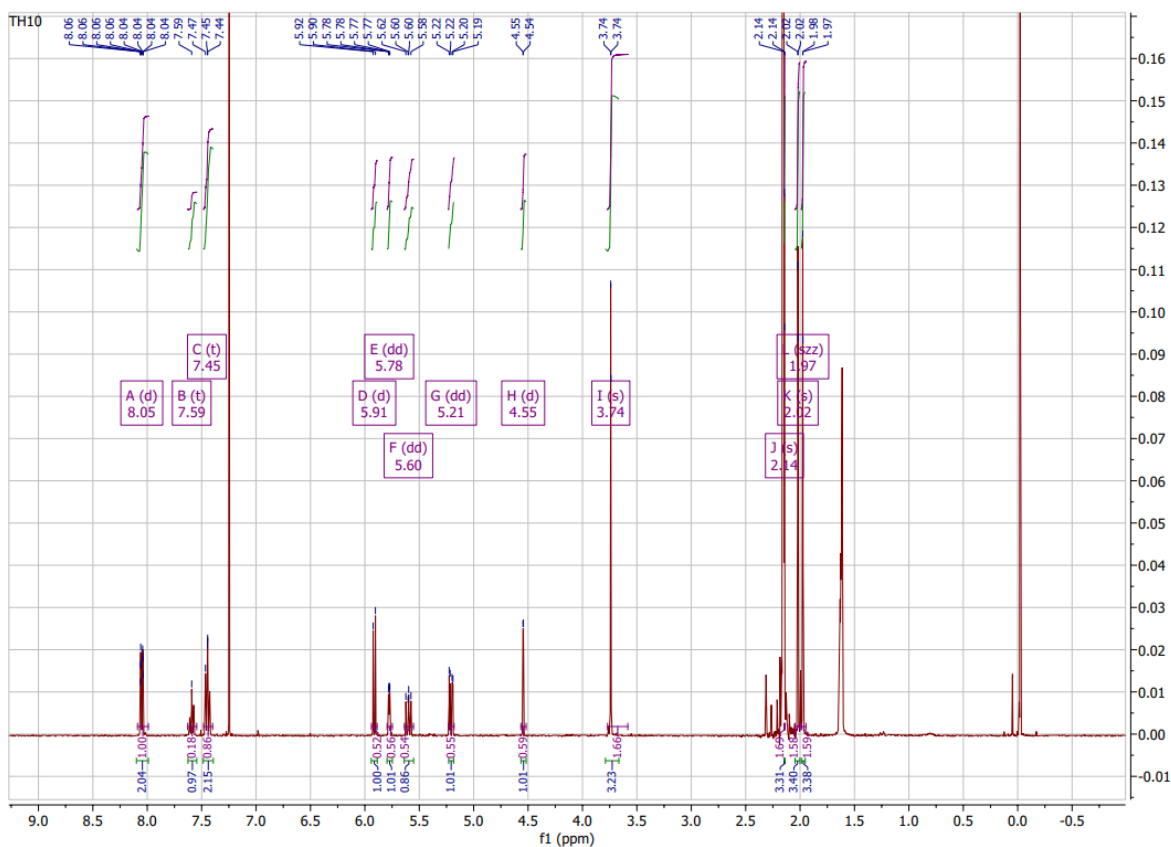
Figure 34. *^{1}H-NMR spectrum of* **(4)**. *Note that alphabetic labels are assigned in Table 1. The singlet at δ 7.26 ppm represents the solvent residual peak of CHCl$_3$ in CDCl$_3$, the quartet at δ 4.12 ppm and the triplet at 1.26 represents the solvent residual peaks of EtOAc and the singlet at δ 1.56 ppm is a water peak.*

38
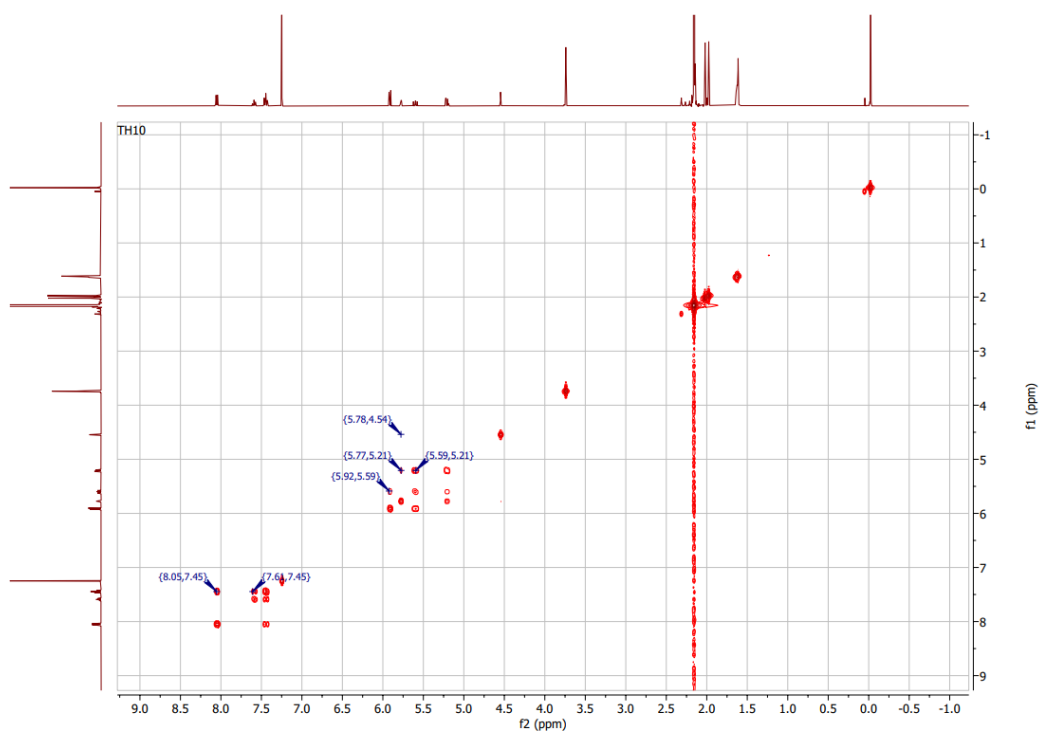
Figure 35. 2D-COSY NMR spectrum of the title compound. Note that labelled signals are assigned in Table 1

Table 1. *Representation of the information of each proton obtained from 1D ^{1}H-NMR spectrum (Figure 35) and 2D COSY NMR spectra (figure 36)*

Atom	Signal Label	δ PPM	Multiplicity	COSY coupling signal(s)
H_1	D	5.91	d	(5.92, 5.59) H_2
H_2	F	5.60	dd	(5.92, 5.49) H_1 (5.59, 5.21) H_3
H_3	G	5.21	dd	(5.59, 5.31) H_2 (5.77, 5.32) H_4
H_4	E	5.78	dd	(5.77, 5.21) H_3 (5.78, 4.54) H_5
H_5	H	4.55	d	(5.78, 4.54) H_4
H_6	I	3.74	s	-
Ac-CH$_3$	J	2.14	s	-
Ac-CH$_3$	K	2.02	s	-
Ac-CH$_3$	L	1.97	3	-
Ar-H$_1$	B	7.59	t	(7.61, 7.45) H_2
Ar-H$_2$	C	7.45	t	(7.61, 7.45) H_1 (8.05, 7.45) H_3
Ar-H$_3$	A	8.05	d	(8.05, 7.45) H_2

1H NMR data shows that it is the β anomer that has been synthesised. The *J* value for the anomeric carbon is 8.3 Hz. This is indicative of a β compound as the dihedral angle is approximately 180 degrees, whereas an alpha compound

would have a dihedral angle of approximately 60 degrees which would alter the J value to roughly 2.7 Hz.

^{13}C-NMR signals were interpreted using 2D-HSQC NMR and literature values. ^{13}C-NMR signals are assigned and summarised in Table 2.
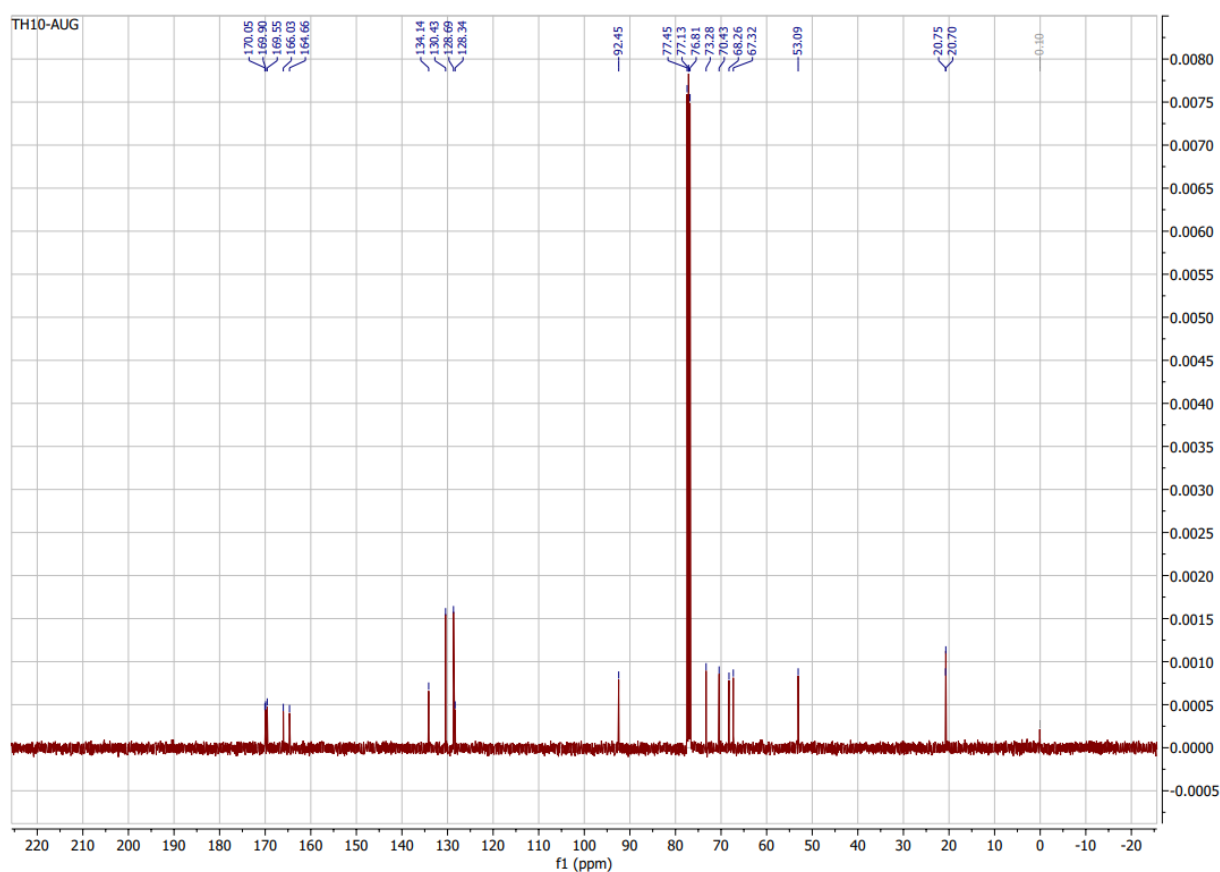
Figure 36. *^{13}C-NMR spectrum of the title compound. Note that peaks are labels are assigned in table 2.*
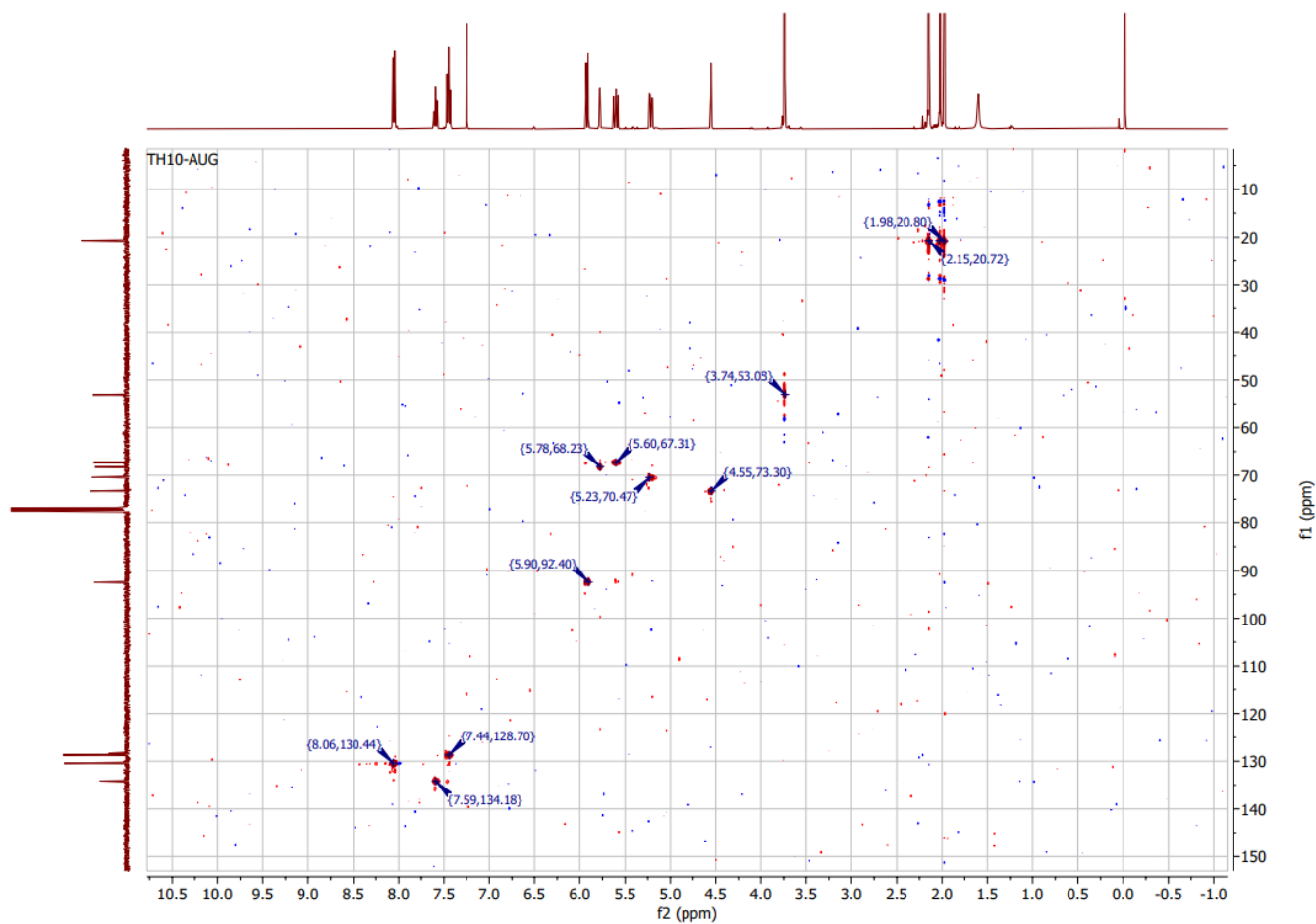
Figure 36. HSQC of the title compound that shows one bond correlation between C and H within the compound all assignments are shown in table 2.

Table 2. *Representation of the information of each carbon obtained from 1D ^{13}C-NMR spectrum (Figure 37) and 2D HSQC NMR spectra (Figure 38)*

Atom	^1H δ ppm	HSQC signal	^{13}C Signal
C_1	5.93	(5.90, 92.40)	92.45
C_2	5.61	(5.60, 67.31)	67.32
C_3	5.23	(5.32, 70.57)	70.53
C_4	5.79	(5.78, 68.32)	68.26
C_5	4.55	(4.55, 73.30)	73.28
C_7	3.76	(3.74, 53.03)	53.09
Acetate OAc -CHs	2.14 2.02 1.97	(2.15, 20.72) (2.03, 20.72) (1.98, 20.80)	20.70 20.75
C=O	-	-	170.05 169.90 169.55 166.03 164.66
Ar-C_1	7.60	(7.59, 134.18)	134.14
Ar-C_2	7.46	(7.44, 128.70)	128.69
Ar-C_3	8.07	(8.06. 130.44)	130.43

2.3 Calibration and Anomerisation Experiments

The second part of this thesis investigated the anomerisation reaction. This study looked at the rate of anomerisation and how it was affected by standard temperature and catalyst concentration using three (**5**), **(6),** and **(7**) compounds synthesised by Dr. Fiach Meaney during his PhD study. The following reactions were carried out using the original compounds synthesised by Dr. Meaney and were not synthesised throughout the course of this research. NMR data for each compound can be found in Appendix 9.

Anomerisation reactions were monitored using ^{1}H-NMR spectroscopy in CDCl$_3$. The rate of the reaction was determined by monitoring the decreases in concentration the β reactant. This was done by measuring the integration of the β hydrogen (H-1 anomeric proton) to the residual CHCl$_3$ peak that is present in the NMR spectrum when using CDCl$_3$ and an NMR solvent throughout the reaction.

This analysis posed the question of how NMR integration and anomer concentration were correlated, therefore, calibration studies were carried out to understand how compound concentration affects NMR signal intensity and integration.

2.3.1 Calibration Experiments

The general procedure for calibration experiments was as follows: 0.0040g of the compound of interest was dissolved in 0.4 mL of $CDCl_3$. An NMR was taken of the solution and the ratio of the integration of the anomeric hydrogen peak vs the residual $CHCl_3$ peak at 7.26 ppm was found. This solution was then emptied into a round bottom flask and diluted with 0.4ml of CDCl3. 0.4 mL of this solution was measured out with a syringe and transferred into an NMR tube. This gave an assumed concentration of 0.0020g. An NMR of this solution was taken and again the ratio of the integration of the anomeric hydrogen peak vs the residual $CHCl_3$ peak at 7.26 ppm was found. This process was repeated two more times to give solutions with an assumed concentration of 0.0010g and 0.0005g and the integration ratio of the anomeric carbon and the residual $CHCl_3$ peak was found for each.

This experimentally determined ratio was plotted against the assumed concentration to give a graph that showed the integration ratio between the anomeric signal and $CHCl_3$. It was shown that compound concentration and integral ratio had a power relationship as determined using Microsoft Excel (Graph 1).
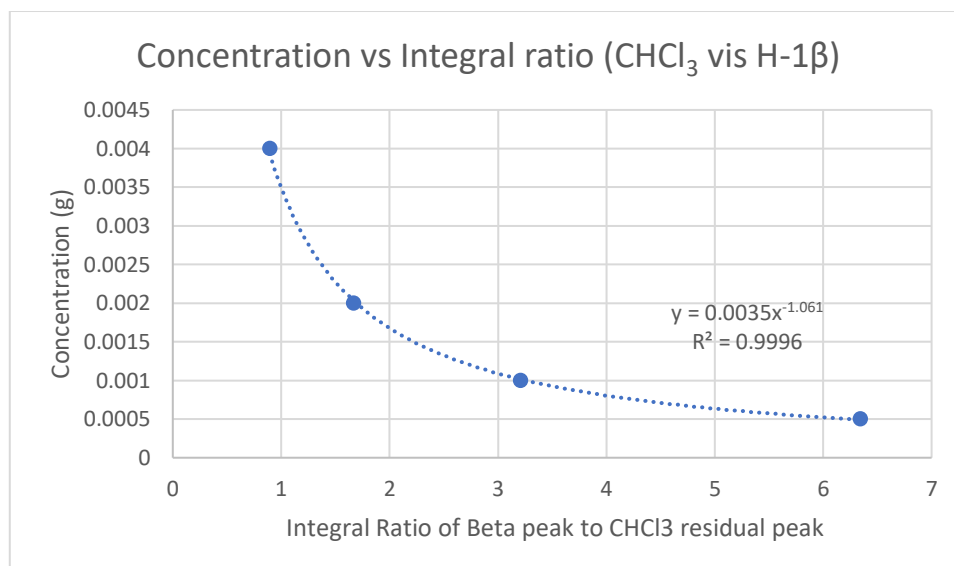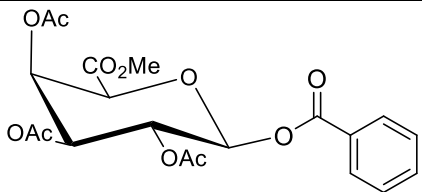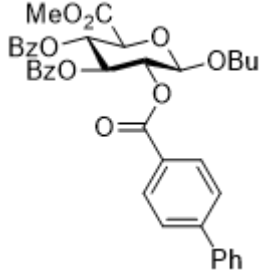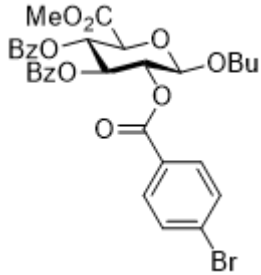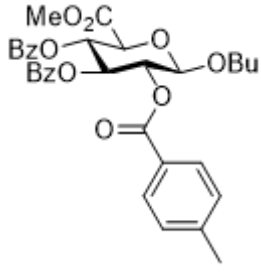
Graph 1. *Concentration vs integral ratio of (4) showing a power relationship.*

Using the equation of the line obtained from the graph produced, a formula was derived to calculate concentration from NMR integration. Where $(\beta:CDCl_3)$ is the integral ratio between the anomeric peak and reference $CHCl_3$

This calibration experiment was done for all three compounds used throughout this study and the results are summarized in Table 3. All calibration data can be found in Appendix 2.

Table 3. *Formulae derived from calibration experiment for each compound.*

Derived Calibration Formulae	
(4)	$Conc = 0.0035 \times (\beta:CHCl_3)^{-1.095}$

(5)	Conc = 0.0035 x (β:CHCl$_3$)$^{-1.061}$
(6)	Conc = 0.0035 x (β:CHCl$_3$)$^{-1.087}$
(7)	Conc = 0.003 x (β:CHCl$_3$)$^{-1.105}$

Each compound had a similar relationship between concentration and integration.

2.3.2 Anomerisation Reactions General Procedure

The general procedure for the anomerisation experiments was as follows: An NMR tube was dried in an oven overnight. 0.0040g of the compound to be anomerised was measured out into the NMR tube. The compound was then

dissolved in 0.30 mL of CDCl$_3$ that had been dried for a minimum of two days over 4 Å molecular sieves. All glassware used throughout these reactions was oven and flame-dried prior to use. One molar equivalent of anhydrous SnCl$_4$ in catalyst in liquid form was added to the NMR tube containing the dissolved carbohydrate compound and mixed thoroughly by shaking the NMR tube. The NMR tube was placed in a water bath to ensure the temperature of the reaction remained constant. An NMR spectrum of the reaction was taken every 15-30 minutes for approximately 5 hours (Figure 39).

In some of the reactions, a white precipitate formed. This is suspected to be the formation of tin (IV) hydroxide (SnO$_4$) or Tin Oxide (SnO$_2$) that formed on contact with water within the reaction vessel or from the NMR tube glass surface. (SnCl$_4$ +4H$_2$O → Sn(OH)$_4$ (↓) +4HCl) (SnCl4+ 2H$_2$O→ SnO$_2$ + 4HCl). In reactions where the water had been adequately removed by flame drying all glassware and ensuring the CDCl$_3$ had been dried using 4Å molecular sieves, the precipitate did not form.

An NMR reading was taken after 24 hours to determine the equilibrium concentration of the reaction.

The reaction mixture was then diluted with EtOAc, washed with a potassium bisulfate solution (KHSO$_4$), saturated NaHCO$_3$, brine, and then dried with Na$_2$SO$_4$. The solution was filtered, the solvent was removed under reduced pressure, and an NMR spectrum of the residue was taken.

Using the calibration equation derived from the calibration experiment, the concentration of the β anomer was determined at each time point. This concentration was plotted against time in seconds to show the rate of conversion of β to α anomer (Graph 2).

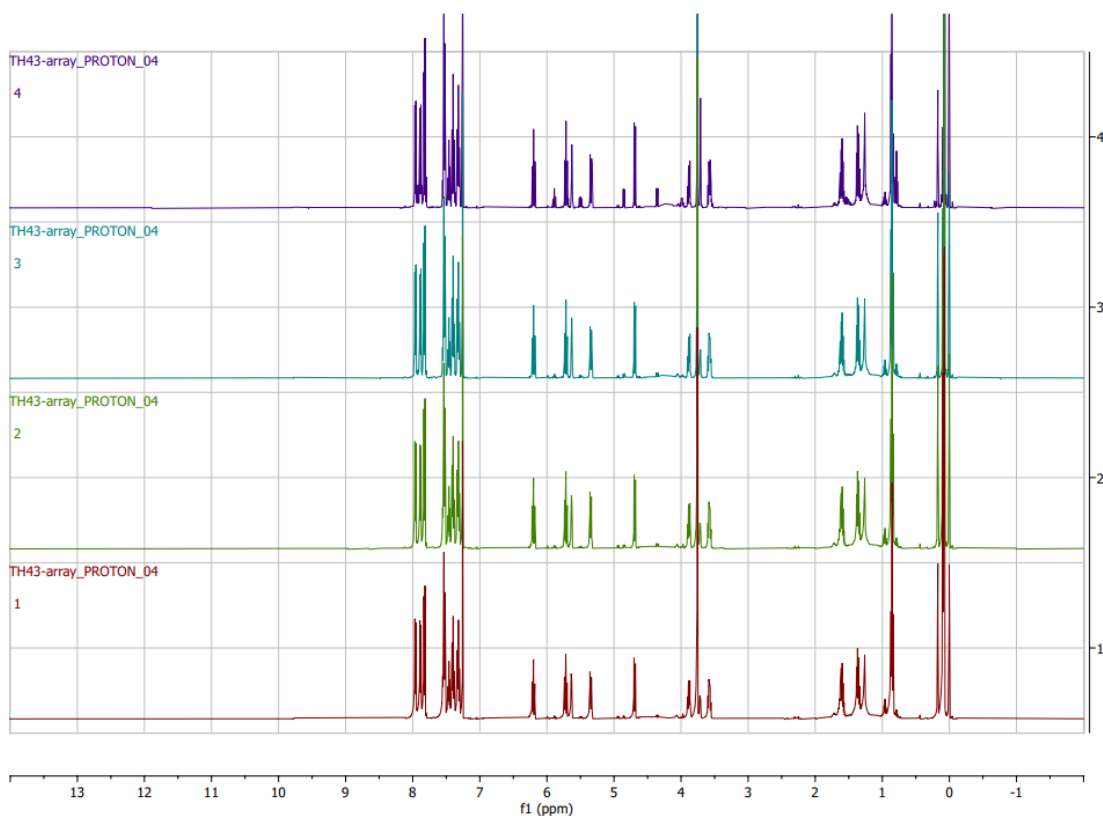*Figure 37.* ^{1}H-NMR graphs of **(6)** taken at increasing time points, with 1 being time 0 h and 8 being after 6 h. Intermediate scans were collected but only a few are shown here to enable peak changes to be ascertained.
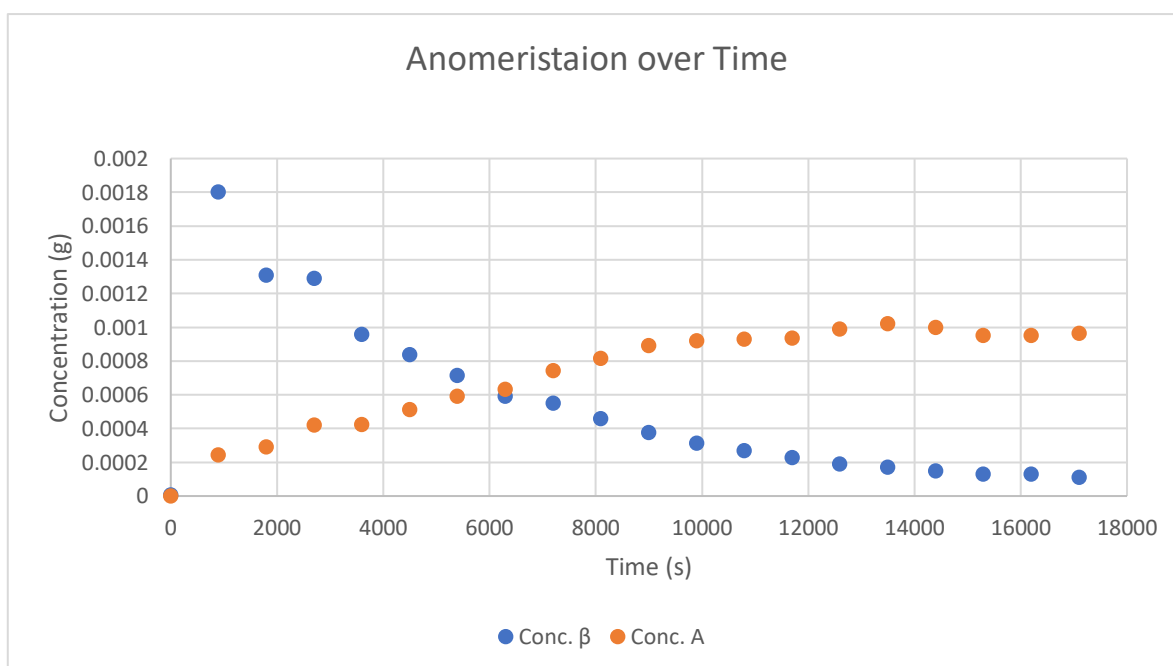
Graph 2. Concentration of anomers vs time for compound **(6)** at 45 Degrees

In Graph 2, the concentration of the α anomer never reaches the same the total concentration of β anomer within the reaction. The NMR does not show any indication of alternate products forming during the reaction, therefore this discrepancy in anomer concentraions may be due to variation in conditions between the calibration experiments and the anomerisation experiments. The calibration experiments were not done in the presence of tin and it is likely that the the product and/or the reactant within the anomerisation reaction is complexed with the Sn present in the solution. This could have an effect on the intensity of the integration. This could be examine further by working up the reaction when it has approx a 50:50 concentration of anomer and examining the relative integrations.

Using the experimentally determined concentrations of the β anomer, k values for each reaction were determined using the first-order equation for reversible kinetics using the following formula[30]:

$$\ln\left(\frac{[\beta]_o - [\beta]_e}{[\beta]_t - [\beta]_e}\right) = -(k_f + k_r)$$

Equation 2. First order reversible kinetics

Minus the natural log of these k (s^{-1}) values were plotted against time (s) to give a straight-line plot in the form y= mx + c where the slope m is the overall rate constant for the reaction (Graph 3).
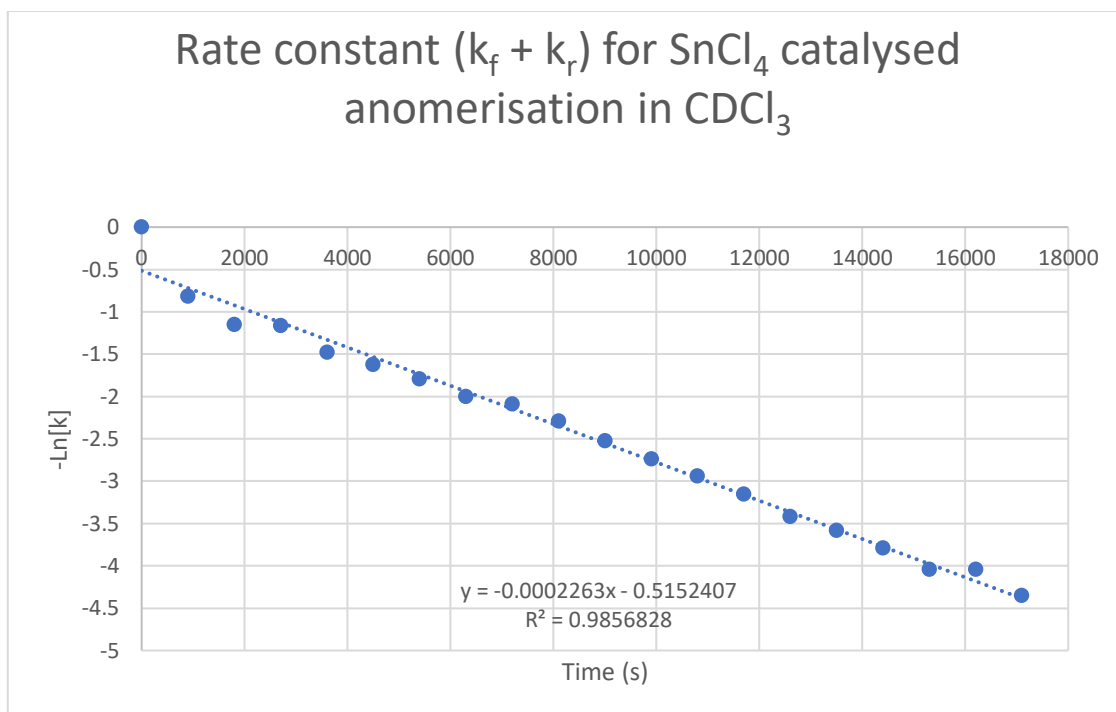
Graph 3. *graph of -Ln(k) vs time for (6) at 45 Degrees*

2.3.3 Anomerisation of compound (4)

Anomerisation of synthesized compound **(4)** was carried out according to the general procedure above. This experiment was conducted at room temperature. Rate constant k was calculated, and the results are summarized in the table below (Table 4). Graphical data of this experiment can be found in appendix 3

Table 4. *Rate constant for compound (4)*

	$k\ (s^{-1})$
(4)	5×10^{-5}

51

This calculated rate constant was relatively slow for an acetelated uronic acid derivative with this high a catalyst concentration in comparison to previously calculated rate constants for these kinds of compounds in the Murphy group. For example, Dr Fiach Meany calculated the rate constant for the uronic acid derivative for the acetelated galaturonic acid an OBu group on the anomeric carbon as 7×10^{-6} while using half the equivalents of catalyst. [35] O-CO group is much more electron withdrawing than an O-alkyl group and therefore reduces the reactivity. This result led to an interest in the rates of other uronic acid derivatives and their rate constants.
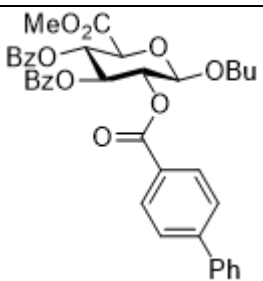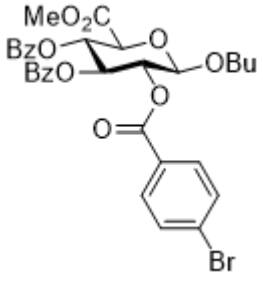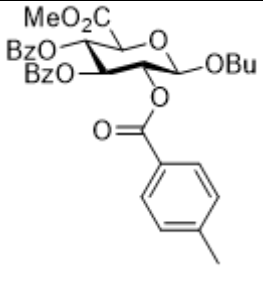
2.3.4 Variable Temperature Studies

As previously stated, temperature affects the rate of reactions, with reaction rates generally increasing with increasing temperature. This section of research aimed to investigate the rate constants of different uronic acid derivatives and the effect of increasing temperature on the rate of anomerisation, and to use this data to calculate the activation energy of the reaction.

The anomerisation reactions were carried out as stated per the general procedure above. The anomerisation reaction was carried out for the three different compounds **(5)**, **(6),** and **(7)** at three different temperatures: 25°C, 35°C, and 45°C. to determine the effect an increased temperature had on the rate constant of the reaction. The temperature was varied by changing the temperature of the water bath that the NMR tube was placed in for the duration

of the reaction. Calculated rate constants are summarized below (Table 4). All kinetic data for compounds **(5)**, **(6)** and **(7)** can be found in appendix 4-6.

Table 5- summary of experimentally derived rate constants (k)

	k (s⁻¹) (25°C)	k (s⁻¹) (35°C)	k (s⁻¹) (45°C)
(5)	0.00037	0.00047	0.00058
(6)	0.00005	0.00016	0.00023
(7)	0.00012	0.00018	0.00064

Rate constants increased with increasing temperature as expected. Compound **(5)** shows the highest k values across the temperatures which can be attributed to it containing an electron donating group Ph. Compound **(7)** also shows higher

k values, particularly at 45°C. This value is unexpectedly large and may be an outlier due to an error such as the addition of more $SnCl_4$ than planned. This data point will be excluded in the calculation of E_a. Electron donating group will enhance conjugation through mesomeric effects therefore increasing the rate. Compound **(6)** shows the smallest k value which is likely due to bromine's electron withdrawing effects which again due to the mesomeric effect decreasing the rate.

Calculated rate constants were of similar magnitude to previously calculated rate constants at RT, reported to be 197×10^{-6}, 120×10^{-6} and 232×10^{-6} for **(4)**, **(5)** and **(6)** respectively with variation likely due to differing concentrations of catalyst used in previous experiments. [35]

Using the calculated rate constants, the activation energy of the reaction can be calculated using the following equation derived from the Arrhenius equation[52]:

$$\ln k = \frac{-E_a}{RT} + \frac{1}{T}$$

Equation 5. Arrhenius equation in linear form

This is done by plotting the log of the rate constants against 1/T (Graph 4)

The graph gives a line with the equation:

$$Ln\, k = \left(\frac{Ea}{R}\right)\left(\frac{1}{T}\right) + LnA$$

Equation 6. Equation of the line when ln(k) vs 1/T is plotted.

Where k is the rate constant, E_a is the activation energy, R is the universal gas constant, T is the temperature and A is a constant related to the geometry needed for reaction to occur.

Therefore, the slope of the line can be used to calculate the activation energy using the following equation:

$$m = \frac{E_a}{R}$$

Equation 7. *Slope of the line*

Where R is the universal gas constant (8.314 J mol^{-1} K^{-1}). Calculated activation energies for each of the three compounds are summarized in Table 5. All graphical data for the determination of E_a can be found in Appendix 7.
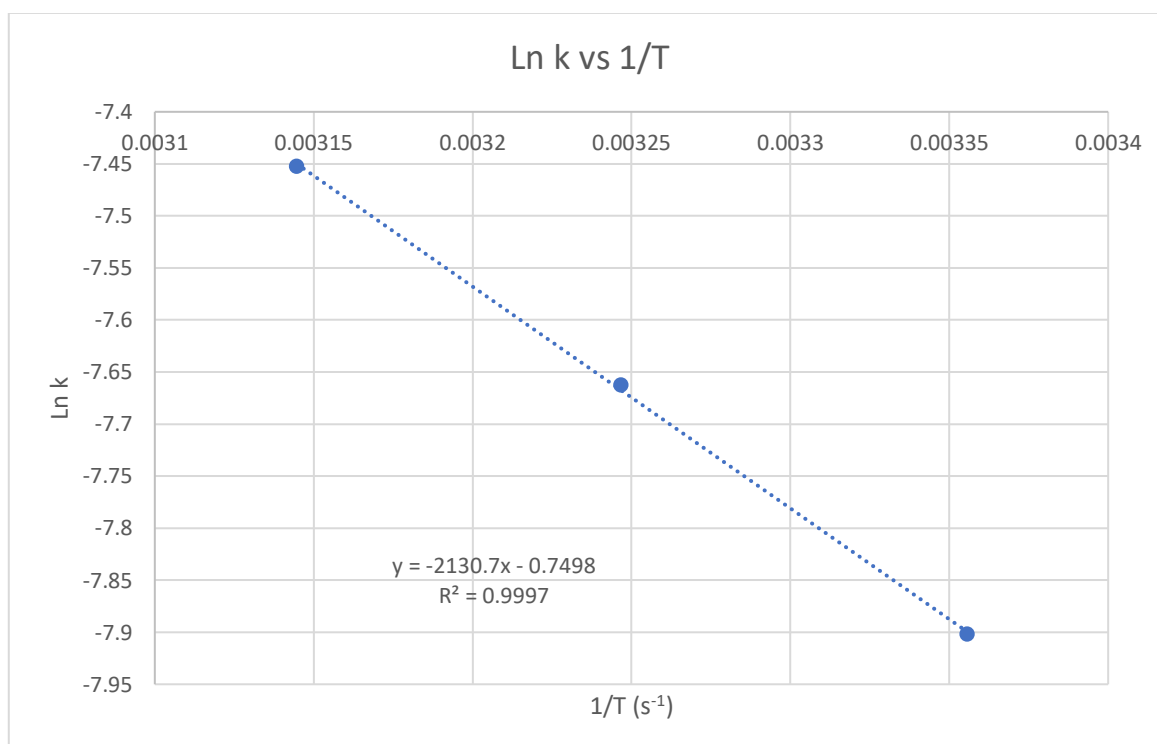
Graph 4. *ln k vs 1/T where m=E_a/R for compound **(5)***

Table 6. Summary of calculated activation energies

	Calculated Activation Energy
(5)	17.71 KJ/Mol
(6)	60.43 KJ/Mol
(7)	30.94 /Mol

The activation energy for each compound was calculated. Compound **(4)** which has a phenyl group on the C-2 substituent showed the lowest activation energy. Compounds (5) and (6) which had a bromide and a methyl group on the C-2

substituent had higher activation energies with compound (6) being marginally higher.

2.3.5 Catalyst concentration studies

Catalyst concentration can affect the rate of a reaction, with the rate expected to increase with increasing catalyst concentration. This section of research looked at the effect of differing catalyst concentrations on the rate of the anomerisation reaction.

The anomerisation reactions were carried out as stated per the general procedure using compound **(5)** but with the molar equivalent of the catalyst varying. 0.5, 1 and 2 equivalents of $SnCl_4$ were the concentrations used for this study. The results of this experiment are summarized in Table 6 and Graph 5. All data for concentration experiments can be found in Appendix 8.

*Table 7. Calculated rate constants for **(5)** at varying catalyst concentration*

Catalyst Equivalents	Moles	$(k_r + k_f)$
0.5 equivalents	3×10^{-6}	2.5×10^{-4}
1 equivalent	6×10^{-6}	3.9×10^{-4}
2 equivalents	1.2×10^{-5}	4.0×10^{-4}
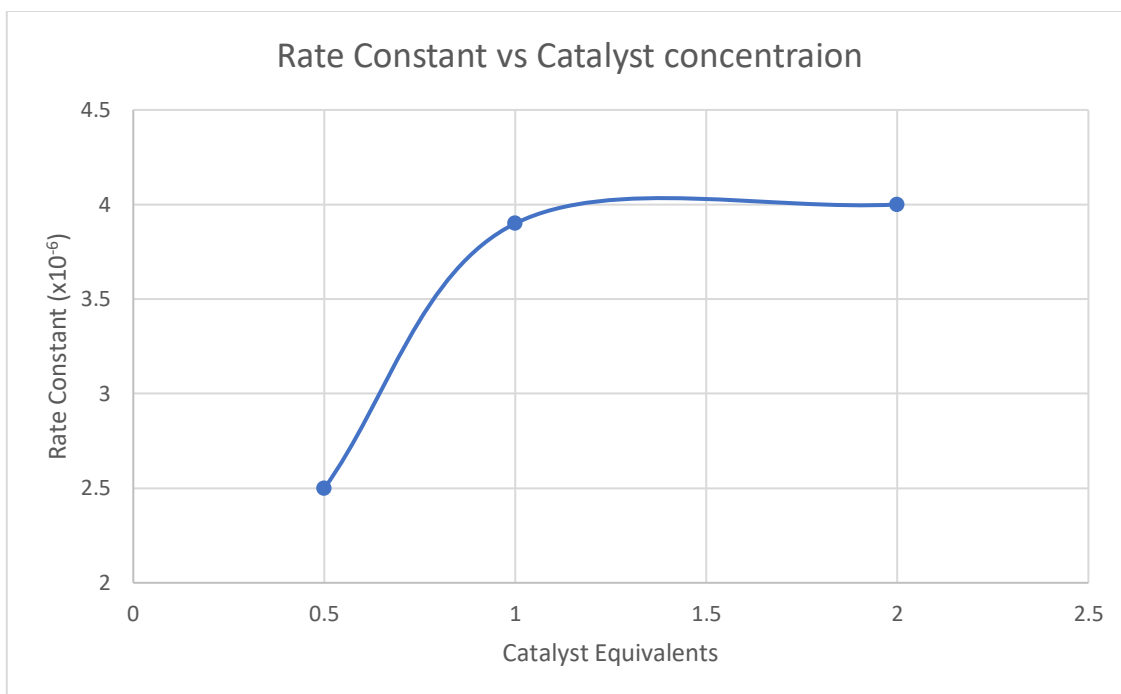
Graph 5. *Relationship between the calculated rate constant and catalyst concentration*

As expected, increasing the catalyst concentration increases the rate of reaction. There was a significant increase in the rate constant when catalyst concentration was increased from 0.5 to one equivalent, while there was a much smaller increase in the rate constant when concentration was increased from one to two equivalents. T. It seems that once the catalyst to reactant ratio goes above 1:1 the rate does not increase any more. It appears that a relatively stable complex between the catalyst and reactant/product forms. Dissociation must occur for another catalyst molecule to affect the reaction, therefore this data supports a mechanism that involves only one molecule of $SnCl_4$ in the rate determining step of the anomerisation reaction.

3. Conclusion

A new galacturonic acid substrate was synthesised. The kinetics of the anomerisation reaction of this compound at room temperature was determined to be 5×10^{-5}. This was relatively slow in comparison to other uronic acid anomerisation reactions with catalyst concentrations at the high level of 1 equivalent.

The anomerisation reaction of three previously synthesised galacturonic acid substrates were investigated at a range of temperatures to determine the activation energy of the anomerisation reaction for these compounds. The rate of reaction increased with temperature as was expected. Compound 7 had an unexpectedly large jump in measured k value at 45°C, this is more than likely due to human error and was taken as an outlier and excluded form E_a calculations. It was clear that substituents on the C-2 influenced the rate of the reaction, with EDG's showed a lower rate constant while EWG's showed a higher rate constant due to mesomeric effects that enhance or reduce conjugation. It can be concluded that the addition of these groups can have a major influence on reaction rates and incorporation into molecules can make the reaction more commercially viable.

The effect of catalyst concentration was also examined using one of the galacturonic acid (compound **(5)**) substrates. It was shown that the rate of anomerisation increased with catalyst concentration with the rate increase plateauing at a 1:1 ratio and going above this ratio does not have a benefit. This is because a 1:1 complex is formed and dissociation must occur for another catalyst molecule to influence the reaction, this supports a mechanism that involves only one $SnCl_4$ molecule in the rate determining step of this reaction. ,

More work needs to be done to ensure these results are reproduceable and to determine the uncertainty of the calculations.

4. Future Work

As compound (4) was only anomerised at one temperature, this could be repeated at more temperatures to obtain the activation energy for this compound also. Using HPLC the α and β anomers could be separated to fully characterise the α derivative of this compound.

The activation energy of three compound were examined, anomerisations for more of these uronic acid derivatives that contain different groups of varying electron donating and electron withdrawing effects such as OH, NH_2, or NO_2on the C2 substituent could be examined, to ascertain with greater confidence, the effect these groups have on the activation energy of the anomerisation reaction.

For the catalyst concentration experiment, only one glucopyranosiduronic acid was examined. It would be interesting if this experiment could be carried out for more of these uronic acid compounds with differing EWG and EDG on the para position of the C2 substituent along with glucopyranosides with these same substituents to see the difference in the effect of the catalyst on these compounds. Anomerisation at a variety of temperatures to determine E_a could be carried out using different concentrations of catalyst.

All anomerisation reactions were only conducted once, and these experiments could be repeated, and error bars could be added to graphs.

5. Experimental

NMR spectra were recorded with either a 500 MHz Agilent spectrometer or JEOL 400 MHz spectrometer. The d1 of the spectrometers was 1 s. Data is reported as: chemical shift (δ) in ppm; multiplicities indicated as s (singlet), d (doublet), t (triplet), dd (double doublet), dt (doublet of triplets) m (multiplet) or overlapping signals; coupling constants (J) are given in Hertz (Hz). Chemical shifts are reported relative to internal standard $CDCl_3$ (δ 7.25) for ^{1}H and $CDCl_3$ (d 77.0) for [13]C. ^{1}H-NMR signals were assigned with the aid of COSY and ^{13}C signals were assigned with the aid of HSQC and HMBC. NMR spectra of known compounds were in good agreement with previously reported data.

High-resolution mass spectra were measured in positive mode using a Waters LCT Mass Spectrometry instrument.

TLC was performed with aluminium sheets coated with silica gel and visualised with UV and charring with 5% H_2SO_4 in MeOH. Flash chromatography was carried out with silica gel 60 (0.040-0.630 mm) and using a stepwise solvent polarity gradient correlated with TLC mobility. Chromatography and reaction solvents, toluene, CH_2Cl_2, EtOAc, MeOH, and cyclohexane were obtained from Sigma Aldrich. Dry CH_2Cl_2 was obtained from a Pure Solv™ Solvent Purification System. CDCl3 was obtained from Sigma Aldrich and dried using 4Å molecular sieves. Optical rotation readings were taken with a Schmidt and Haensch UniPol L1000 at the sodium D line at 20°C. Unless otherwise stated, compounds were obtained from suppliers without further purification. All chemical compounds were drawn using ChemDraw 21.0.0. All anomerisation experiments were conducted once.
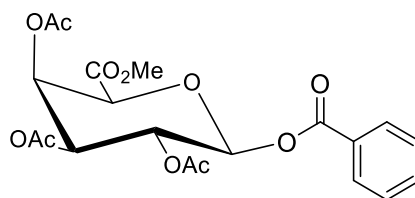
2,3,4-Tri-O-acetyl-β-D-galactopyranosiduronic acid, methyl ester (4): Acetic anhydride (28.5 cm^3, 301 mmol) and sulfuric acid (0.1 cm^3, 2 mmol) were combined on ice and allowed to stir for 20 mins under an inert nitrogen atmosphere. The solution was returned to room temperature and D-galacturonic acid (5 g 23.6 mmol) was added and stirred for 2 h. The solution was cooled again on ice and MeOH was added to quench the reaction. The reaction solution was partitioned with EtOAc and H$_2$O. The organic layer was washed with H$_2$O and brine and dried with Na$_2$SO$_4$, filtered, and concentrated to yield the acetylated compound (1) which was used immediately without purification. (1) was dissolved in DMF. NaHCO$_3$ (4.00 g, 48 mmol) and CH$_3$I was added to the solution and left to stir at room temperature overnight. The reaction solution was diluted with H$_2$O and extracted into EtOAc. The organic layer was washed with H$_2$O and brine and dried with Na$_2$SO$_4$ filtered and concentrated. Flash chromatography (gradient elution of 15 to 25 % EtOAc in cyclohexane) gave the protected uronic acid compound (2) to give 2.9 g over two steps (2.9 g, 37%).

Then (2) was dissolved in dry CH$_2$Cl$_2$. HBr was added (10 cm^3, 30% AcOH) and stirred at room temperature for 2 h and then was poured on an ice-water mixture in a separating funnel. The mixture was separated, and the aqueous layer was washed with CH$_2$Cl$_2$. The organic layer was neutralised with saturated aqueous NaHCO$_3$. Organic layer was dried with Na$_2$SO$_4$, filtered, and

62

concentrated to produce glycosyl bromide (3) which was used immediately without further purification.

The (3) was dissolved in CH_2Cl_2 and stirred over 4Å

molecular sieves for 20 mins. In a separate flask CH_2Cl_2 (35 cm^3), Ag_2CO_3 (3.75 g, 11 mmol) and benzoic acid (2.70 g, 22.00 mmol) along with a catalytic amount of I_2 (0.1 g, O.8 mmoles) were combined an allowed to stir for 15 mins. The flask was covered with aluminium foil to shield the mixture from light, at this point the glycosyl bromide mixture was added dropwise to the flask. The mixture was left to stir for 16 h. The mixture was then diluted with EtOAc and filtered through celite. The mixture was concentrated and purified by flash chromatography (gradient elution of 22 % EtOAc in cyclohexane). Chromatography of the residue yielded 1.049g of the title compound as a white solid over 4 steps (1.05 g, 11.4 %).

^{1}H NMR (400 MHz, CDCl$_3$) δ 8.05 (d, J= 8.3, 2H, Ar-H), 7.59 (t, J=8.3, 1H, Ar-H), 7.45 (m, 2H, Ar-H), 5.91 (d, J= 8.3 Hz, 1H, H-1), 5.78 (dd, J= 3.5, 1.4Hz, 1H, H-4), 5.60 (dd, J= 10., 8.3 Hz, 1H, H-2), 5.21 (dd, J= 10.5, 3.5, 1H, H-3), 4.55 (d, J= 1.4 Hz, 1H, H-5), 3.76 (s, 3H, CO$_2$Me), 2.14 (s, 3H, CH$_3$), 2.02 (s, 3H, CH$_3$), 1.97 (s, 3H, CH$_3$); ^{13}C NMR (126 MHz CDCl$_3$) δ 170.05, 169.90, 169.55, 166.03, 164.66 ((CH$_3$)C=O), 134.17, 130.43, 128.69, 128.35 (Ar-C), 92.45 (C-1), 73.28 (C-5) 70.53 (C-3), 68.26 (C-4),67.32 (C-2), 53.09 (CO$_2$Me), 20.70, 20.75 (Ac)

ESI-HRMS cacld. For C$_{20}$H$_{22}$O$_{11}$Na 461.1059, found m/z 461.1057 [M+Na]$^+$

General procedure for calibration experiments:

0.0040g of the compound of interest was dissolved in 0.4 mL of CDCl$_3$. An NMR was taken of the solution and the ratio of the integration of the anomeric

hydrogen peak vs the residual $CHCl_3$ peak at 7.26 ppm was found. This solution was then emptied into a round bottom flask and diluted with 0.4ml of CDCl3.

0.4 mL of this solution was measured out with a syringe and transferred into a clean and oven dried NMR tube. This gave the solution an assumed concentration of 0.0020g. An NMR of this solution was taken and again the ratio of the integration of the anomeric hydrogen peak vs the residual $CHCl_3$ peak at 7.26 ppm was found. This dilution process was repeated two more times to give solutions with an assumed concentration of 0.0010g and 0.0005g and the integration ratio of the anomeric carbon and the residual $CHCl_3$ peak was found for each.

This experimentally determined ratio was plotted against the assumed concentration to give a graph that showed the integration ratio between the anomeric signal and $CHCl_3$. It was shown that compound concentration and integral ratio had a power relationship as determined using Microsoft Excel

General procedure for the anomerisation reaction:

 An NMR tube was dried in an oven overnight. 0.0040g of the uronic acid derivative to be anomerised was weighed into the NMR tube. The compound was then dissolved in 0.30 mL of $CDCl_3$ that had been distilled and dried over 4 Å molecular sieves. All glassware used throughout these reactions was oven and flame-dried prior to use. $SnCl_4$ was diluted with $CDCl_3$ in a round bottom flask to ensure a volume containing one molar equivalent of catalyst that could be accurately measured with a syringe (approx. 0.05ml of $SnCl_4$ in 5 mL of $CDCl_3$). One molar equivalent of $SnCl_4$ catalyst was added to the NMR tube containing the dissolved carbohydrate compound and mixed thoroughly by shaking the

NMR tube. The NMR tube was placed in a water bath to ensure the temperature of the reaction remained constant throughout the reaction. An NMR spectrum of the reaction was taken every 15-30 minutes for approximately 5 hours.

An NMR reading was then taken after 24 hours once the reaction had reached equilibrium.

The reaction mixture was then diluted with EtOAc, washed with a potassium bisulfate solution (KHSO$_4$), saturated NaHCO$_3$, brine, and then dried with Na$_2$SO$_4$. The solution was filtered, the solvent was removed under reduced pressure, and an NMR spectrum of the residue was taken.
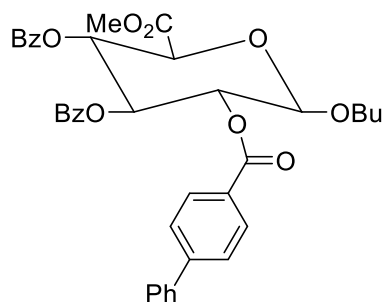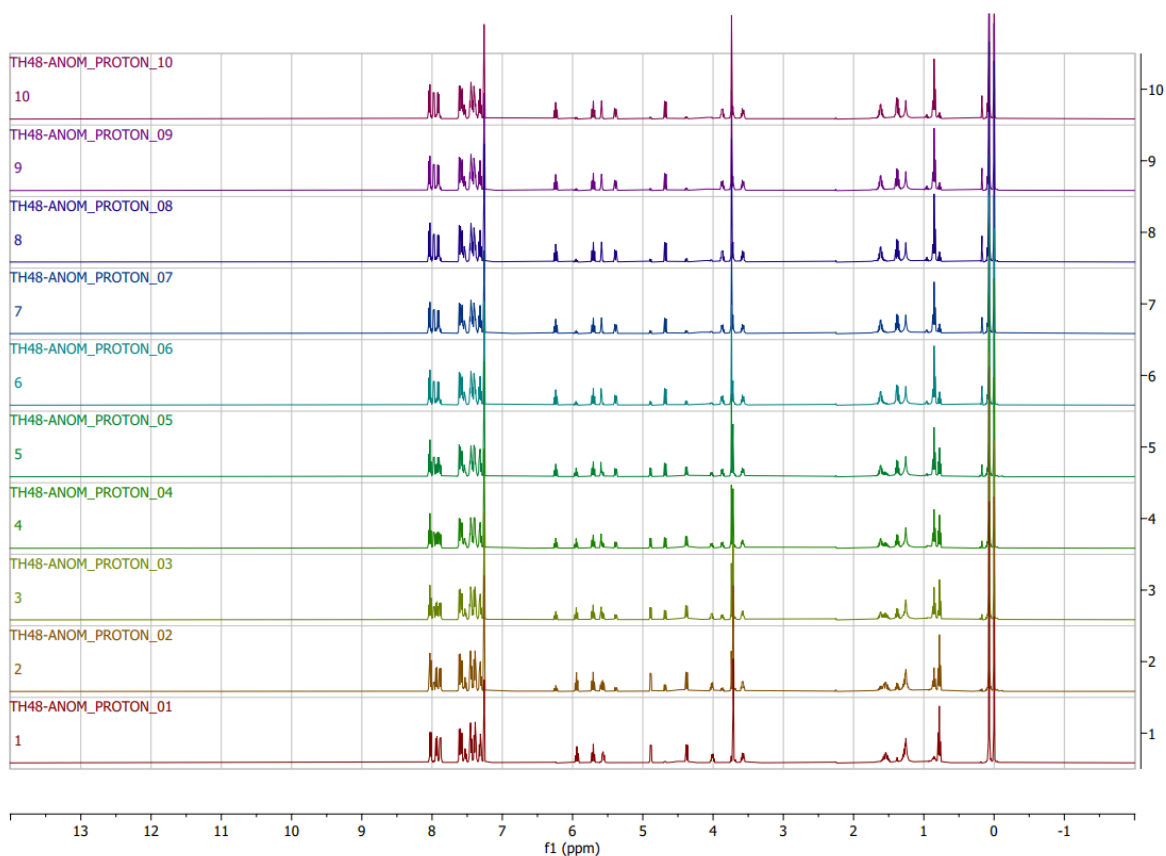
Butyl 2-O-(4-phenylbenzoyl)-3,4-di-O-benzoyl-α-D-glucopyranosiduronic acid, methyl ester (5) ^{1}H-NMR (400 MHz, cdcl3) δ 8.01 (d, 2H, Ar-H), 7.92 (d, 2H, Ar-H), 7.86 (d, 2H, Ar-H), 7.58 (overlapping signals, 4H, Ar-H), 7.51 (m, 1H, Ar-H), 7.43 (overlapping signals, 3H, Ar-H), 7.38 (overlapping signals, 3H, Ar-H), 7.31 (m, 2H, Ar-H), 5.91 (t, J=9.4 Hz, 1H, H-3), 5.68 (t, J=9.5 Hz, 1H, H-4), 5.53 (dd, J=9.5 Hz, 1H, 7.5 Hz, H-2), 4.85 (d, J=7.5 Hz, 1H, H-1), 4.34 (d J=9.5 Hz, 1H, H-5), 3.97 (dt, J=9.6, 6.4 Hz, 1H, proton of OCH_2), 3.69 (s, 3H, CO_2Me), 3.55 (dt, J=9.7, 6.7 Hz, 1H, proton of OCH_2); ^{13}C NMR (126 MHz $CDCl_3$) δ 167.58 (CO_2Me), 165.82, 165.31, 164.95 (Ar-C=O), 146.06, 139.98, 133.55, 133.45, 130.39, 129.96, 129.91, 129.02, 128.81, 128.85, 128.56, 128.45, 128.29, 128.03, 127.36, 127.14 (Ar-C & Ar-CH), 101.29 (C-1), 73.05 (C-5), 72.24 (C-3), 71.70 (C-2), 70.37 (overlapping signals, C-4 & OCH_2), 53.02 (CO_2Me), 31.40 (Butyl Methylene), 18.98 (Butyl Methylene), 13.74 (CH_3).

NMR Data for alpha anomer

^{1}H-NMR (400 MHz, cdcl3) δ 8.04 (d, J=8.3 Hz, 2H, Ar-H), 7.98 (d, J=8.2 Hz, 2H, Ar-H), 7.91 (d, J=8.2 Hz, 2H, Ar-H), 7.60 (overlapping signals, 4H, Ar-H), 7.56 (t, J=8.2 Hz, 1H, Ar-H), 7.45 (overlapping signals, 3H, Ar-H), 7.39 (overlapping signals, 3H, Ar-H), 7.32 (t, J=7.8 Hz, 2H, Ar-H), 6.27 (t, J=9.9 Hz, H-3),5.78 (t, J=9.8 Hz, 1H, H-4), 5.44 (d, J=3.6 Hz, 1H, H-1) 5.36 (dd, J=9.8, 3.6, 1H, H-2) 4.77 (d, J=10.1 Hz, 1H, H-5) 3.93 (m, 1H, proton of OCH_2) 3.81 (s, 3H, CO_2Me), 3.64 (m, 1H, proton of

OCH$_2$), 1.63 (overlapping signals, 2H butyl methylene), 1.38 (overlapping signals butyl methylene), 0.85 (t, J=7.4 Hz, 3H, CH$_3$).

The NMR data is in good agreement with that reported in literature.[35]

Graph 6 *- NMR of anomerisation of (5) at 25°C*
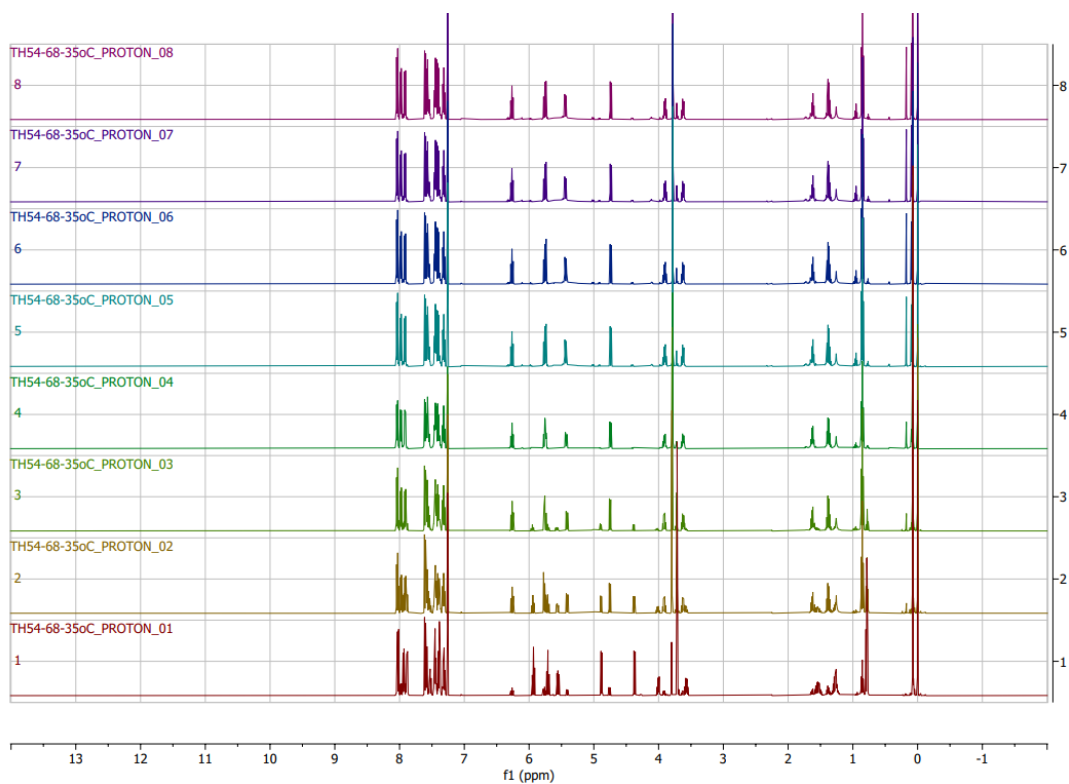
***Graph 7**- NMR of anomerisation of (5) at 35°C*
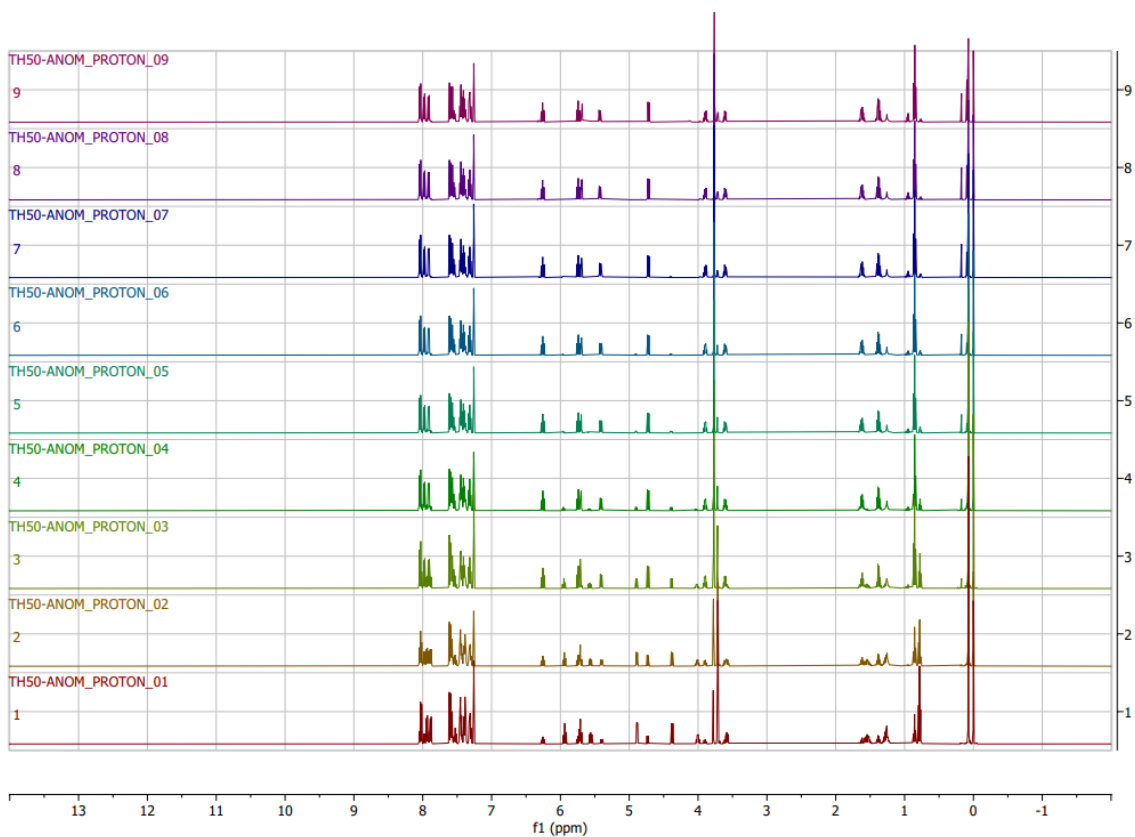
***Graph 8**- NMR of anomerisation of (5) at 45°C*
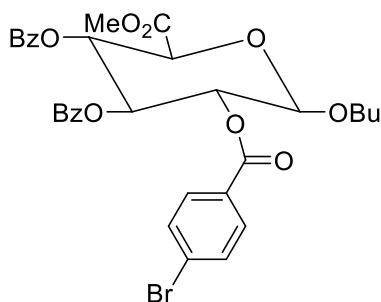
Butyl 2-O-(4-methylbenzoyl)-3,4-di-O-benzoyl-α-D-glucopyranosiduronic acid, methyl ester (6) ^{1}H-NMR (400 MHz, cdcl3) δ 7.91 (d, 2H, Ar-H), 7.84 (d, 2H, Ar-H), 7.80 (d, 2H, Ar-H), 7.51 (overlapping signals, 3H, Ar-H), 7.45 (t, J=7.4 Hz, 1H, Ar-H), 7.37 (t, J-7.7 Hz, 2H, Ar-H), 7.30 (t, J=7.7 Hz, 2H, Ar-H), 5.86 (t, 1H, H-3), 5.67 (t, 1H, H-4), 5.48 (t, 1H, H-2), 4.82 (d, J=7.5 Hz, 1H, H-1), 4.31 (d, J=9.6 Hz, 1H, H-5), 3.96 (dt, J=9.6, 6.3 Hz, 1H, proton of OCH$_2$), 3.69 (s, 3H, CO$_2$Me), 3.53 (dt, J=9.7, 6.7 Hz, 1H, proton of OCH$_2$)); ^{13}C NMR (126 MHz CDCl$_3$) δ 167.36, 165.18, 164.35, 154.53 (4x Ar-C=O), 133.54, 133.53, 131.85, 131.34129.92, 129.89 128.82, 128.73, 128.57, 128.45,128.22, 128.15 (Ar-C & Ar-CH), 101.13 (C-1), 73.04 (C-5), 72.16 (C-3), 71.97 (C-2), 70.35, 70.24 (overlapping signals, C-4 and OCH$_3$), 53.04 (CO$_2$Me), 31.35 (butyl methylene), 18.95 (butyl methylene), 13.17 (CH$_3$)

NMR data for alpha anomer

^{1}H-NMR (400 MHz, cdcl3) δ 7.96 (d, *J*=6.6 Hz, 2H, Ar-H), 7.92 (d, *J*=6.6 Hz, 2H, Ar-H), 7.86 (d, *J*=6.6 Hz, 2H. Ar-H), 7.53 (overlapping signals, 3H, Ar-H), 7.46 (t, *J*=6.6 Hz, 1H, Ar-H), 7.39 (t, *J*=6.6 Hz, 2H, Ar-H), 7.32 (t, *J*=6.6 Hz, 2H, Ar-H), 6.16 (t, *J*=9.8 Hz, 1H, H-3), 5.69 (t, *J*=9.7 Hz, 1H, H-4), 5.44 (d, *J*=3.7 Hz, 1H), 5.32 (dd, *J*= 10.1, 3.6 Hz, 1H), 5.64 (d, *J*=10.0 Hz, 1H), 3.99 (dt, *J*=9.7, 6.6 Hz, 1H, proton of OCH$_2$), 3.72 (s, *J*=10.9 Hz, 3H, CO$_2$Me), 3.54 (dt, *J*=9.7, 6.6 Hz, 2H), 1.59

(overlapping signals, 2H, butyl methylene), 1.35 (overlapping signals, 2H, butyl methylene), 0.85 (t, *J*=7.4 Hz, 3H).

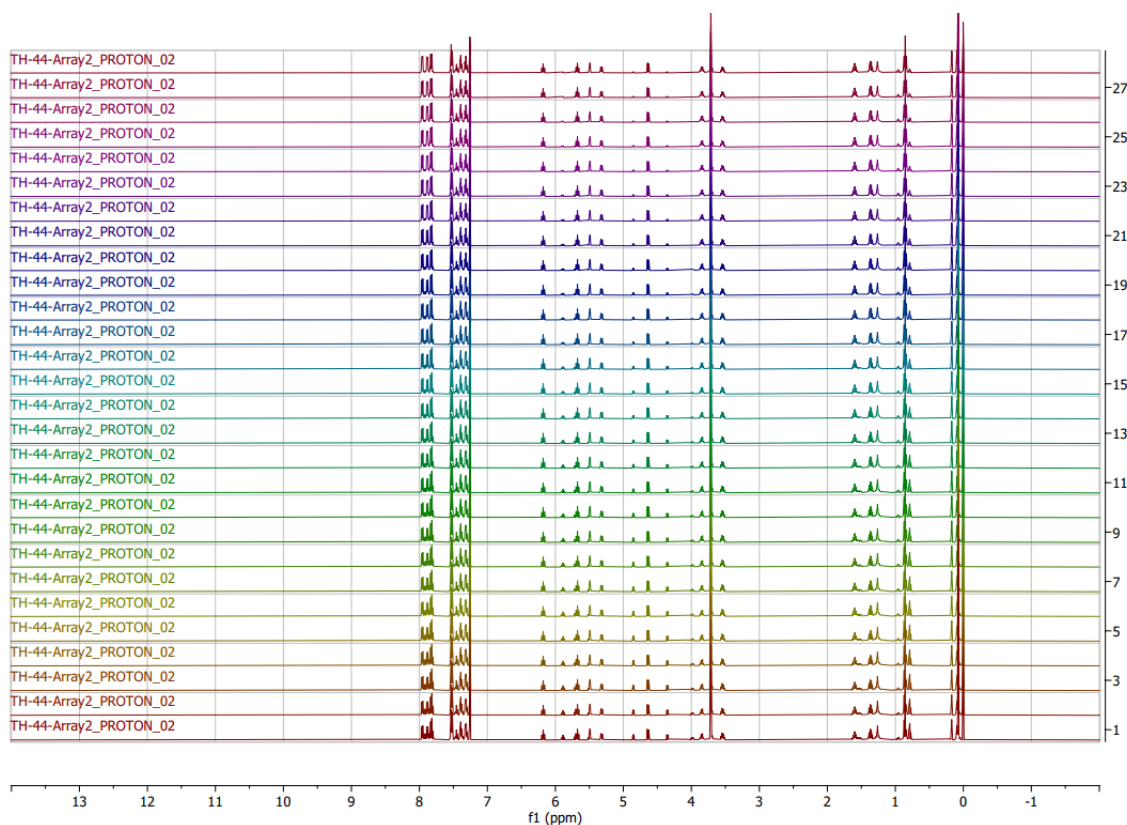The NMR data is in good agreement with that reported in literature.[35]

Graph 9-NMR of anomerisation of (6) at 25°C
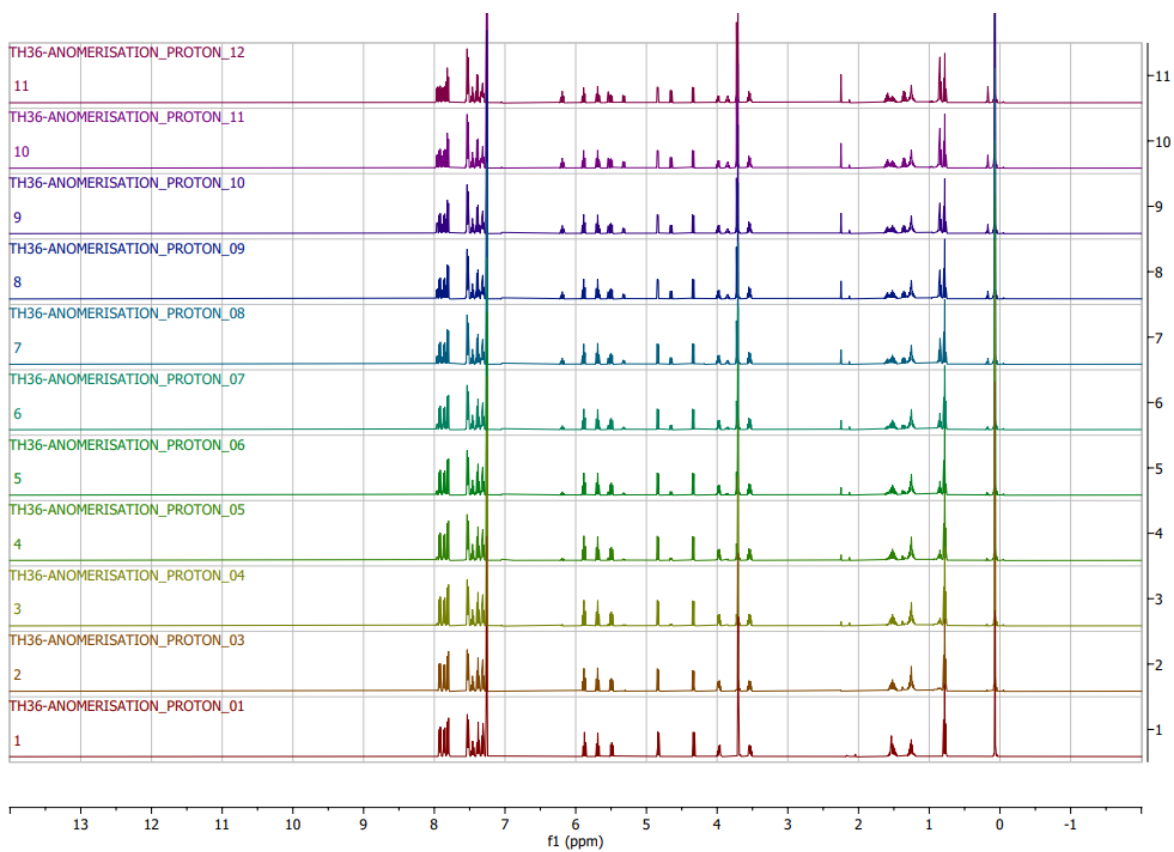
Graph 10- *NMR of anomerisation of (6) at 35°C*
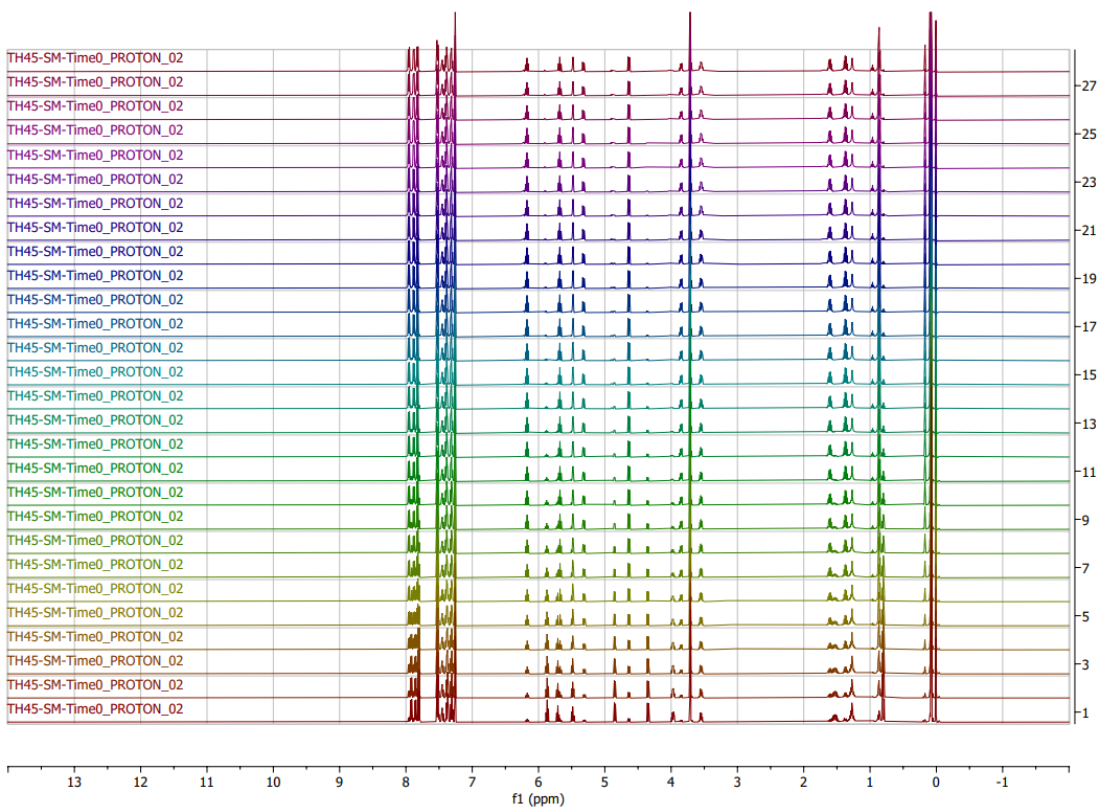
Graph 11- *NMR of (6) at 45*

BzO—MeO₂C
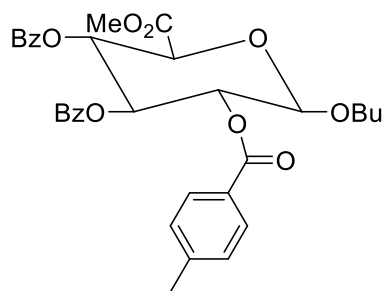
Molecular Weight: 590.62500

Butyl 2-O-(4-methylbenzoyl)-3,4-di-O-benzoyl-α-D-glucopyranosiduronic acid, methyl ester (7): ^{1}H-NMR (400 MHz, cdcl3) δ 7.91 (d, 2H, Ar-H), 7.84 (overlapping signals, 4H, Ar-H), 7.51 (t, J=7.4 Hz, 1H, Ar-H), 7.43 (t, J=7.8, 7.0 Hz, 1H, Ar-H), 7.37 (t, J=7.8, 7.0 Hz, 2H, Ar-H), 7.29 (m, 2H, Ar-H) 7.16 (d, 2H, Ar-H), 5.87 (t, J=9.4 Hz, 1H, H-3), 5.66 (t, J=9.5 Hz, 1H, H-4), 5.50 (t,J=9.4, 7.5 Hz 1H, H-2), 4.82 (d, J=7.5, 1H, H-1), 4.32 (d, J=9.5 Hz, 1H, H-5), 3.95 (dt, J=9.7, 6.4 Hz, 1H, proton of OCH₂), 3.69 (s, 3H, CO₂Me), 3.52 (dt, J=9.6 Hz, 1H, proton of OCH₂), 2.35 (s, 3H, Ar-H), 0.76 (t, J=7.4, 3H, CH₃)); ^{13}C NMR (126 MHz CDCl₃) δ 167.50 (CO₂Me), 165.69, 165.19, 165.02 (3x Ar-C), 143.95, 133.41, 133.27, 129.84, 129.80, 129.06, 128.88, 128.84, 128.43, 128.31, 126.55 (Ar-C & Ar-CH), 101.23 (C-1), 72.98 (C-5), 72.19 (C-3), 71.43 (C-2), 70.27 (C-4), 70.22 (OCH₂), 52.87 (CO₂Me), 31.30 (butyl methylene), 21.65 (butyl methylene), 18.86 (butyl methylene), 13.16 (CH₃)

NMR data for alpha anomer

^{1}H-NMR (400 MHz, cdcl3) δ 7.96 (d, *J*=7.4 Hz, 2H, Ar-H), 7.89 (overlapping signal, 4H, Ar-H), 7.55 (t, *J*=7.4 Hz, 1H), 7.43 (overlapping signals, 3H, Ar-H), 7.31 (t, *J*=7.6 Hz, 2H, Ar-H), 7.18 (d, *J*=8.0 Hz, 2H, Ar-H), 6.24 (t, *J*=9.9 Hz, 1H, H-3), 5.75 (t, *J*=9.9 Hz, 1H, H-4), 5.60 (d, *J*= 3.6, 1H, H-1), 5.41 (dd, *J*= 10.2, 3.6 Hz, 1H, H-2), 4.74 (d, *J*=10.1 Hz, 1H, H-5), 3.90 (dt, *J*=10.1, 6.5 Hz, 1H, proton of OCH₂), 3.71

72

(s, 3H, Ar-Me), 1.60 (overlapping signals, 2H, Butyl Methylene), 1.36 (overlapping signals 2H, butyl methylene), 0.84 (t, J=7.4 Hz, 3H, CH_3).

The NMR data is in good agreement with that reported in the literature.[35]
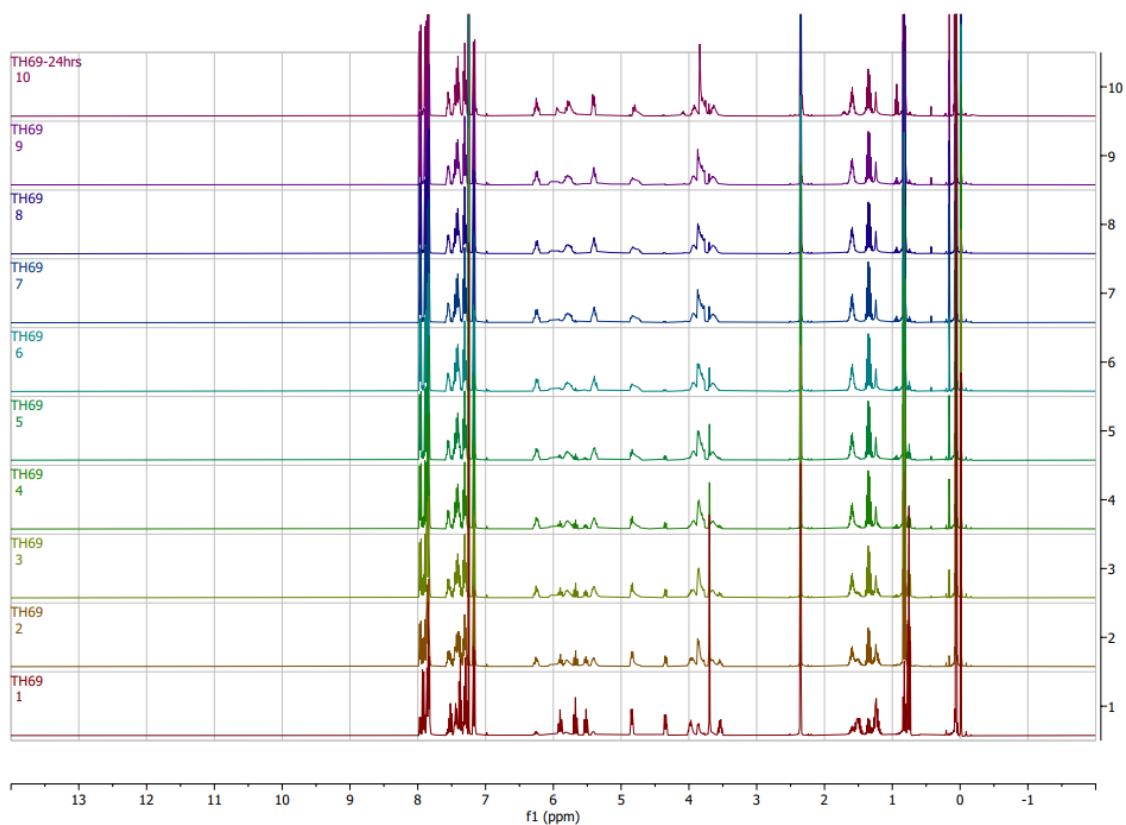
Graph 12- *NMR of anomerisation of (7) at 25°C*
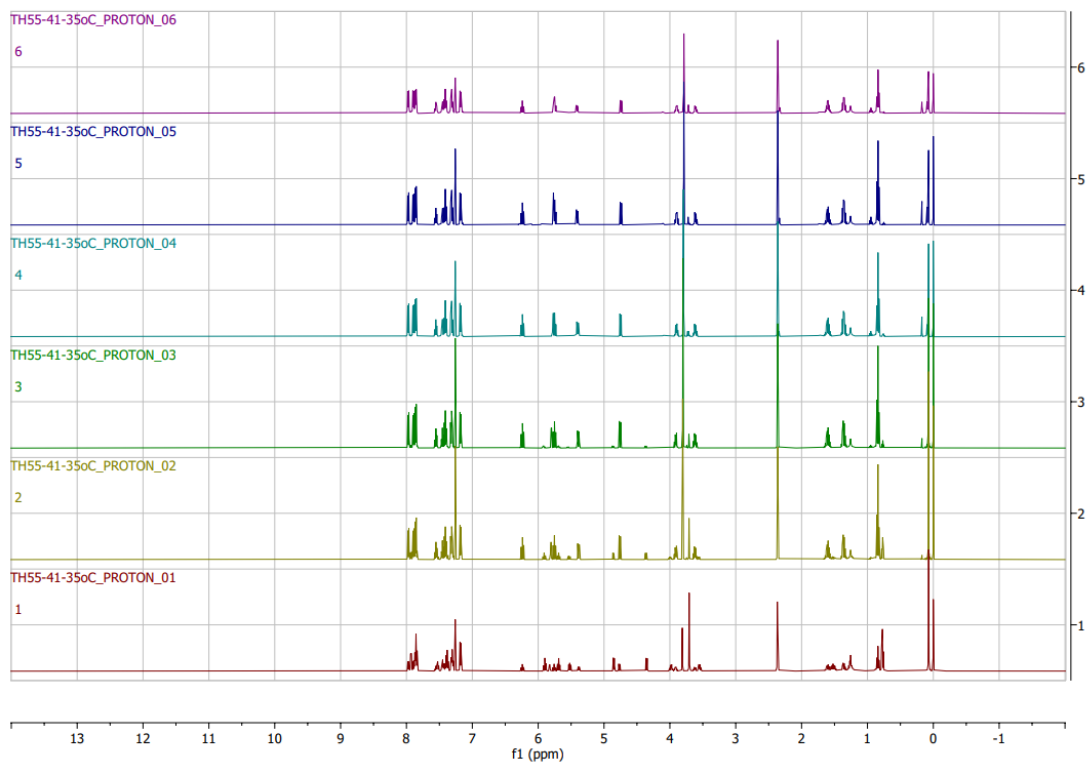
***Graph 13**- NMR of anomerisation of (7) at 35°C*
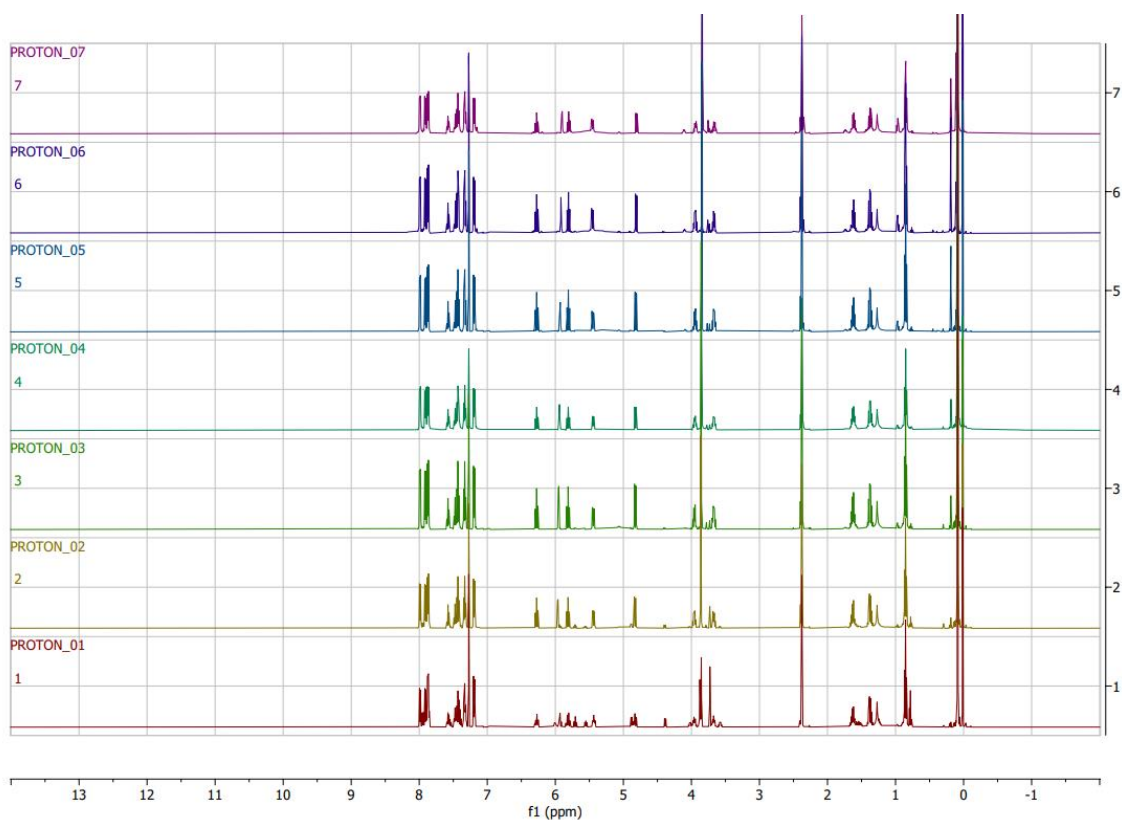
***Graph 14**- NMR of anomerisation of (7) at 45°C*

74

6. Reference

1 Carbohydrate | Definition, Classification, & Examples | Britannica, https://www.britannica.com/science/carbohydrate, (accessed 22 February 2023).

2 John F. Robyt, *Essentials of Carbohydrate Chemistry*, Springer, 1998.

3 L. Cole and P. R. Kramer, *Human Physiology, Biochemistry and Basic Medicine*, Elsevier, 2016.

4 Carbohydrates: Types & Health Benefits, https://my.clevelandclinic.org/health/articles/15416-carbohydrates, (accessed 2 June 2023).

5 F. Hossain and P. R. Andreana, *Pharmaceuticals*, , DOI:10.3390/ph12020084.

6 X. Cao, X. Du, H. Jiao, Q. An, R. Chen, P. Fang, J. Wang and B. Yu, *Acta Pharm Sin B*, 2022, **12**, 3783–3821.

7 D. B. Werz and P. H. Seeberger, *Chem. Eur. J*, 2005, **11**, 3194–3206.

8 B. K. Brandley and R. L. Schnaar, *J Leukoc Biol*, 1986, **40**, 97–111.

9 Francesca Vasile, Maddalena Panigada, Antonio Siccardi, Donatella Potenza and Guido Tiana, *Int J Mol Sci*, , DOI:10.3390/ijms19051267.

10 S. Naithani, S. S. Komath, A. Nonomura and G. Govindjee, *J Plant Physiol*, , DOI:10.1016/j.jplph.2021.153531.

11 N. E. Zachara, *Lecture 2,* .

12 H. Ghazarian, B. Idoni and S. B. Oppenheimer, *Acta Histochem*, , DOI:10.1016/j.acthis.2010.02.004.

13 S. G. Sáyago-Ayerdi, Y. Rossez, F. Evgeny, A. Semchenko, D. Garrido, K. J. González-Morelo and M. Vega-Sagardía, *Frontiers in Microbiology* , , DOI:10.3389/fmicb.2020.591568.

14   J. Rg Breitling and M. Aebi, *Cold Spring Harb Perspect Biol*, ,
      DOI:10.1101/cshperspect.a013359.

15   A. H. Merrill, *Encyclopedia of Cell Biology*, Elsevier, 2022, vol. 1.

16   Glycolipids - Latest research and news | Nature,
      https://www.nature.com/subjects/glycolipids, (accessed 26 July 2023).

17   G. E. Kapellos and T. S. Alexiou, *Modeling Momentum and Mass
      Transport in Cellular Biological Media: From the Molecular to the Tissue
      Scale*, Elsevier Inc., 2013.

18   Glycoproteins and Human Disease - Inka Brockhausen, William Kuhns -
      Google Books,
      https://books.google.ie/books?hl=en&lr=&id=Tyn7CAAAQBAJ&oi=fnd&p
      g=PA2&dq=Glycoproteins+and+their+relationship+to+human+disease&o
      ts=ZSyijpQc6F&sig=31nRHMJpvBBxIi9P17OhrpQZyMo&redir_esc=y#v=on
      epage&q=Glycoproteins%20and%20their%20relationship%20to%20hum
      an%20disease&f=false, (accessed 18 July 2023).

19   Gentamicin (Injection Route) - Mayo Clinic,
      https://www.mayoclinic.org/drg-20074471?p=1, (accessed 18 July 2023).

20   Paxlovid: a medicine for treating COVID-19 - HSE.ie,
      https://www2.hse.ie/conditions/paxlovid/, (accessed 19 July 2023).

21   A. Gabba, R. Attariya, S. Behren, C. Pett, J. C. van der Horst, H. Yurugi, J.
      Yu, M. Urschbach, J. Sabin, G. Birrane, E. Schmitt, S. J. van Vliet, P.
      Besenius, U. Westerlind and P. V. Murphy, *J Am Chem Soc*, 2022, **145**,
      13027–13037.

22   Doxorubicin (Adriamycin, Rubex) Chemotherapy Drug Information,
      https://chemocare.com/chemotherapy/drug-info/doxorubicin.aspx,
      (accessed 11 July 2023).

23   K. Liu, X. Jiang and P. Hunziker, *Nanoscale*, 2016, **8**, 16091.

24   M. C. Hewitt, D. A. Snyder and P. H. Seeberger, *J. AM. CHEM. SOC*, 2002, **124**, 13431–13436.

25   M. Zuffo, A. Stucchi, J. Campos-Salinas, M. Cabello-Donayre, M. Martínez-García, E. Belmonte-Reche, J. M. P Erez-Victoria, J. L. Mergny, M. Freccero, J. C. Morales and F. Doria, *European Journal of Medicinal Chemistry* , 2019, **163**, 54–66.

26   W. Zhang, W. Mu, H. Wu and Z. Liang, *Appl Microbiol Biotechnol*, 2019, **103**, 9335–9344.

27   J. J. Bennett and P. V Murphy, *Carbohydr Res*, 2023, **529**, 108845.

28   Conformations and Cyclic Forms of Sugars, https://chem.libretexts.org/Bookshelves/Organic_Chemistry/Map%3A_O rganic_Chemistry_(Vollhardt_and_Schore)/24%3A_Carbohydrates%3A_P olyfunctional_Compounds_in_Nature/24.02%3A_Conformations_and__C yclic__Forms__of_Sugars, (accessed 3 May 2023).

29   16.4: Cyclic Structures of Monosaccharides - Chemistry LibreTexts, https://chem.libretexts.org/Bookshelves/Introductory_Chemistry/Basics _of_General_Organic_and_Biological_Chemistry_(Ball_et_al.)/16%3A_Ca rbohydrates/16.04%3A_Cyclic_Structures_of_Monosaccharides, (accessed 12 April 2023).

30   W. Pilgrim and P. V Murphy, *J. Org. Chem*, 2010, **75**, 18.

31   The Haworth Projection – Master Organic Chemistry, https://www.masterorganicchemistry.com/2018/01/11/haworth-projections/, (accessed 12 April 2023).

32   C. ; Li, S. ; Wang, Z. A. Marel, G. A. Van Der and J. D. C. Codee, 2021, 200–227.

33   L. Flutto, *Encyclopedia of Food Sciences and*, Elsevier, 2003.

34   Heparin (Intravenous Route, Subcutaneous Route) Description and Brand Names - Mayo Clinic, https://www.mayoclinic.org/drugs-supplements/heparin-intravenous-route-subcutaneous-route/description/drg-20068726, (accessed 16 June 2023).

35   F. Meany, National University of Ireland, Galway , 2022.

36   C. O'Brien, M. Poláková, N. Pitt, M. Tosin and P. V. Murphy, *Chemistry - A European Journal*, 2007, **13**, 902–909.

37   Galacturonic Acid - an overview | ScienceDirect Topics, https://www.sciencedirect.com/topics/medicine-and-dentistry/galacturonic-acid, (accessed 6 July 2023).

38   L. K. Mydock and A. V Demchenko, *Org Biomol Chem*, 2010, **8**, 497–510.

39   Igarashi Kikuo, *THE KOENIGS-KNORR REACTION*, .

40   13.10: Protecting Groups in Organic Synthesis - Chemistry LibreTexts, https://chem.libretexts.org/Bookshelves/Organic_Chemistry/Basic_Principles_of_Organic_Chemistry_(Roberts_and_Caserio)/13%3A_Polyfunctional_Compounds_Alkadienes_and_Approaches_to_Organic_Synthesis/13.10%3A_Protecting_Groups_in_Organic_Synthesis, (accessed 11 July 2023).

41   M. Schelhaas and H. Waldmann, *Angew. Chem.*, 1996, **35**, 2056–2083.

42   Z. Zhang, I. R. Ollmann, X.-S. Ye, R. Wischnat, T. Baasov and C.-H. Wong, *J. Am. Chem. Soc.*, , DOI:10.1021/ja982232s.

43   Chemeurope, https://www.chemeurope.com/en/encyclopedia/Anomer.html, (accessed 15 May 2023).

44   The Key Difference Between Alpha And Beta Glucose, https://www.vedantu.com/neet/difference-between-alpha-and-beta-glucose, (accessed 2 November 2023).

45   J. McConathy and M. J. Owens, *Primary Care Companion J Clin Psychiatry*, 2003, **5**, 70–73.

46   R. Porta, M. Benaglia and A. Puglisi, *OPR&D*, 2015, 2–25.

47   A. Corma and H. García, *Chem Rev*, , DOI:10.1021/cr030680z.

48   P. Krawczuk, 2005.

49   Mutarotation: The α,β Sugars Interconversion, https://psiberg.com/mutarotation/, (accessed 30 July 2023).

50   Polarimetry - Principle, Definition, Instrumentation, https://www.priyamstudycentre.com/2021/12/polarimetry-principle.html, (accessed 1 August 2023).

51   Activation energy (article) | Khan Academy, https://www.khanacademy.org/science/ap-biology/cellular-energetics/enzyme-structure-and-catalysis/a/activation-energy, (accessed 5 July 2023).

52   6.2.3.1: Arrhenius Equation - Chemistry LibreTexts, https://chem.libretexts.org/Bookshelves/Physical_and_Theoretical_Chemistry_Textbook_Maps/Supplemental_Modules_(Physical_and_Theoretical_Chemistry)/Kinetics/06%3A_Modeling_Reaction_Kinetics/6.02%3A_Temperature_Dependence_of_Reaction_Rates/6.2.03%3A_The_Arrhenius_Law/6.2.3.01%3A_Arrhenius_Equation, (accessed 19 August 2023).

53   Anomeric effect, https://www.chem.ucalgary.ca/courses/351/Carey5th/Ch25/ch25-3-2.html, (accessed 18 August 2023).

54   Y. Singh and A. V Demchenko, *Chemistry (Easton)*, 2019, **25**, 1461–1465.

7. Appendix

Appendix 1:

LC-MS Data for 2,3,4-tri-O-acetyl-β-D-galactopyranosiduronic acid, methyl ester

Custom Workflow Report

Agilent | Trusted Answers

Sample Information

Name	TH	Data File Path	D:\Projects\Masshunter data\Data\Trish Holland\TH_10.d
Sample ID		Acq. Time (Local)	2/28/2023 10:18:49 AM (UTC+00:00)
Instrument	PC-CZC2257BQT	Method Path (Acq)	D:\Projects\Masshunter data\Methods\GF_POS_DAD.m
MS Type	QTOF	Version (Acq SW)	6200 series TOF/6500 series Q-TOF (11.0.221.1)
Inj. Vol. (ul)	2	IRM Status	Success
Position	P1-B2	Method Path (DA)	D:\Projects\Masshunter data\Data\Trish Holland\TH_10.d\Results\Qual\Version4\GF_POS_DAD.m
Plate Pos.		Target Source Path	
Operator	SYSTEM (SYSTEM)	Result Summary	1 qualified (1 targets)

Sample Chromatograms
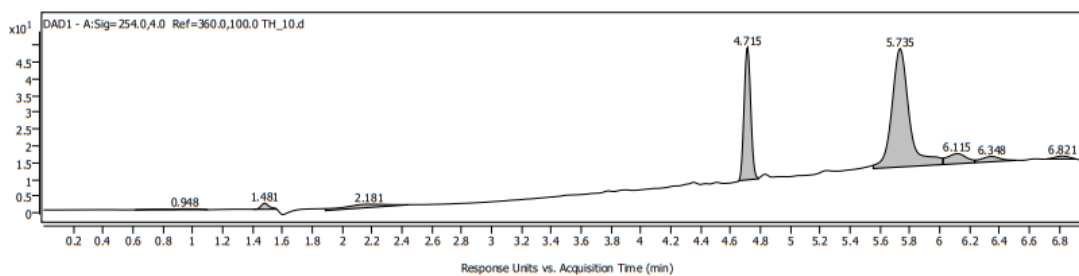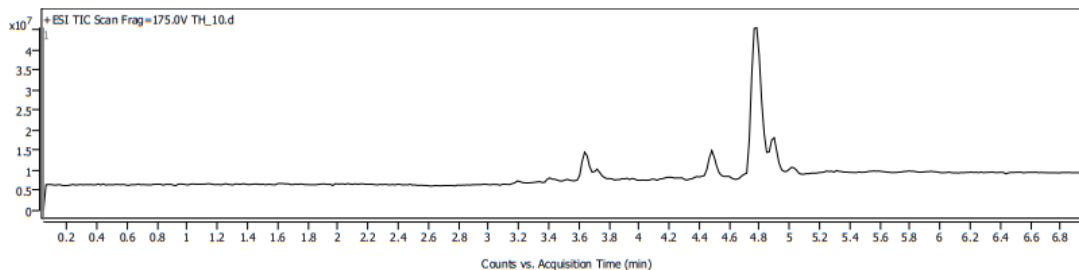
Chromatogram Peaks

Peak	RT	Height	Area	Area %
1	0.948	0	4	1.42
2	1.481	2	7	2.45
3	2.181	1	20	7.12
4	4.715	39	122	42.58
5	5.735	35	286	100.00
6	6.115	3	27	9.53
7	6.348	2	14	5.03
8	6.821	1	6	2.01
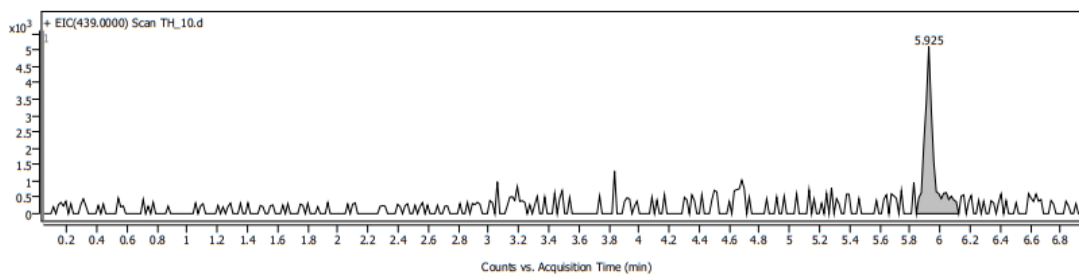
Chromatogram Peaks

Peak	RT	Height	Area	Area %
1	5.925	5104	21125	100.00

Custom Workflow Report

Agilent | Trusted Answers

Compound Summary

Cpd	Name	Formula	RT	Mass	CAS	ID Source	Score	Score (Lib)	Score (DB)	Score (MFG)	Algorithm
1		C20 H22 O11	4.898	438.1166		FBF	99.69				FBF

Compound Details

Cpd. 1: C20 H22 O11

Name	Formula	RT	RI	Mass	Score	Algorithm	Lib/DB
	C20 H22 O11	4.898		438.1166	99.69	FBF	

Species	m/z	Score (Lib)	Num Spectra	Score (DB)	Score (MFG)	Score (RT)
(M+NH4)+ (M+Na)+ (M+K)+	456.1505 461.1057 477.0798					

Compound ID Table

Name	Formula	Species	RT	RT Diff	Mass	CAS	ID Source	Score	Score (DB)	Score (MFG)
	C20 H22 O11	(M+NH4)+ (M+Na)+ (M+K)+	4.898		438.1166		FBF	99.69		

Compound Chromatograms (overlaid)   Structure
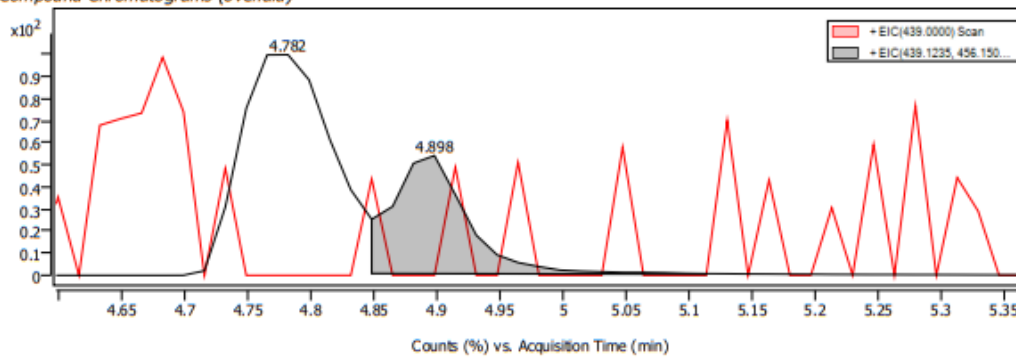
Counts (%) vs. Acquisition Time (min)

Compound Chromatograms (overlaid)

Counts (%) vs. Acquisition Time (min)

Compound Chromatogram(s)

Counts vs. Acquisition Time (min)

81

Agilent | Trusted Answers
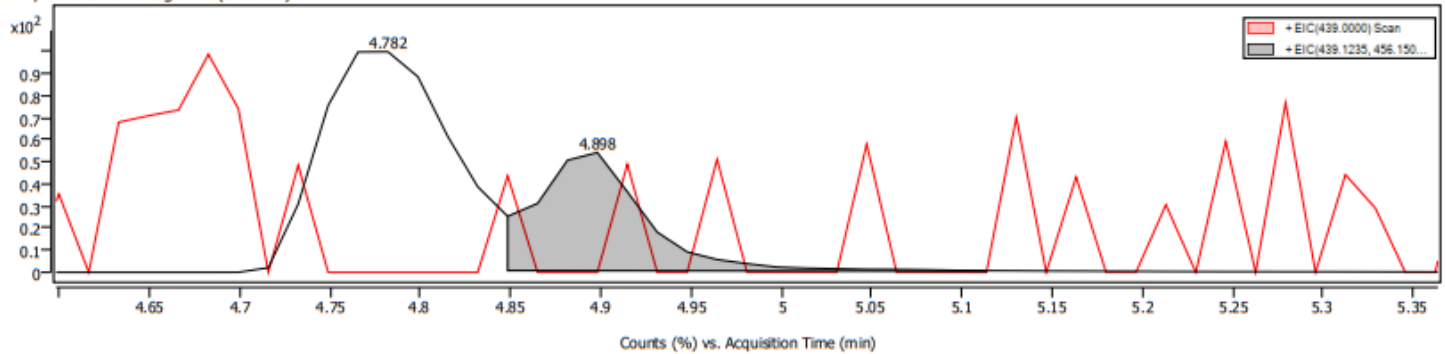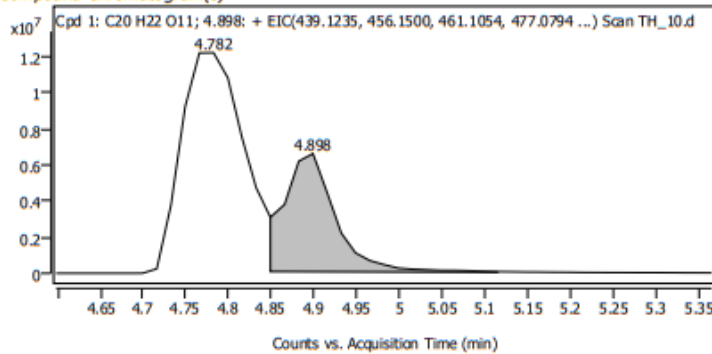
Compound Spectra (overlaid)

Cpd 1: C20 H22 O11; 4.898: + FBF Spectrum (rt: 4.848-4.865, 4.915-4.948 min) TH_10.d Subtract
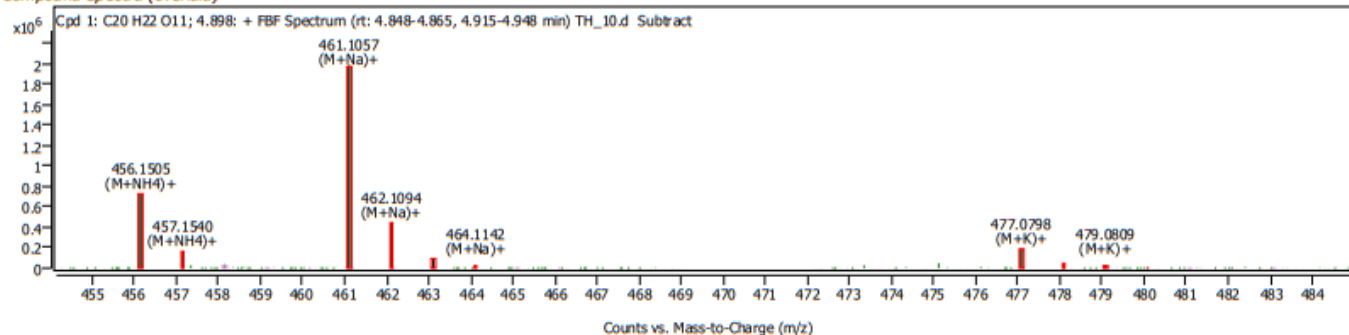
Spectrum Peaks

m/z	Z	Abund	Diff (ppm)	Height %	Height % (Calc)	Ion Species	Formula
456.1505	1	729061	1.08	100.00	100.00	(M+NH4)+	C20H22O11
457.1540	1	165325	1.33	22.68	22.71	(M+NH4)+	C20H22O11
461.1057	1	1986730	0.51	100.00	100.00	(M+Na)+	C20H22O11
462.1094	1	437138	1.21	22.00	22.30	(M+Na)+	C20H22O11
463.1111	1	93784	0.22	4.72	4.63	(M+Na)+	C20H22O11
464.1142	1	11679	1.01	0.59	0.66	(M+Na)+	C20H22O11
477.0798	1	188334	0.86	100.00	100.00	(M+K)+	C20H22O11
478.0828	1	41886	0.13	22.24	22.32	(M+K)+	C20H22O11
479.0809	1	22635	1.06	12.02	11.85	(M+K)+	C20H22O11
480.0822	1	4576	-1.47	2.43	2.27	(M+K)+	C20H22O11

Compound Spectra

Cpd 1: C20 H22 O11; 4.898: + FBF Spectrum (rt: 4.848-4.865, 4.915-4.948 min) TH_10.d Subtract
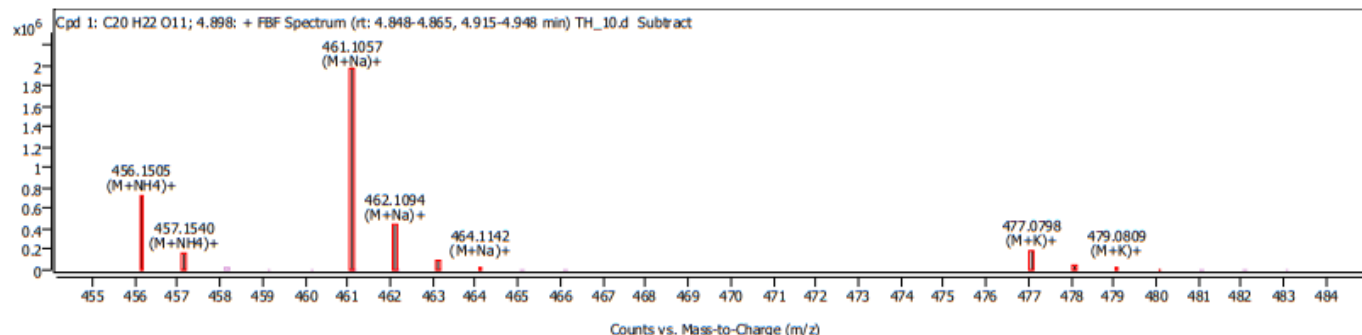
Spectrum Peaks

m/z	m/z (Calc)	Diff (ppm)	Abund	Height %	Height % (Calc)	Ion Species	Z
456.1505	456.1500	1.08	729061	100.00	100.00	(M+NH4)+	1
457.1540	457.1533	1.33	165325	22.68	22.71	(M+NH4)+	1
461.1057	461.1054	0.51	1986730	100.00	100.00	(M+Na)+	1
462.1094	462.1088	1.21	437138	22.00	22.30	(M+Na)+	1
463.1111	463.1110	0.22	93784	4.72	4.63	(M+Na)+	1
464.1142	464.1137	1.01	11679	0.59	0.66	(M+Na)+	1
477.0798	477.0794	0.86	188334	100.00	100.00	(M+K)+	1
478.0828	478.0828	0.13	41886	22.24	22.32	(M+K)+	1
479.0809	479.0804	1.06	22635	12.02	11.85	(M+K)+	1
480.0822	480.0829	-1.47	4576	2.43	2.27	(M+K)+	1

Cpd 1: C20 H22 O11; 4.898: + Scan (rt: 4.848-4.865, 4.915-4.948 min, 5 scans) TH_10.d
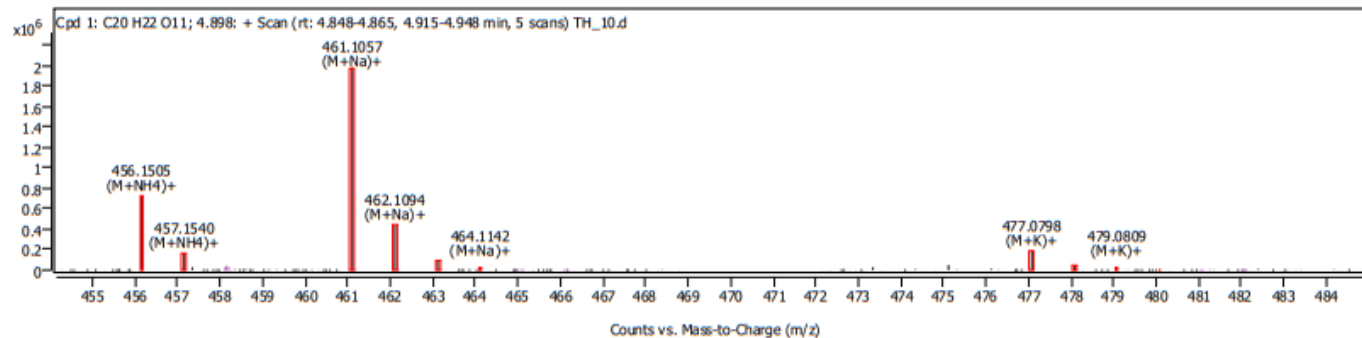
Appendix 2:

Calibration data for compounds **(4)**, **(5)**, **(6)** and **(7)**:

Calibration curve for compound **(4)**
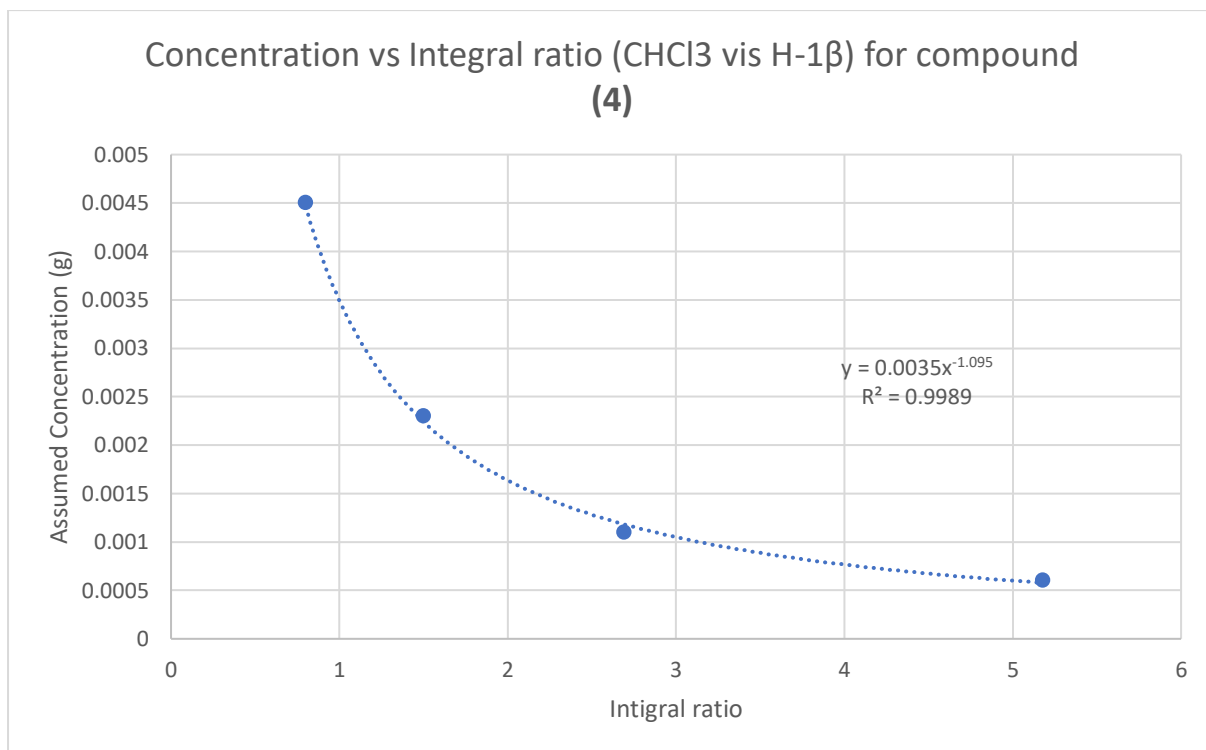
Calibration curve for compound **(5)**

Calibration curve for compound (6)

Concentration vs Integral ratio (CHCl$_3$ vis H-1β) for compound **(6)**

$y = 0.0035x^{-1.087}$
$R^2 = 0.9823$

Assumed Concentration (g) vs Integral Ratio

Calibration curve for compound (7)

Concentration vs Integral ratio (CHCl$_3$ vis H-1β) for compound **(7)**

$y = 0.0032x^{-1.105}$
$R^2 = 1$

Assumed Concentration vs Integral Ratio
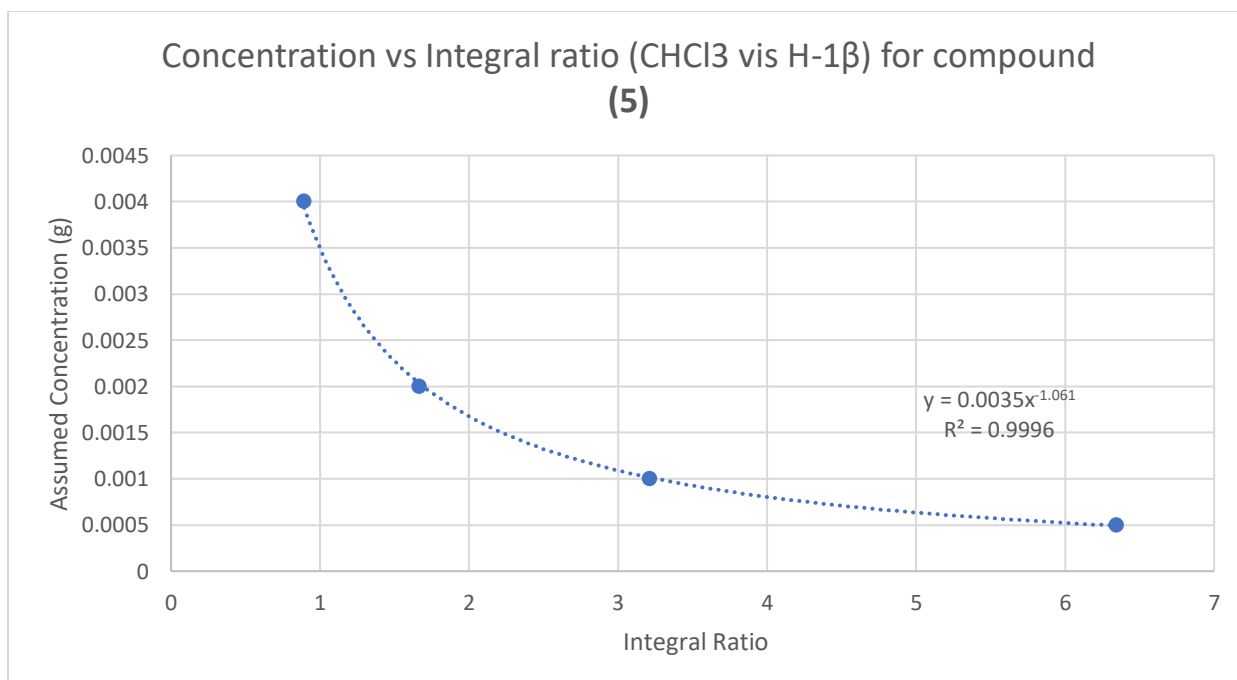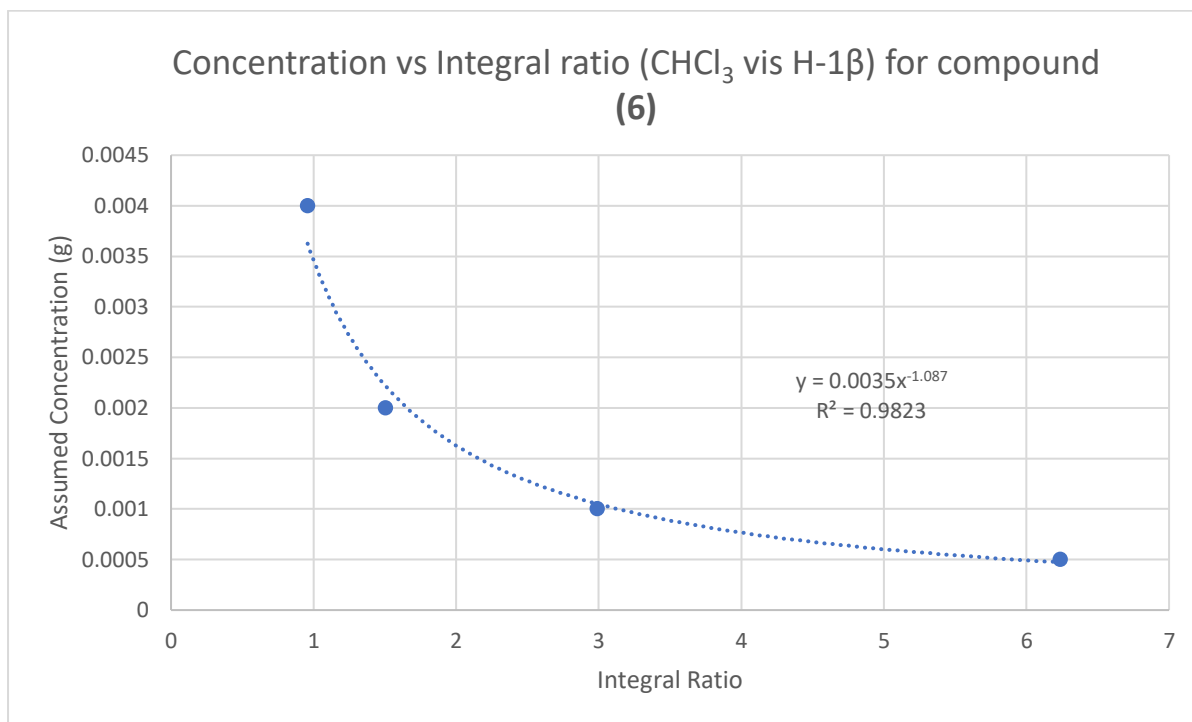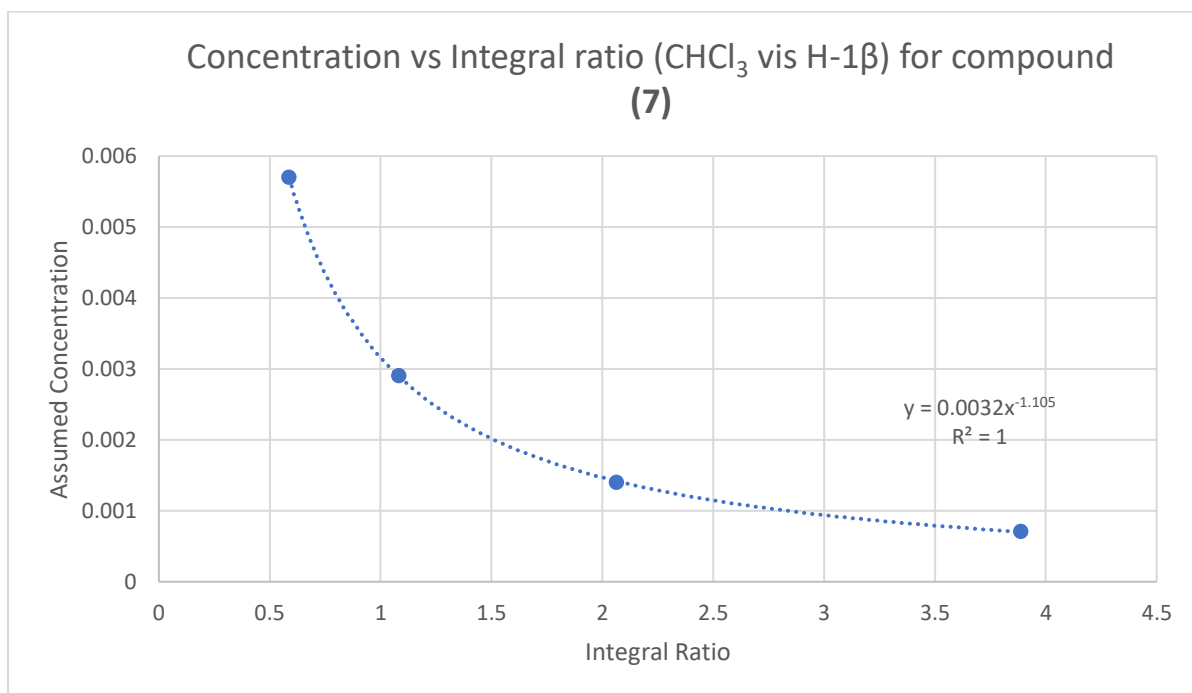
Appendix 3

Kinetic data for compound (4)
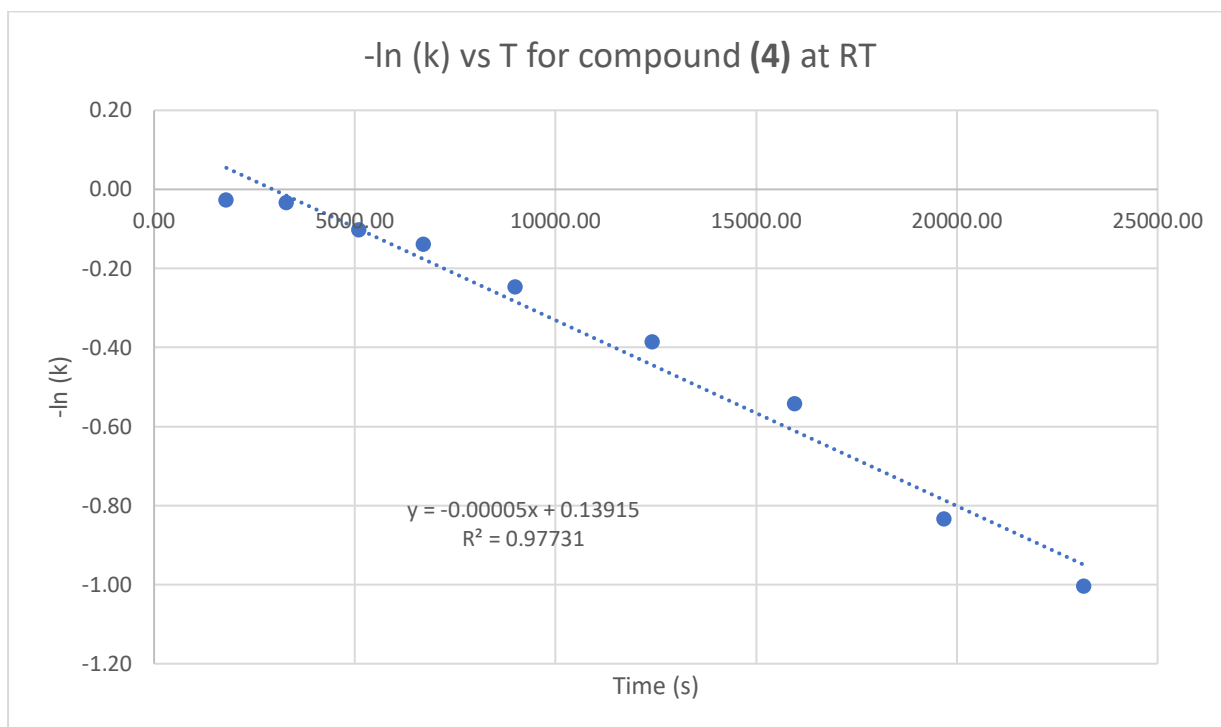
-ln (k) vs T for compound **(4)** at RT

$y = -0.00005x + 0.13915$
$R^2 = 0.97731$

Time (min)	Time (s)	Integration β	Integration CHCL3	Ratio H-1beta:CHCl3	assumed Conc. β	[B]o-[β]e/[β]t-[β]e	Ln[K]	-Ln[K]
30.00	1800.00	0.32	0.29	0.91	0.0039	1.03	0.03	-0.03
55.00	3300.00	0.34	0.31	0.91	0.0039	1.03	0.03	-0.03
85.00	5100.00	0.32	0.31	0.97	0.0036	1.11	0.10	-0.10
112.00	6720.00	0.31	0.31	1.00	0.0035	1.15	0.14	-0.14
150.00	9000.00	0.30	0.33	1.10	0.0032	1.28	0.25	-0.25
207.00	12420.00	0.29	0.36	1.24	0.0028	1.47	0.39	-0.39
266.00	15960.00	0.26	0.37	1.42	0.0024	1.72	0.54	-0.54
328.00	19680.00	0.23	0.42	1.83	0.0018	2.30	0.83	-0.83
386.00	23160.00	0.19	0.40	2.11	0.0015	2.73	1.00	-1.00

Kinetic data for compound **(5)**

Calculated rate constants for **(5)** at 25°C
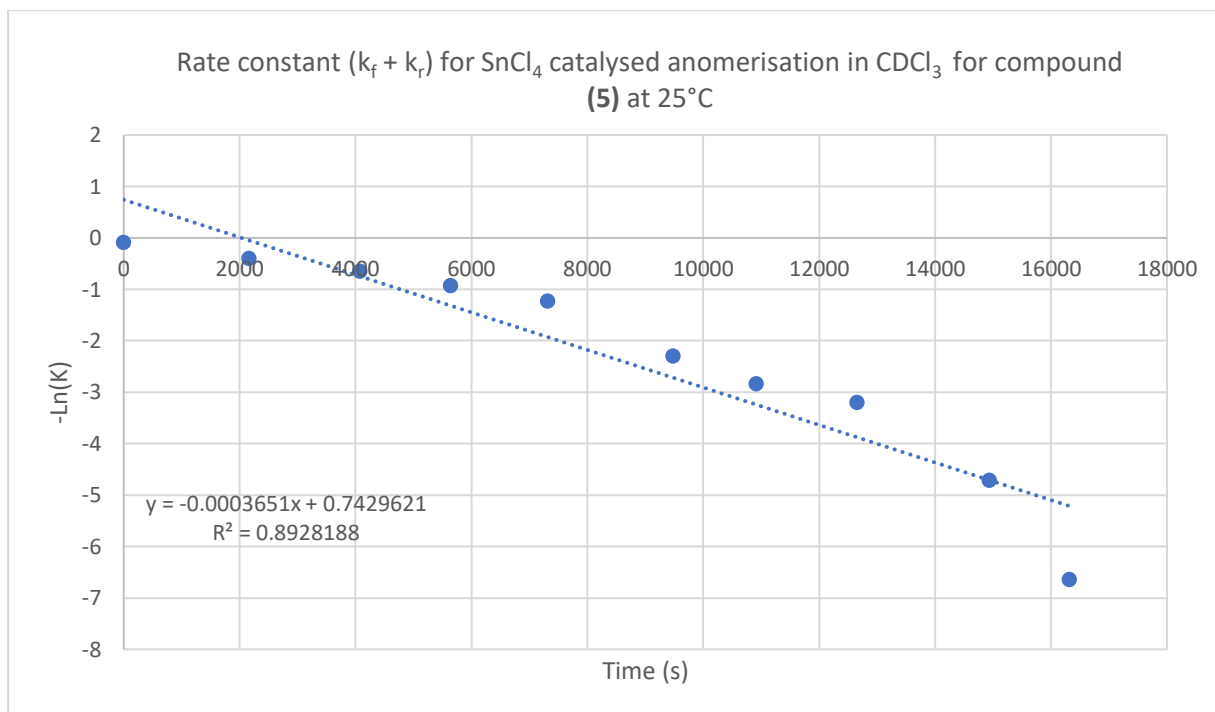
Rate constant ($k_f + k_r$) for SnCl$_4$ catalysed anomerisation in CDCl$_3$ for compound **(5)** at 25°C

$y = -0.0003651x + 0.7429621$
$R^2 = 0.8928188$

Time (min)	Time (s)	Integration β	Integration CHCL3	Ratio H-1beta:CHCl3	assumed Conc. β	[β]o-[β]e/[β]t-[β]e	Ln[K]	-Ln[K]
0.00	0.00	0.94	1.73	1.84	0.00183	1.10	0.09	-0.09
36.00	2160.00	0.74	1.78	2.41	0.00138	1.50	0.41	-0.41
68.00	4080.00	0.59	1.75	2.97	0.00110	1.93	0.66	-0.66
94.00	5640.00	0.49	1.82	3.71	0.00087	2.55	0.94	-0.94
122.00	7320.00	0.37	1.74	4.70	0.00068	3.46	1.24	-1.24
158.00	9480.00	0.19	1.78	9.37	0.00033	10.00	2.30	-2.30
182.00	10920.00	0.15	1.82	12.13	0.00025	17.27	2.85	-2.85
211.00	12660.00	0.13	1.80	13.85	0.00022	24.69	3.21	-3.21
249.00	14940.00	0.10	1.87	18.70	0.00016	112.41	4.72	-4.72

Calculated rate constants for **(5)** at 35°C

Rate constant (k_f + k_r) for SnCl$_4$ catalysed anomerisation in CDCl$_3$ for compound **(5)** at 35°C

$y = -0.0002x - 0.8188$
$R^2 = 0.916$

(x-axis: Time (s), y-axis: -ln[K])
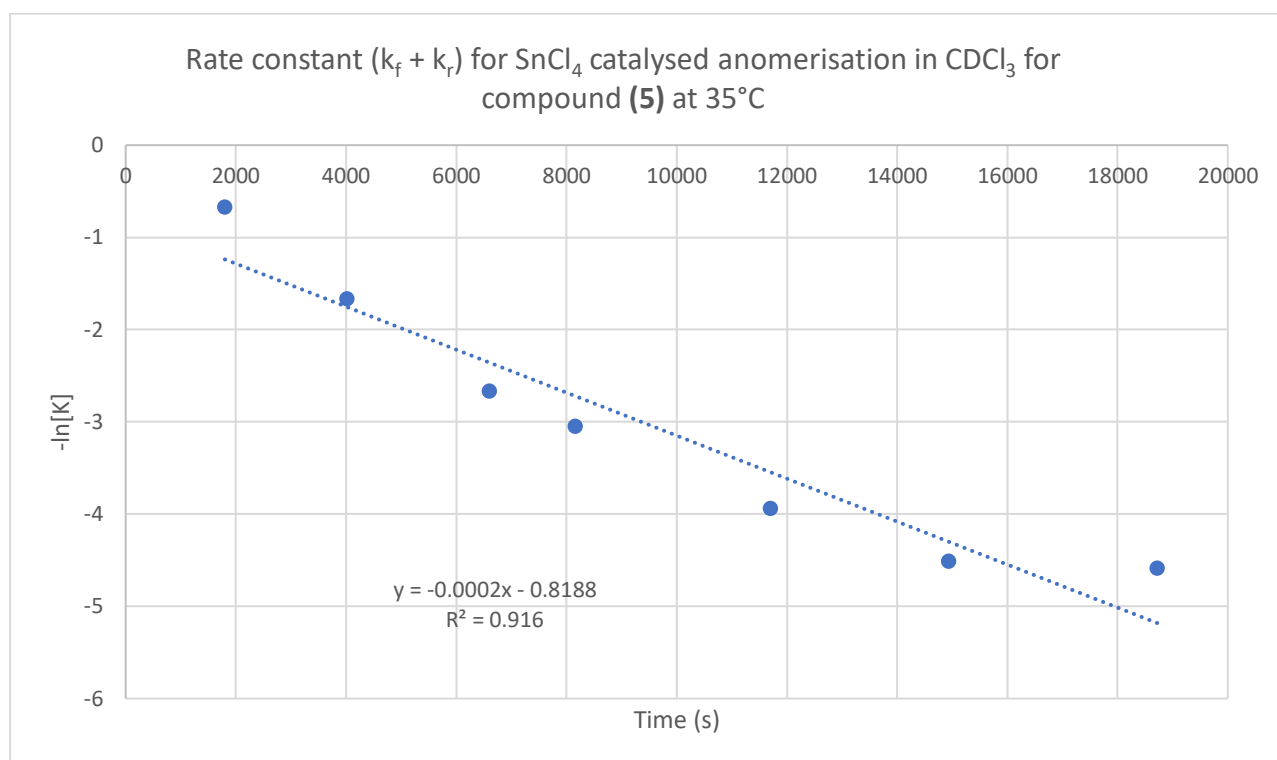
Time (min)	Time (s)	Integration β	Integration CHCL3	Ratio H-1beta:CHCl3	assumed Conc. B	[B]o-[β]e/[β]t-[β]e	Ln[K]	-Ln[K]
10.00	600.00	0.93	1.27	1.37	0.00251	1.61	0.48	-0.48
52.00	3120.00	0.54	1.54	2.85	0.00115	3.70	1.31	-1.31
87.00	5220.00	0.24	1.24	5.17	0.00061	7.55	2.02	-2.02
152.00	9120.00	0.06	1.17	19.50	0.00015	72.18	4.28	-4.28
239.00	14340.00	0.04	1.15	28.75	0.00010	1104.90	7.01	-7.01
240.00	14400.00	0.04	1.12	28.00	0.00010	614.39	6.42	-6.42

Calculated rate constants for **(5)** at 45°C
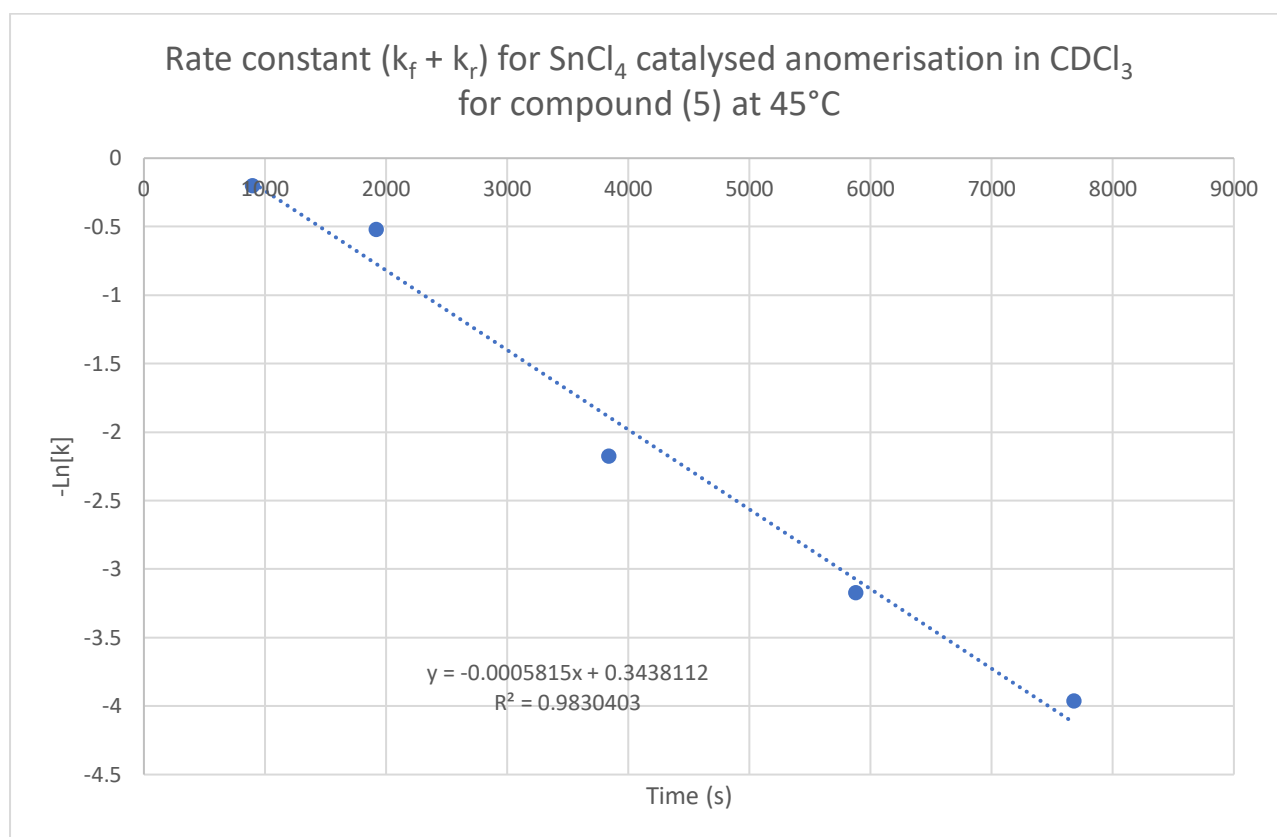
Rate constant ($k_f + k_r$) for SnCl$_4$ catalysed anomerisation in CDCl$_3$ for compound (5) at 45°C

$$y = -0.0005815x + 0.3438112$$
$$R^2 = 0.9830403$$

X-axis: Time (s)
Y-axis: -Ln[k]

Time (min)	Time (s)	Integration β	Integration CHCL3	Ratio H-1beta:CHCl3	assumed Conc. β	[B]o-[β]e/[β]t-[β]e	Ln[K]	-Ln[K]
15.00	900.00	1.03	1.09	1.06	0.0033	1.23	0.20	-0.20
32.00	1920.00	0.65	0.91	1.40	0.0024	1.68	0.52	-0.52
64.00	3840.00	0.30	0.82	5.13	0.0006	8.82	2.18	-2.18
98.00	5880.00	0.15	0.77	8.89	0.0003	23.86	3.17	-3.17
128.00	7680.00	0.09	0.80	11.71	0.0003	52.68	3.96	-3.96

Calibration curve for compound **(6)**

Concentration vs Integral ratio ($CHCl_3$ vis H-1β) for compound **(6)**

$y = 0.0035x^{-1.087}$
$R^2 = 0.9823$

Calculated rate constants for **(6)** at 25°C

Rate constant ($k_f + k_r$) for $SnCl_4$ catalysed anomerisation in CDCl3 for compound **(6)** at 25°C

$y = -0.00004x + 0.03253$
$R^2 = 0.99278$
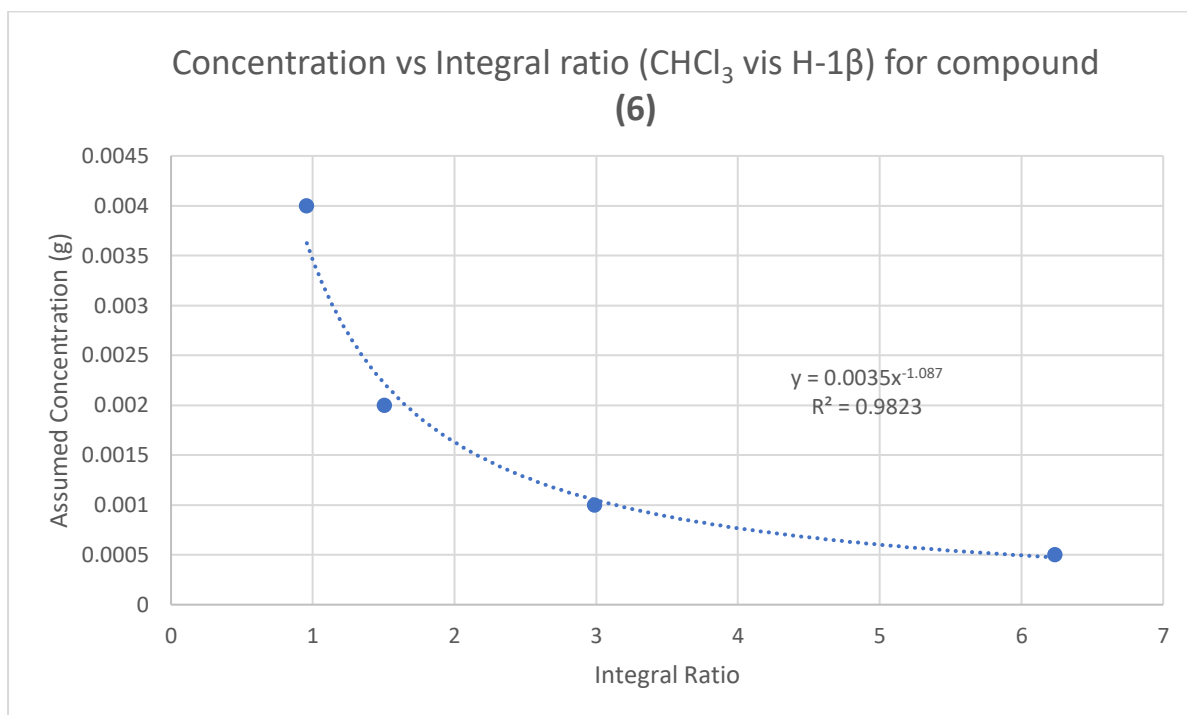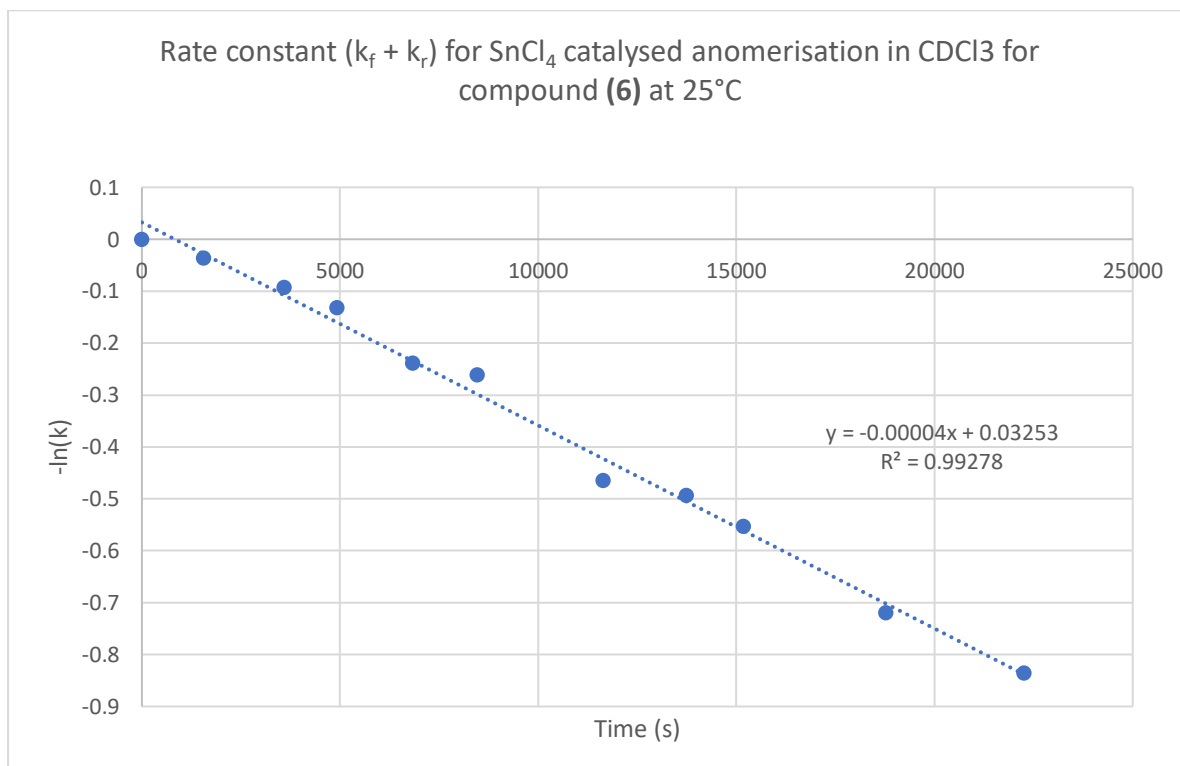
Time (min)	Time (s)	Integration β	Conc. β	[B]o-[β]e/[β]t-[β]e	Ln[K]	-Ln[K]
0.00	0.00	0.94	0.00061	0.01	-4.68	4.68
26.00	1560.00	0.92	0.00059	0.01	-4.65	4.65
60.00	3600.00	0.87	0.00056	0.01	-4.60	4.60
82.00	4920.00	0.83	0.00054	0.01	-4.56	4.56
114.00	6840.00	0.76	0.00049	0.01	-4.46	4.46
141.00	8460.00	0.74	0.00048	0.01	-4.44	4.44
194.00	11640.00	0.62	0.00040	0.01	-4.26	4.26
229.00	13740.00	0.60	0.00039	0.01	-4.23	4.23
253.00	15180.00	0.57	0.00037	0.02	-4.18	4.18
313.00	18780.00	0.49	0.00032	0.02	-4.04	4.04
371.00	22260.00	0.44	0.00029	0.02	-3.94	3.94

Calculated rate constants for **(6)** at 35°C
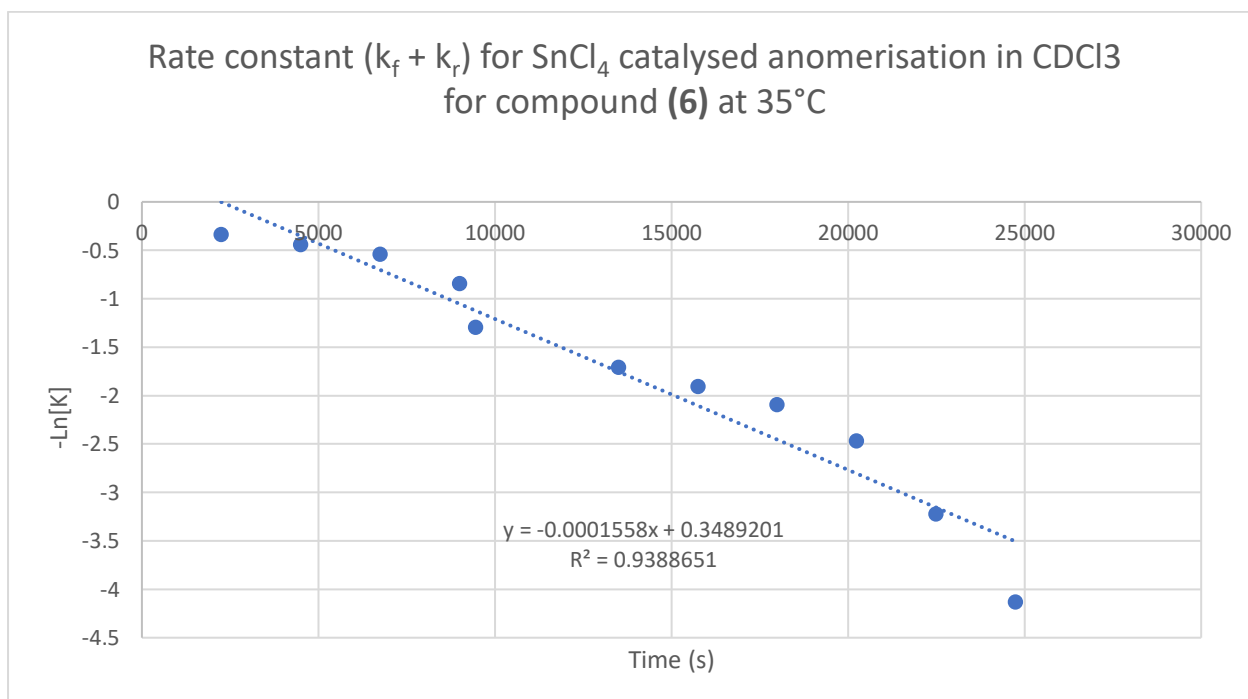
Rate constant ($k_f + k_r$) for SnCl$_4$ catalysed anomerisation in CDCl3 for compound **(6)** at 35°C

$y = -0.0001558x + 0.3489201$
$R^2 = 0.9388651$

Time (min)	Time(sec)	Integration β	Integration of CHCl3	Ratio of H1 beta:CHCl3	Conc. β	[B]o-[β]e/[β]t-[β]e	Ln[K]	-Ln[K]
37.50	2250.00	0.95	1.24	1.31	0.00261	1.40	0.34	-0.34

75.00	4500.00	0.86	1.25	1.45	0.00233	1.56	0.45	-0.45
112.50	6750.00	0.77	1.24	1.60	0.00210	1.72	0.54	-0.54
150.00	9000.00	0.58	1.26	2.16	0.00151	2.33	0.85	-0.85
157.50	9450.00	0.36	1.25	3.44	0.00091	3.66	1.30	-1.30
225.00	13500.00	0.23	1.25	5.42	0.00056	5.54	1.71	-1.71
262.50	15750.00	0.18	1.26	6.85	0.00043	6.75	1.91	-1.91
300.00	18000.00	0.14	1.24	8.65	0.00034	8.12	2.09	-2.09
337.50	20250.00	0.08	1.26	14.89	0.00019	11.85	2.47	-2.47

Calculated rate constants for **(6)** at 45°C
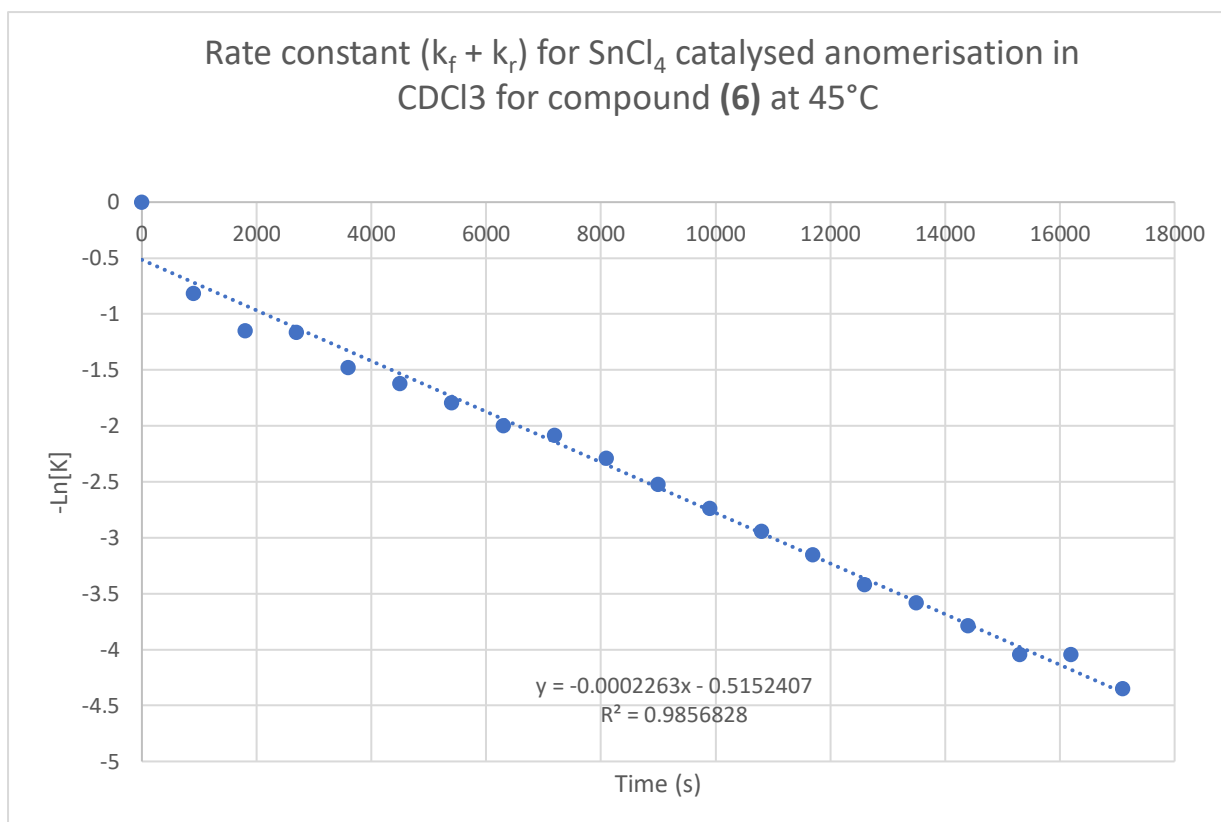
Rate constant ($k_f + k_r$) for $SnCl_4$ catalysed anomerisation in CDCl3 for compound **(6)** at 45°C

$y = -0.0002263x - 0.5152407$
$R^2 = 0.9856828$

Time (min)	Time(sec)	Integration β	Integration of CHCl3	Ratio of H1 beta:CHCl3	Conc. β	[B]o-[β]e/[β]t-[β]e	Ln[K]	-Ln[K]
15.00	900.00	0.82	1.51	1.84	0.00180	2.26	0.82	-0.82
30.00	1800.00	0.68	1.68	2.47	0.00131	3.15	1.15	-1.15
45.00	2700.00	0.59	1.48	2.51	0.00129	3.21	1.17	-1.17
60.00	3600.00	0.51	1.68	3.29	0.00096	4.39	1.48	-1.48
75.00	4500.00	0.44	1.64	3.73	0.00084	5.07	1.62	-1.62
90.00	5400.00	0.38	1.64	4.32	0.00071	6.02	1.80	-1.80
105.00	6300.00	0.32	1.64	5.13	0.00059	7.40	2.00	-2.00
120.00	7200.00	0.28	1.54	5.50	0.00055	8.06	2.09	-2.09
135.00	8100.00	0.23	1.49	6.48	0.00046	9.87	2.29	-2.29
150.00	9000.00	0.19	1.48	7.79	0.00038	12.47	2.52	-2.52
165.00	9900.00	0.16	1.47	9.19	0.00031	15.49	2.74	-2.74
180.00	10800.00	0.14	1.49	10.64	0.00027	18.95	2.94	-2.94
195.00	11700.00	0.12	1.48	12.33	0.00023	23.42	3.15	-3.15
210.00	12600.00	0.10	1.47	14.70	0.00019	30.63	3.42	-3.42
225.00	13500.00	0.09	1.46	16.22	0.00017	35.98	3.58	-3.58
240.00	14400.00	0.08	1.46	18.25	0.00015	44.20	3.79	-3.79
255.00	15300.00	0.07	1.46	20.86	0.00013	57.08	4.04	-4.04
270.00	16200.00	0.07	1.46	20.86	0.00013	57.08	4.04	-4.04
285.00	17100.00	0.06	1.44	24.00	0.00011	77.57	4.35	-4.35

Appendix 6: Calibration and kinetic data for compound **(7)**
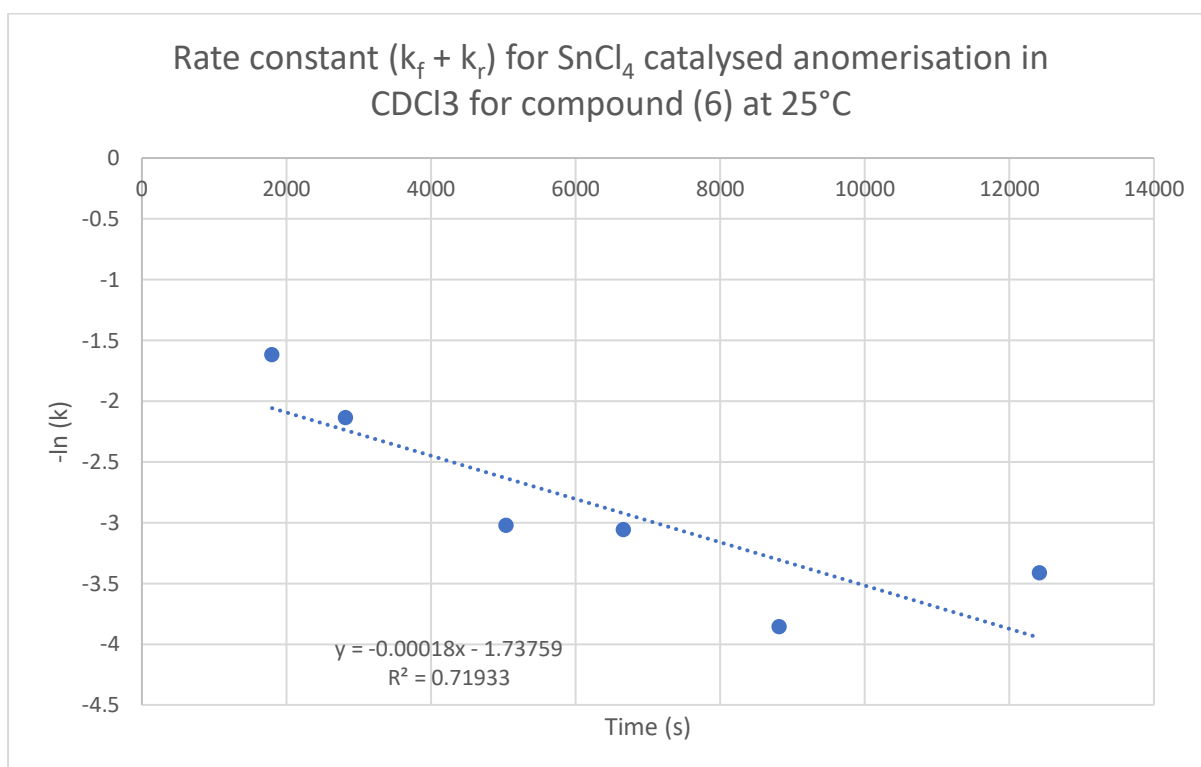
Calibration curve for compound **(7)**
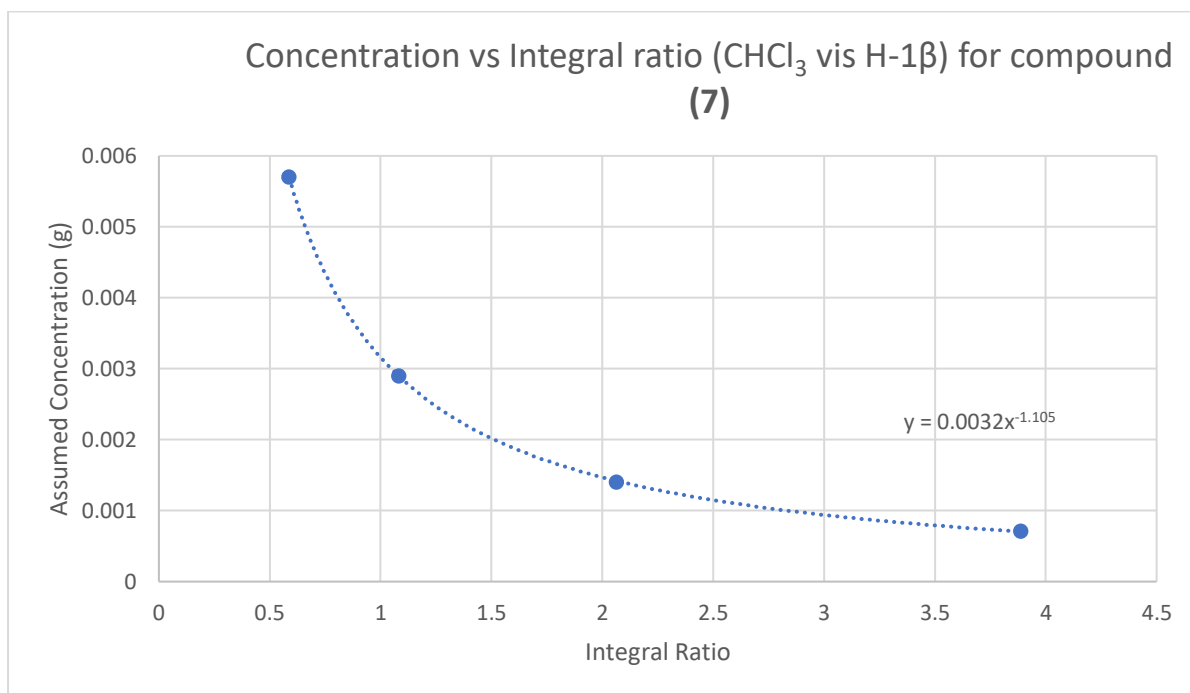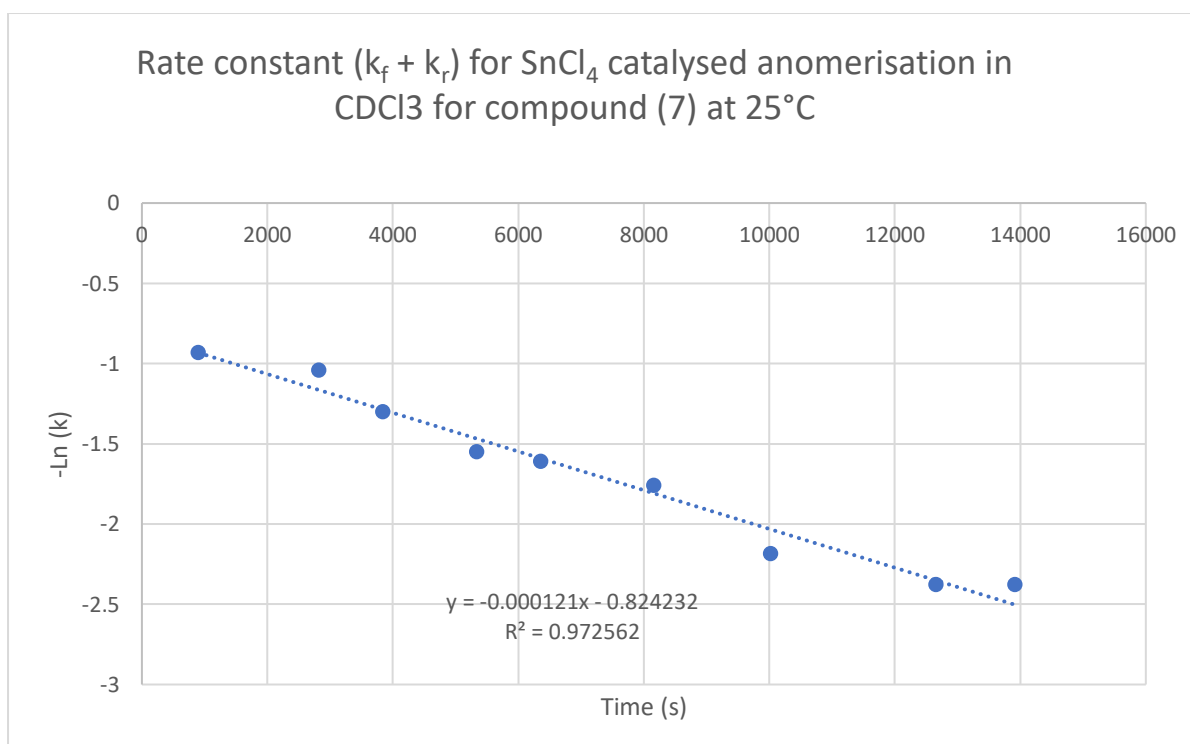
Concentration vs Integral ratio ($CHCl_3$ vis H-1β) for compound **(7)**

$y = 0.0032x^{-1.105}$

Calculated rate constants for **(7)** at 25°C

Rate constant ($k_f + k_r$) for $SnCl_4$ catalysed anomerisation in CDCl3 for compound (7) at 25°C

$y = -0.000121x - 0.824232$
$R^2 = 0.972562$

Time (min)	Time (s)	Integration β	Integration CHCL3	Ratio H-1beta:CHCl3	assumed Conc. β	[B]o-[β]e/[β]t-[β]e	Ln[K]	-Ln[K]
15.00	900.00	0.30	0.52	1.73	0.0020	2.54	0.93	-0.93
47.00	2820.00	0.28	0.52	1.86	0.0018	2.83	1.04	-1.04
64.00	3840.00	0.24	0.52	2.17	0.0015	3.68	1.30	-1.30
89.00	5340.00	0.21	0.52	2.48	0.0013	4.72	1.55	-1.55
106.00	6360.00	0.20	0.51	2.55	0.0013	5.01	1.61	-1.61
136.00	8160.00	0.19	0.52	2.74	0.0012	5.82	1.76	-1.76
167.00	10020.00	0.16	0.52	3.25	0.0010	8.89	2.19	-2.19
211.00	12660.00	0.15	0.52	3.47	0.0009	10.78	2.38	-2.38
232.00	13920.00	0.15	0.52	3.47	0.0009	10.78	2.38	-2.38

Calculated rate constants for **(7)** at 35°C

Rate constant ($k_f + k_r$) for $SnCl_4$ catalysed anomerisation in CDCl3 for compound (6) at 25°C

$y = -0.00018x - 1.73759$
$R^2 = 0.71933$

Time (min)	Time (s)	Integration β	Integration CHCL3	Ratio H-1beta:CHCl3	assumed Conc. β	[B]o-[β]e/[β]t-[β]e	Ln[K]	-Ln[K]
30.00	1800.00	0.16	0.65	4.06	0.00079	5.06	1.62	-1.62
47.00	2820.00	0.10	0.66	6.60	0.00047	8.46	2.14	-2.14
84.00	5040.00	0.04	0.61	15.25	0.00019	20.58	3.02	-3.02
111.00	6660.00	0.04	0.63	15.75	0.00019	21.30	3.06	-3.06
147.00	8820.00	0.02	0.67	33.50	0.00008	47.43	3.86	-3.86
207.00	12420.00	0.03	0.66	22.00	0.00013	30.36	3.41	-3.41

Calculated rate constants for **(7)** at 45°C
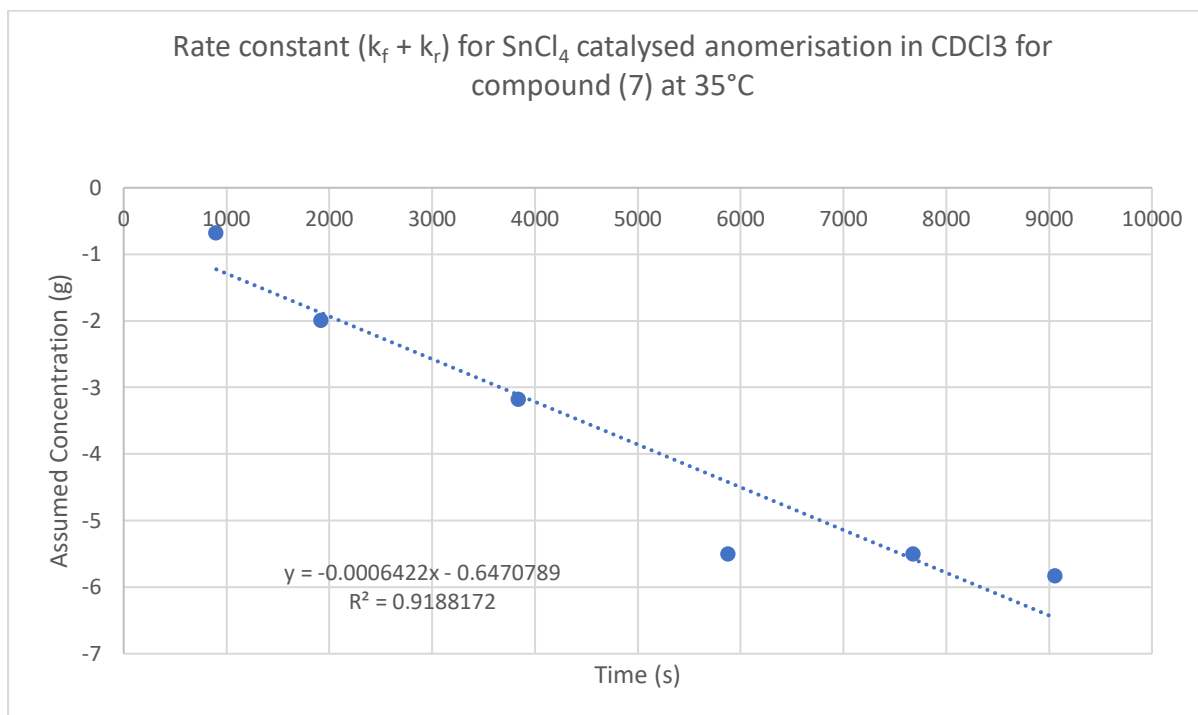
Rate constant ($k_f + k_r$) for SnCl$_4$ catalysed anomerisation in CDCl3 for compound (7) at 35°C

y = -0.0006422x - 0.6470789
R² = 0.9188172

Time (min)	Time (s)	Integration β	Integration CHCL3	Ratio H-1beta:CHCl3	assumed Conc. β	[B]o-[β]e/[β]t-[β]e	Ln[K]	-Ln[K]
15.00	900.00	1.53	2.50	1.63	0.0021	1.97	0.68	-0.68
32.00	1920.00	0.23	1.16	5.04	0.0006	7.32	1.99	-1.99
64.00	3840.00	0.09	1.05	11.67	0.0003	24.01	3.18	-3.18
98.00	5880.00	0.04	1.03	25.75	0.0001	245.72	5.50	-5.50
128.00	7680.00	0.04	1.03	25.75	0.0001	245.72	5.50	-5.50
151.00	9060.00	0.04	1.07	26.75	0.0001	340.33	5.83	-5.83

Graph of the log of the rate constant vs 1/T for compound **(5)**

Ln k vs 1/T for compound (5)

$y = -2130.7x - 0.7498$
$R^2 = 0.9997$

Graph of the log of the rate constant vs 1/T for compound **(6)**

Ln k vs 1/T for compound (6)

$y = -7269.2x + 14.611$
$R^2 = 0.9261$

Graph of the log of the rate constant vs 1/T for compound **(7)**

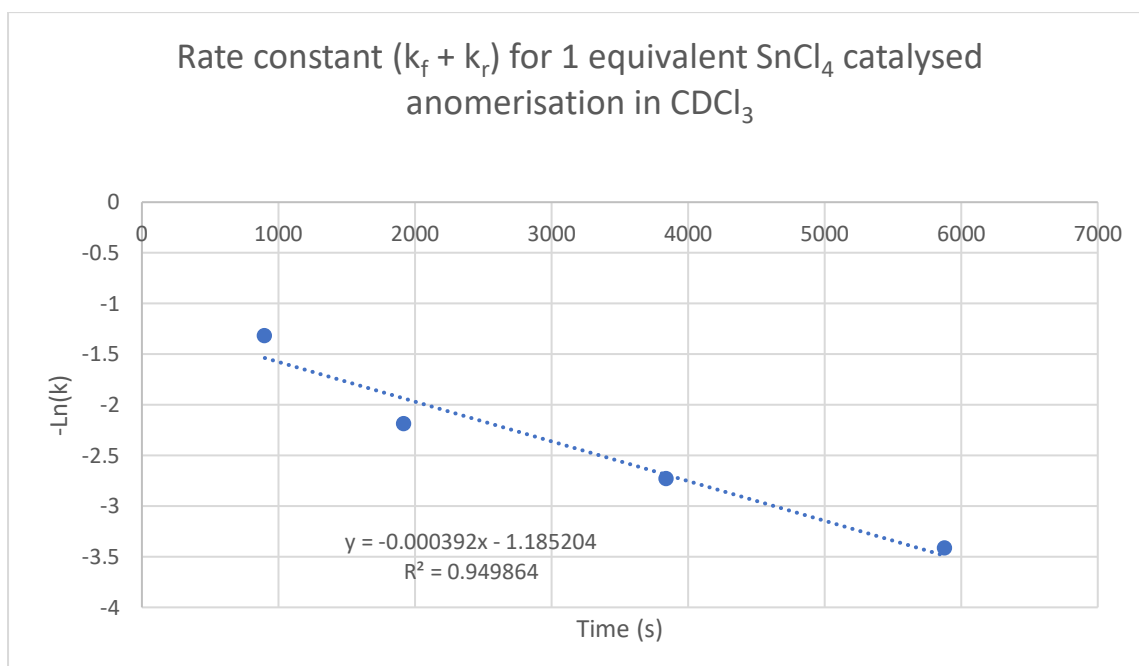Ln K vs 1/T for compound **(7)**

$y = -3721.5x + 3.4603$
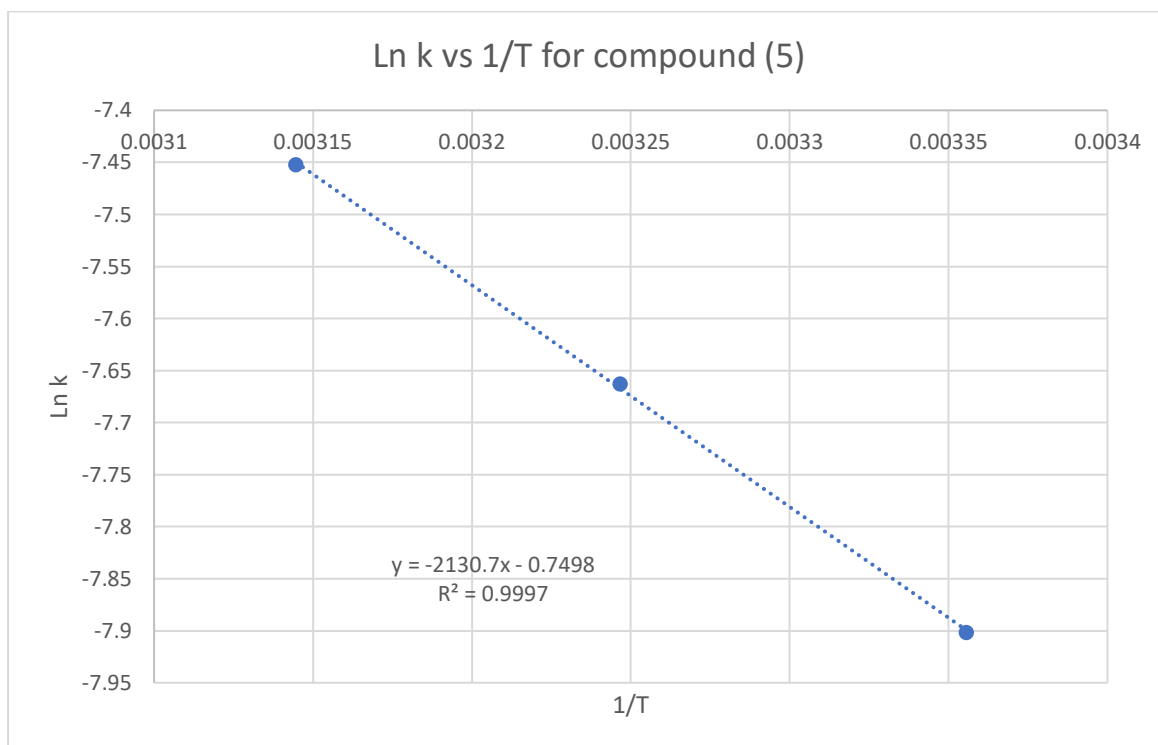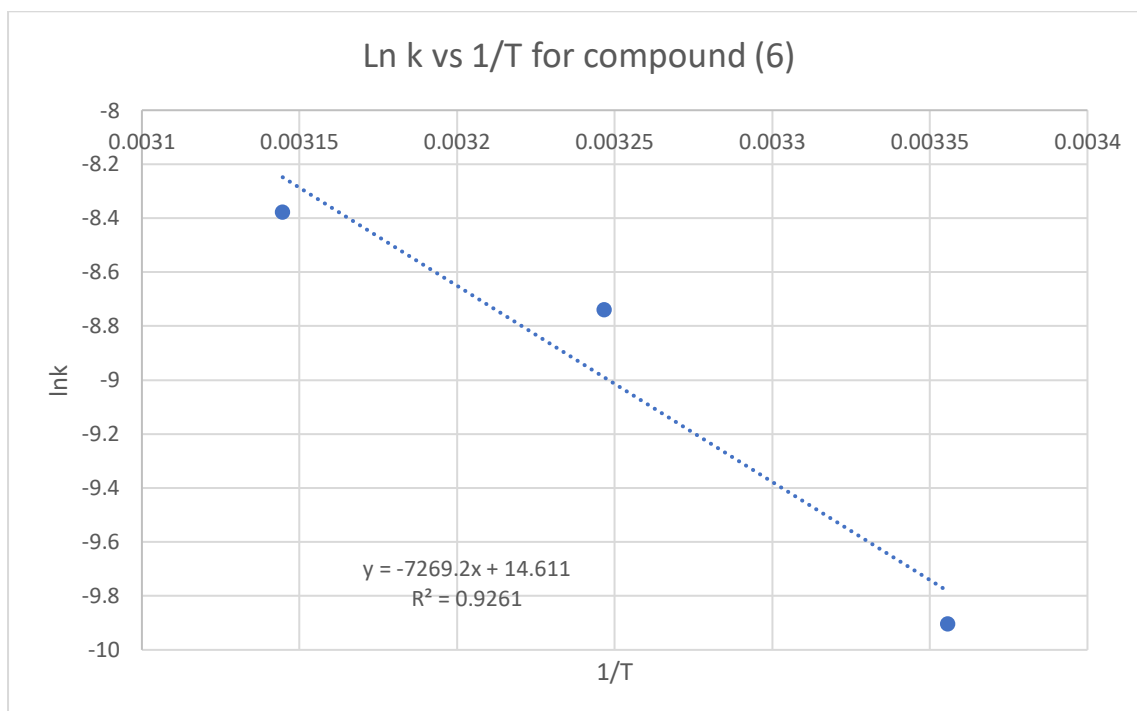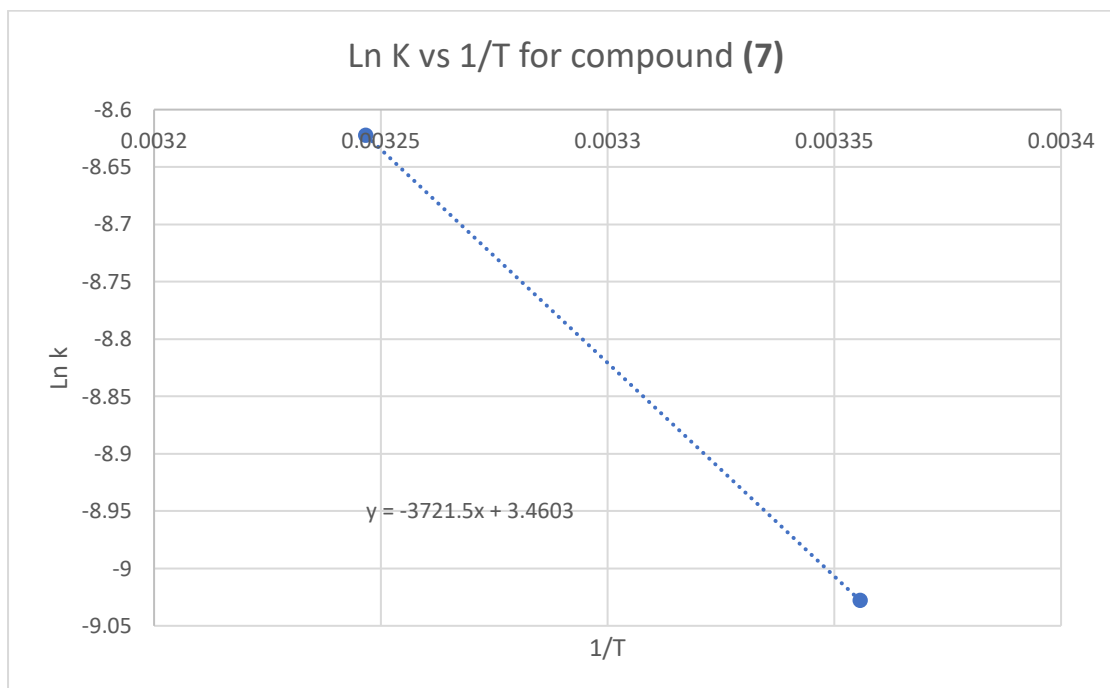
Appendix 8: Graphical data for catalyst concentration experiments

0.5 equivalents:

Rate constant ($k_f + k_r$) for 0.5 equivalent $SnCl_4$ catalysed anomerisation in $CDCl_3$

$y = -0.000250x - 0.475318$
$R^2 = 0.919107$

1 equivalent:

Rate constant ($k_f + k_r$) for 1 equivalent SnCl$_4$ catalysed anomerisation in CDCl$_3$

y = -0.000392x - 1.185204
R² = 0.949864

2 equivalents:

Rate constant ($k_f + k_r$) for 2 equivalent SnCl$_4$ catalysed anomerisation in CDCl$_3$
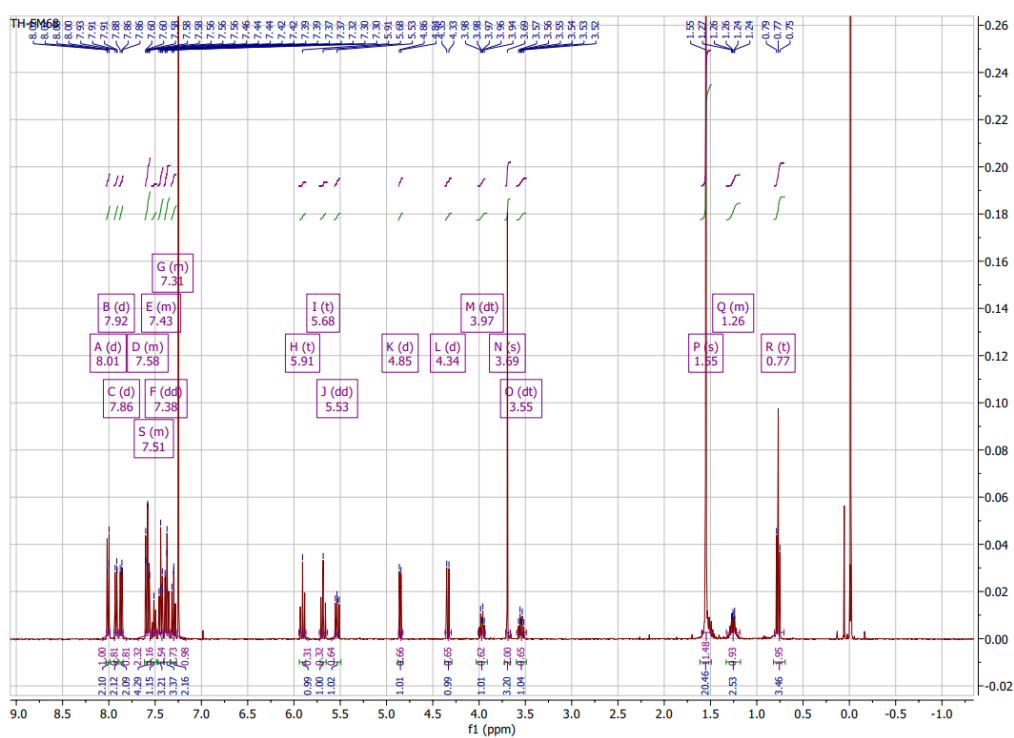
$y = -0.000400x - 0.948805$
$R^2 = 0.967653$
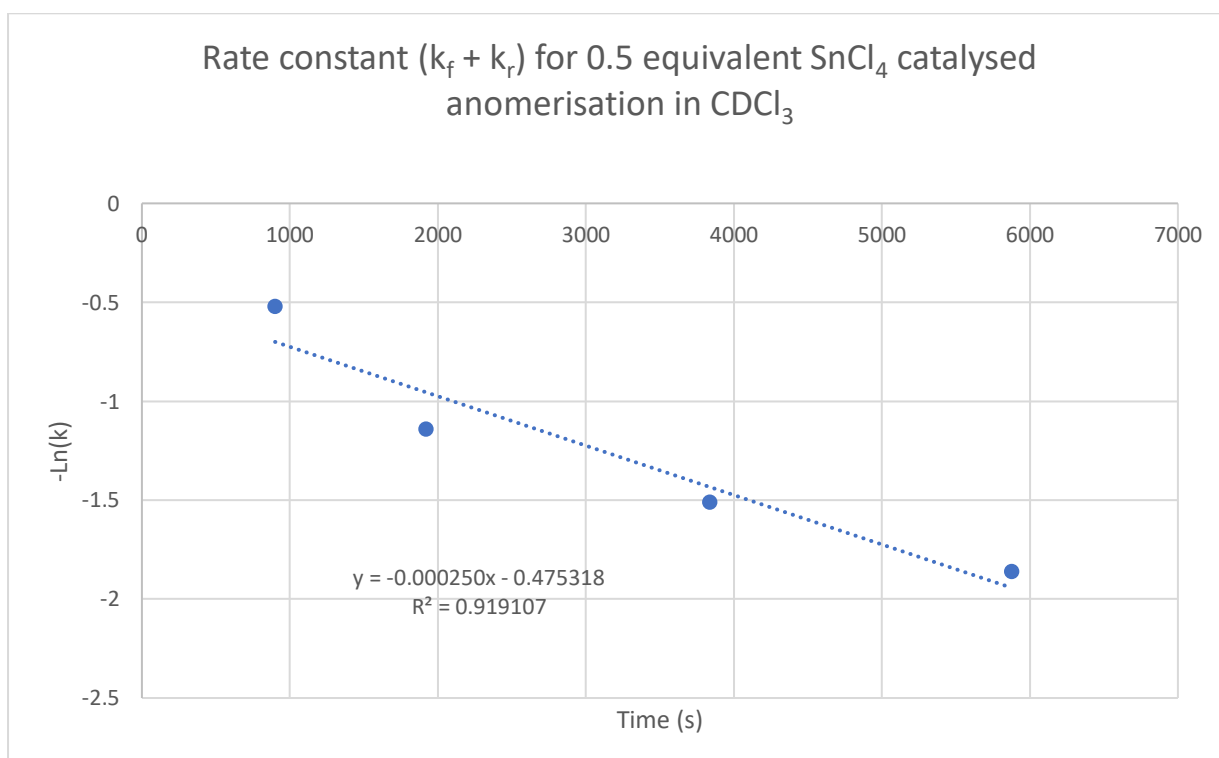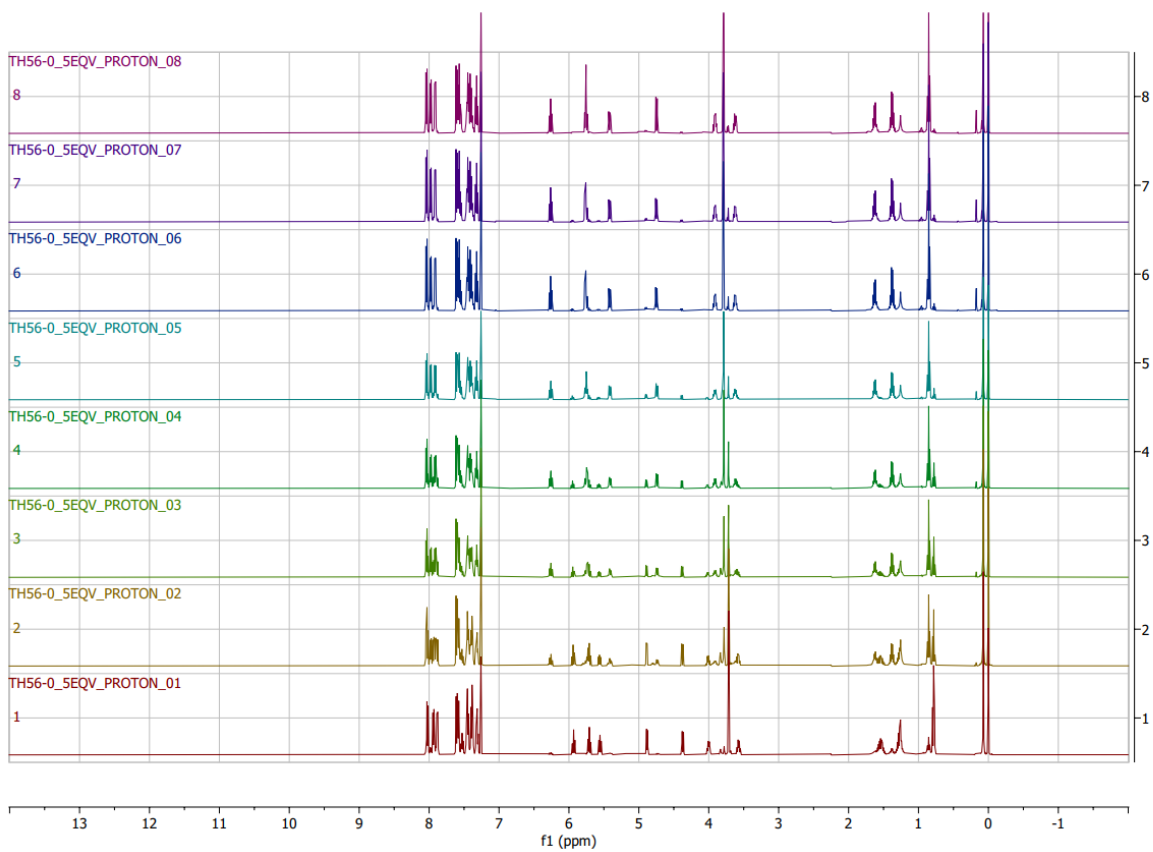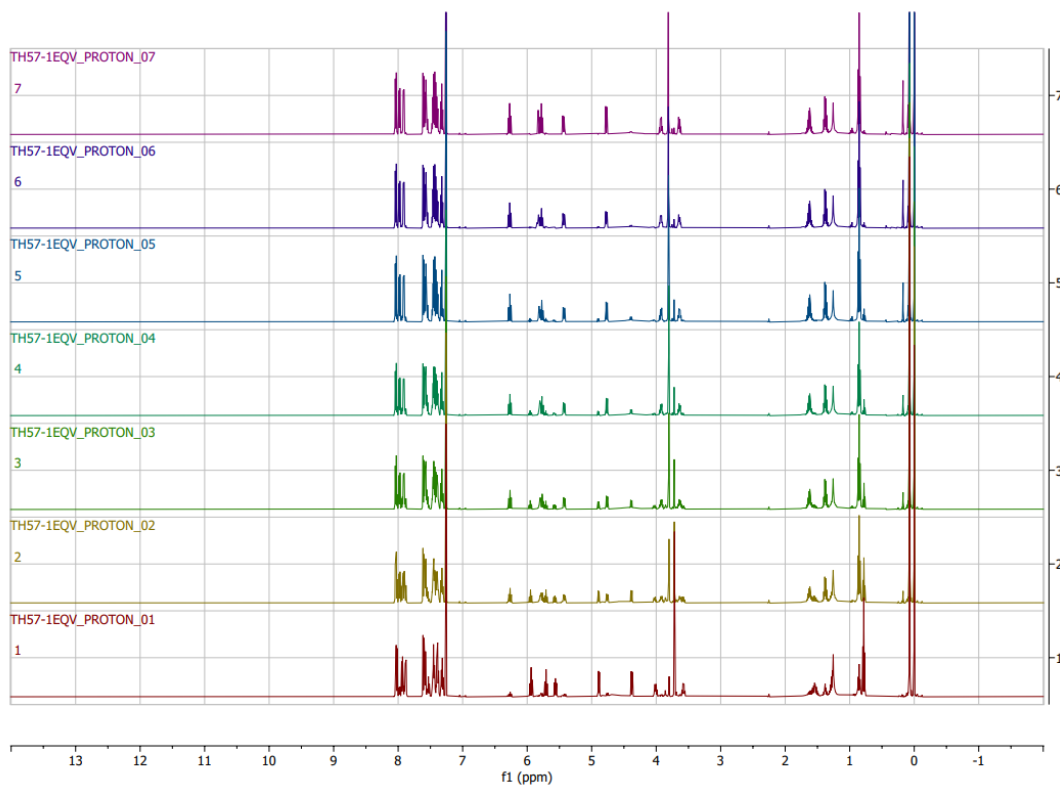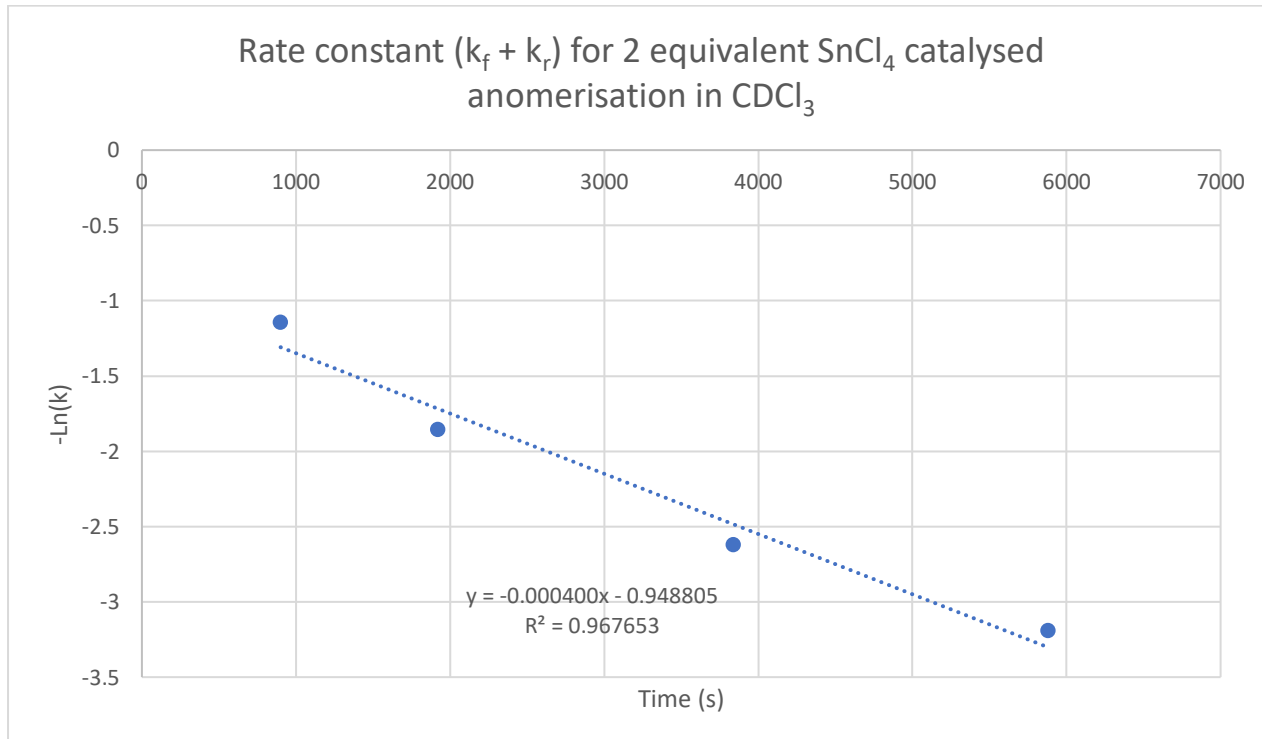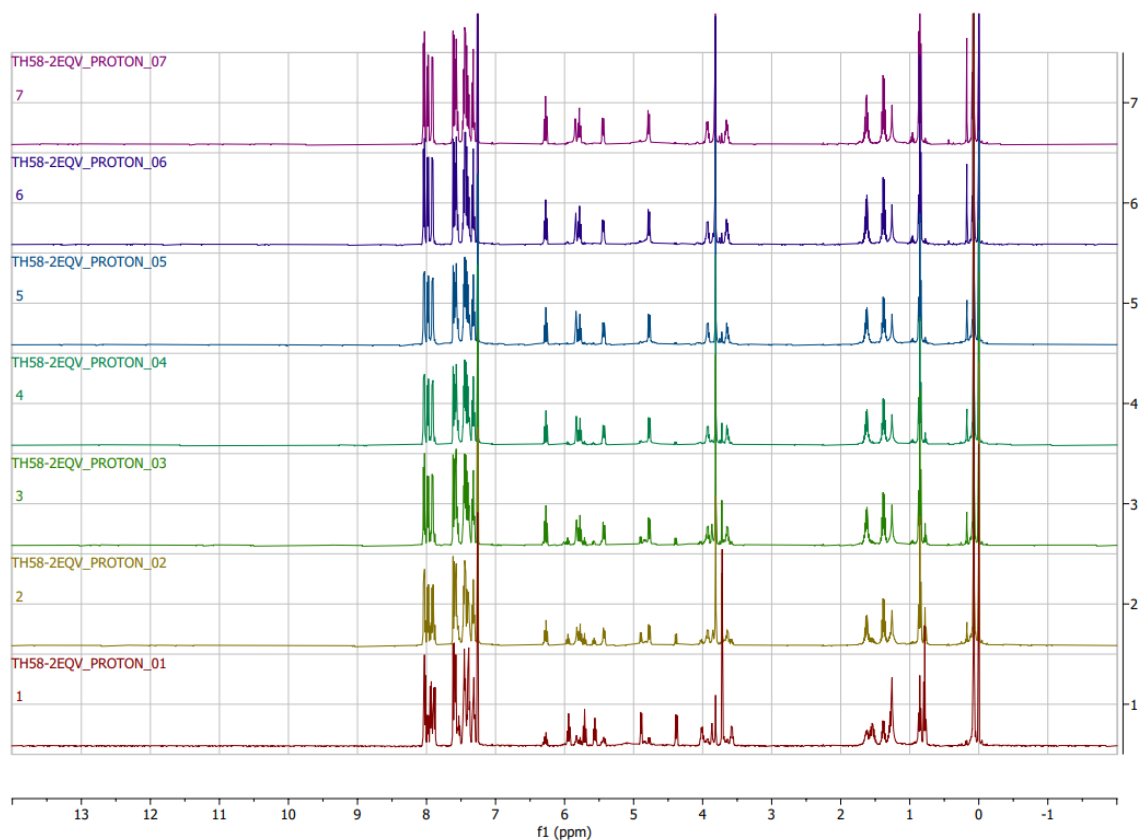
Appendix 9: NMR Data for compounds **(5)**, **(6),** and **(7)**

^{1}H-NMR compound **(5)**

^{13}C-NMR compound **(5)**

TH-68-CARBON

Peaks: 167.58, 165.31, 146.06, 139.98, 133.55, 133.45, 130.39, 129.96, 129.91, 128.56, 128.45, 127.36, 127.14, 101.29, 77.43 CHLOROFORM-D, 77.12 CHLOROFORM-D, 77.00 CHLOROFORM-D, 73.05, 72.24, 71.70, 70.37, 53.02, 31.40, 18.98, 13.74

^{1}H-NMR compound **(6)**

TH-FM93

Label	Shift (ppm)
A (d)	7.91
B (d)	7.84
C (d)	7.80
D (m)	7.51
E (t)	7.45
F (t)	7.37
G (t)	7.30
H (d)	5.86
I (t)	5.67
J (t)	5.48
K (d)	4.82
L (d)	4.31
M (dt)	3.96
N (s)	3.69
O (s)	3.53
P (s)	1.55
Q (s)	1.24
R (t)	0.77
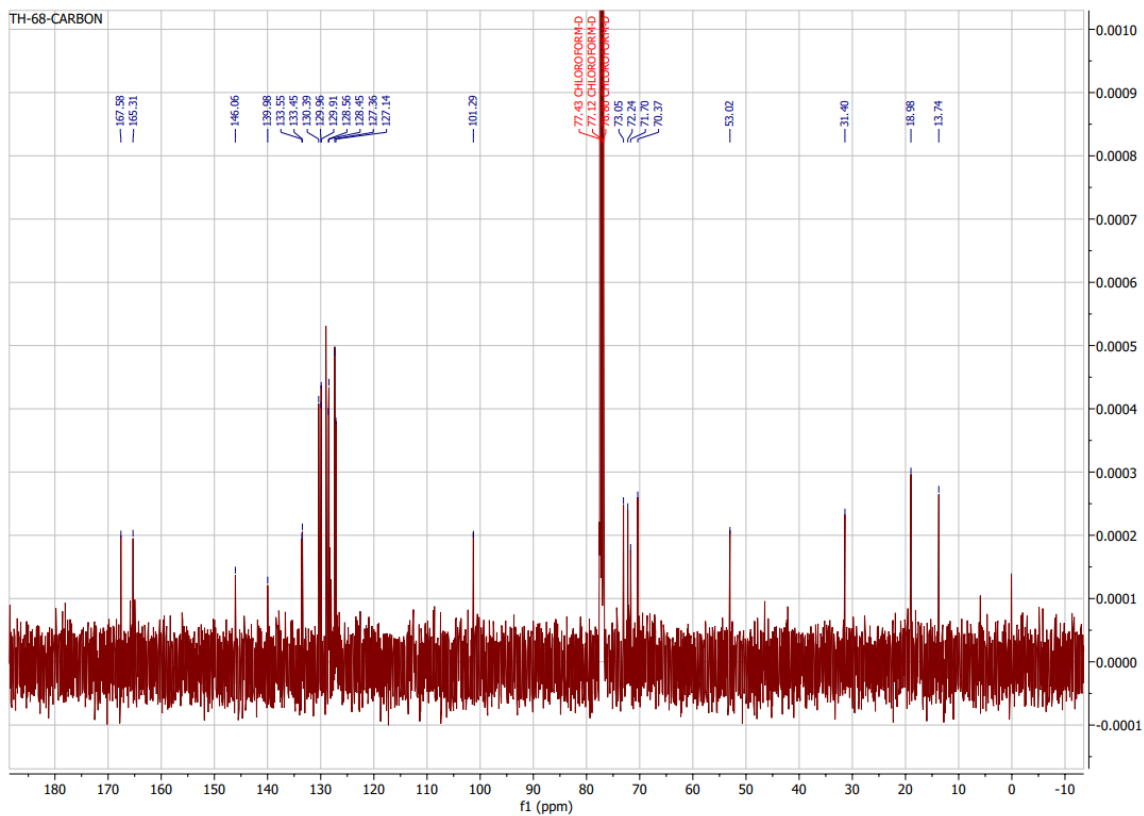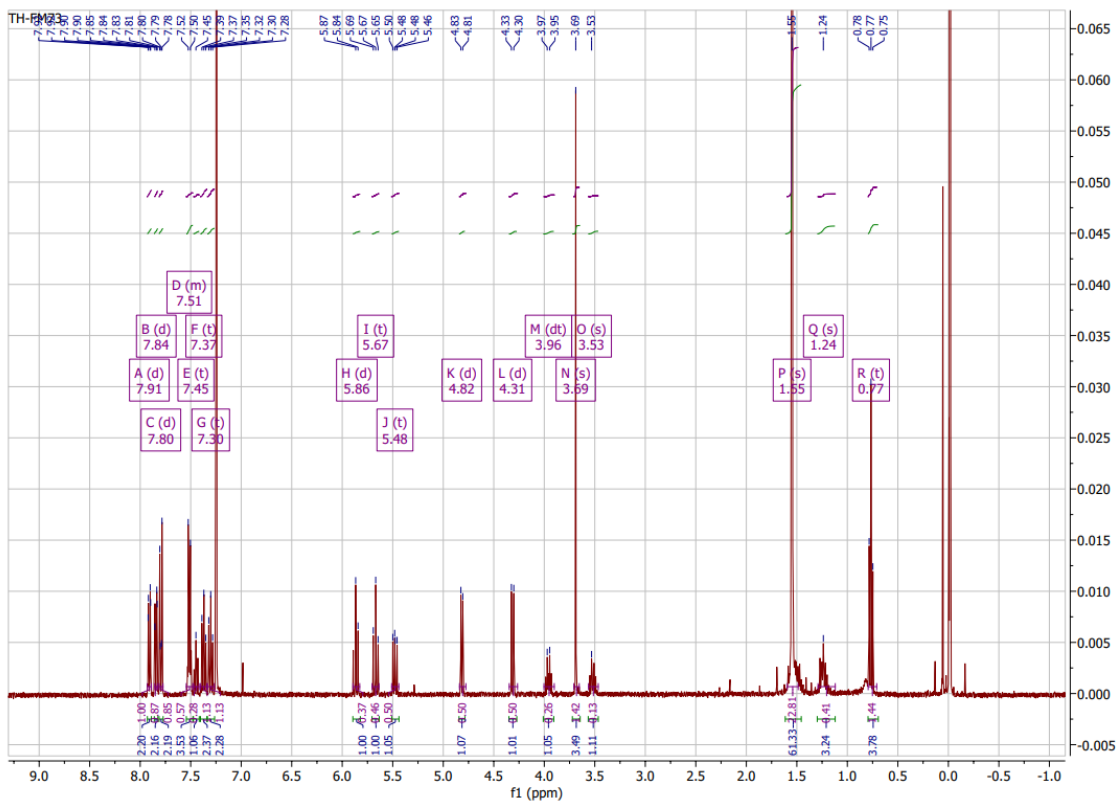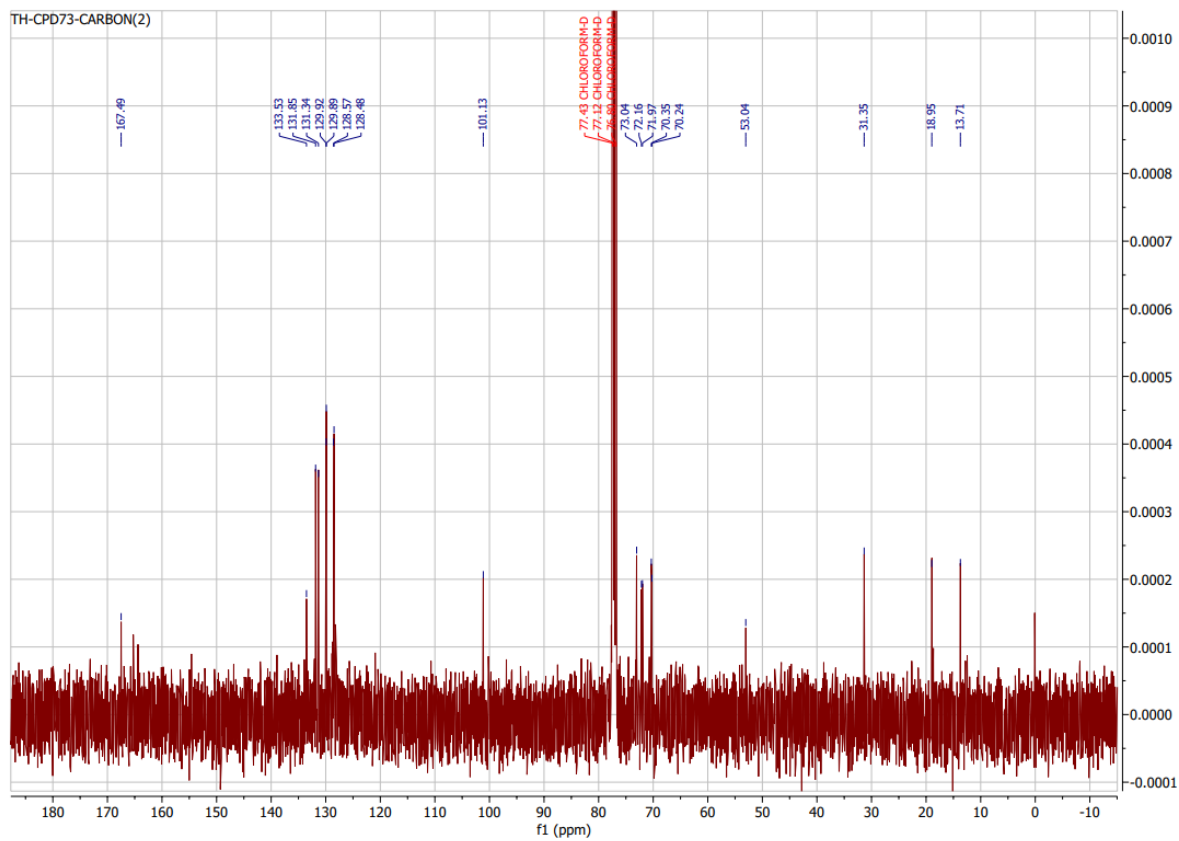
^{13}C-NMR compound **(6)**

^{1}H-NMR compound **(7)**

¹³C-NMR compound **(7)**